Magnetism of Earth, Planetary, and Environmental Nanomaterials

Denis G. Rancourt

Department of Physics
University of Ottawa
Ottawa, Ontario, Canada K1N 6N5

INTRODUCTION

Superparamagnetism, the archetypal small particle phenomenon, was first described by Louis Néel (1949a,b) in the context of rock magnetism. Key features of the underlying micromagnetism had been described by Stoner and Wohlfarth (1948), in the context of industrial magnetic alloys. The physical theory of superparamagnetism was further developed by William Fuller Brown (1963, 1979; see Rubens 1979). Many recent and ongoing additional advances are motivated by the potential for improved nanotechnological applications. One of my main aims in writing this chapter is to help bridge the gap that presently exists between the still largely phenomenological methods of rock and mineral magnetism and rapidly developing fundamental advances in the theory of micromagnetism, the theory of magnetic measurements applied to nanomagnets, and the study of synthetic model systems of ensembles of interacting magnetic nanoparticles. It is hoped that the reader will acquire appreciations of both the underlying atomistic theory of small particle magnetism and the wealth of phenomena involving the magnetism of natural materials, that often have nanoscale structural or chemical features, including their sizes. The reward for taking a more fundamental approach is that magnetism becomes one of the most sensitive probes of such structural and chemical features of complex natural solids and composites.

Magnetism in the Earth sciences

Magnetism is many things in the Earth. Three large areas can be distinguished: (1) geomagnetism, where one is primarily concerned with paleorecords of geomagnetic fields (inclination, intensity, reversals), models of the geodynamo and geomagnetic field generation, or the use of geomagnetic fields for prospecting or probing planetary interiors, (2) magnetic geology (magnetic petrology, magnetic fabric, environmental magnetism), where one is primarily concerned with magnetic rock and mineral records that are used to study petrogenesis, geotectonic activity, weathering, diagenesis, sediment transport, etc., and (3) mineral magnetism, where one is primarily concerned with the magnetic properties of natural samples in order to deduce the underlying mineralogy or individual mineral characteristics. Successes in the first two areas largely depend on the latter area of mineral magnetism, that is the subject of the present chapter. We wish to know the extent to which measured magnetic properties can be used to provide mineralogical identification, quantification, and characterization, of either whole samples or separated solid phase fractions of interest and even down to a single nanoparticle.

Relation to other books and reviews

The book by O'Reilly (1984) is a wonderful first attempt at a general textbook on mineral magnetism, although the outlook is slanted towards rock magnetic methods. The early rock magnetism review by Stacey (1963) has a strong mineral magnetic perspective. Banerjee's review (1991) has a mineral magnetism perspective but does

not deal with particle size effects. Frost (1991) has written a nice survey of magnetic petrology. Researchers such as Rochette and Fillion (1988) and Richter and van der Pluijin (1994) have endeavored to bring novel mineral magnetic methods into rock magnetism. Dunlop and Özdemir (1997) have written an authoritative recent textbook on traditional rock magnetism, that complements the classic text by Nagata (1961) and other important texts (e.g., Stacey and Banerjee 1974, Collinson 1983) and reviews (e.g., Clark 1983). Tarling and Hrouda (1993) concentrate on magnetic fabric applications and good examples in this area can be found in the collection assembled by Benn (1999). Thompson and Oldfield (1986) concentrate on environmental magnetism, Creer et al.. (1983) on baked clays and recent sediments, and Opdyke and Channell (1996) on magnetic stratigraphy, all using mainly rock magnetic methods. Maher and Thompson (1999) have surveyed the use of magnetism in the study of paleoclimates via the sedimentary record. Worm (1998) has reviewed the application of classic alternating field magnetic susceptibility measurements to soils, in relation to pedogenic nanoparticles. There are several books on the theoretical and experimental aspects of geomagnetism and paleomagnetism (e.g., Parkinson 1983, Vacquier 1972, Rikitake and Honkura 1986, Lowes 1989, Jacobs 1991, Backus et al. 1996, Merrill et al. 1998, McElhinny and McFadden 1999, Campbell 2000). A nice recent example of geomagnetic research is provided by Gee et al.. (2000). Dormann et al. (1997) have given a comprehensive review of magnetic relaxation effects arising from superparamagnetism. Dormann (1981) had provided an earlier review. Pankhurst and Pollard (1993) have reviewed Fe oxide nanoparticles. Himpsel et al. (1998) have provided a review of magnetic nanostructures that emphasises technological applications and the underlying relations to electronic structure. The present chapter is the first review to concentrate on the fundamental foundations of both mineral magnetism and the relevant measurement methods, especially in relation to magnetic nanoparticles and nanomaterials. This should serve to illustrate both the opportunities for development of the methods and interpretations and to provide some insight into the magnetic phenomena themselves.

Organization and focus of this chapter

Following a brief interdisciplinary look at magnetic nanoparticles and a brief overview of the magnetism of Earth's crust and surface environments, the core of this chapter is broadly organized into the usual divisions of measurement methods, underlying theory of both the phenomena themselves and the measurement methods, and applications to and interpretations of natural phenomena. As in all observational sciences, however, these three areas are highly interdependent and must not be treated as separate topics. Interpretation of the raw measured data relies on a chosen theoretical framework that in turn is judged appropriate to describe the expected phenomenon, etc. Self-consistency is the result of much trial and error and is only attained once the phenomenon is judged to be understood, such that routine applications can be devised. The mineral magnetism of nanomaterials is a developing area of intense present research where the interplays between measurement, theory, and interpretation must be considered with care. For example, characteristic measurement times may be comparable to intrinsic sample property fluctuation times (e.g., SP supermoment fluctuations compared to the measurement frequency in an alternating field susceptibility measurement) such that calculations that assume thermodynamic equilibrium become inapplicable but stochastic resonance may become relevant. I have made a special effort to illustrate these inter-relationships throughout this chapter, in order to do justice to the area and to enhance the general reader's appreciation of the subject.

Symbols and acronyms

1NN	first nearest neighbour
2NN	second nearest neighbour
a	lattice parameter or particle's long ellipsoidal semi-axis
a-HFO	abiotic hydrous ferric oxide
$<A>_a$	type-a average of A
$<A>(T,H)$	thermal average of A as a function of temperature and field
$\{A_i\}$	set of all values of A_i (for all cations-i in sample or particle)
$\{A_{ij}\}$	set of all values of A_{ij} (for all cation pairs-ij in sample or particle)
AF	antiferromagnetic
b	lattice parameter or particle's short ellipsoidal semi-axis
b-HFO	biotic hydrous ferric oxide
BCC	body centered cubic
χ	magnetic susceptibility ($= \partial M / \partial H$)
χ_o	initial magnetic susceptibility
χ_3	cubic magnetic susceptibility
C	Curie constant (of paramagnetic susceptibility)
CBED	convergent beam electron diffraction
CMEs	collective magnetic excitations
d	particle size (diameter or mean diameter)
d_{QT}	quantum-tunnelling/quantum-blocked transition size
d_{SD}	single-domain/multi-domain transition size
d_{SP}	superparamagnetic/blocked transition size
d_{SR}	characteristic surface region size or thickness
DM	diamagnetic
ε_n	subsystem (cation) eigenenergy in subsystem eigenstate n
e	eccentricity of particle's assumed ellipsoid of revolution shape
E_b	supermoment reversal energy barrier height or barrier function of θ
E_d	dipolar anisotropy energy barrier function
E_n	eigenenergy of system in eigenstate n
E_s	surface anisotropy energy barrier function
E_v	magneto-crystalline anisotropy energy barrier function
EDS	energy dispersive spectroscopy
EELS	electron energy loss spectroscopy
ESC	electronic structure calculation (*ab initio* calculation of electron densities)
ESR	electron spin resonance
f_o	pre-exponential term or attempt frequency in expression for $1/\tau$
FC	field cooling
FCC	face centered cubic
FI	ferrimagnetic
FW	field warming
GBIC	graphite bi-intercalation compound
GIC	graphite intercalation compound
GSC	Geological Survey of Canada
$\mathcal{H}$	Hamiltonian of (total) system (entire solid or particle)

$\mathcal{H}_i$	Hamiltonian of subsystem-i (cation-i)
H	magnetic field
H_o	critical field of induced magnetic moment reversal at T = 0 K
H_{int}	interaction field (local or uniform, static or time-dependent)
$H_{applied}$	applied magnetic field
HFD	hyperfine field distribution
HFO	hydrous ferric oxide (solid precipitate)
HM	high moment (state or phase)
INS	inelastic neutron scattering
$J, J_{ij}, J_{ij}(r_{ij})$	magnetic exchange parameter (energy per interacting pair of moments)
k_B	Boltzmann's constant
k_s	surface anisotropy energy barrier per surface (in J/m^2)
K	single-ion magneto-crystalline anisotropy constant (energy per ion)
K_i	magneto-crystalline anisotropy constant of cation-i
K_v	magneto-crystalline anisotropy energy per volume of the material (= nK/v)
ln(A)	natural logarithm of A
L	orbital angular momentum vector operator (of a cation)
LHT	liquid helium temperature (4.2 K)
LM	low moment (state or phase)
LNT	liquid nitrogen temperature (77 K)
LSSE	Lake Sediment Structure and Evolution (Group)
μ	magnetic moment (atomic or particle or sample)
μ_i	magnetic moment at site-i or on nanoparticle-i
μ_s	magnetic supermoment
μ_{Fe}	atomic magnetic moment on Fe atom
μ_B	Bohr magneton
μ_N	nuclear magneton
m	number of cation moments per net supermoment (m = μ_s/μ = Mv/μ)
M	sample or sublattice magnetization (= μ/V)
M(H)	magnetization as a function of field, at constant temperature
M(T)	magnetization as a function of temperature, at constant field
M(t)	magnetization as a function of time, at constant field and temperature
MC	Monte Carlo (calculation method)
MD	multi-domain or molecular dynamics
MFT	mean field theory
MITE	Metals in the Environment (Project)
MQT	macroscopic quantum tunnelling (of the supermoment orientation)
n	number of moment-bearing cations in a nanoparticle or eigenstate index
<n|A|n>	diagonal matrix element of operator A, using eigenstate |n>
NC	non-collinear
NN	nearest neighbour
$P(H_o)$	probability density distribution of critical reversal fields
$P(m,E_b,H_{int},...)$	joint probability density distribution of m, E_b, H_{int}, and other parameters
P(v)	probability density distribution of particle volumes
PM	paramagnetic
ρ	mass density

RT	room temperature (22 °C)
RTM	reaction transport model
s-Fe	surface complexed or sorbed Fe
S	dimensionless spin angular momentum quantum number (of a cation)
S	dimensionless spin angular momentum vector operator (of a cation)
S, S(T,H)	magnetic viscosity
SAED	selected area electron diffraction
SANS	small angle neutron scattering
SD	single domain
SF	superferromagnetic
SG	spin glass
SP	superparamagnetic
SQUID	superconducting quantum interference device (magnetometer)
SR	surface region (of a nanoparticle)
τ	superparamagnetic reversal fluctuation time (zero field)
τ_+	superparamagnetic dwell time for supermoment mostly parallel to field
τ_-	superparamagnetic dwell time for supermoment mostly antiparallel to field
τ_m	measurement or observation time
θ_{CW}	Curie-Weiss temperature
$\theta_{\mu a}$	angle between supermoment and particle's major axis of elongation
$\theta_{\mu k}$	angle between supermoment and particle's anisotropy axis direction
T	temperature or Tesla
T_{0B}	effective Curie-Weiss temperature due to distribution of barrier energies
T_{0i}	effective Curie-Weiss temperature due to inter-particle interactions
T_C	Curie point or Curie temperature (of a ferromagnet)
T_{oB}	magnetic ordering temperature of the bulk material
T_{peak}	temperature of peak in ZFQ-FW magnetization curve
T_{SP}	superparamagnetic/blocked transition temperature (depends on τ_m)
TEM	transmission electron microscopy
TRM	thermoremanent magnetization
u_r	dimensionless unit vector pointing along a vector r
u_i	dimensionless unit vector pointing along axis-i
u_{ij}	dimensionless unit vector pointing along the straight line between i and j
U_{dd}	dipolar interaction energy (per pair of interacting moments)
v	volume of a nanoparticle
v_{SP}	transition nanoparticle volume between SP and blocked states
VSM	vibrating sample magnetometer
WF	weak ferromagnetic (or canted antiferromagnetic)
Z	partition function
ZFQ	zero field quench

Note: Boldface type is used to represent vector quantities.

This chapter is not a comprehensive review of the many studies concerned with natural magnetic nanoparticles in the Earth, planetary and environmental sciences. Instead, I concentrate on giving a broad overview and key examples and attempt to motivate a deeper than usual examination of forefront fundamental developments. I stress

that the magnetism of nanomaterials and nanoparticles is presently an area of intense and rapid development that touches many fields including technological applications, biology, medicine, chemistry, materials science, condensed matter physics, environmental science, planetary science, information theory, etc. (see below), and that I will primarily focus on the development of mineral magnetism for advanced applications in the Earth, planetary, and environmental sciences.

MAGNETIC NANOPARTICLES EVERYWHERE

In our brains, the animals, space, everywhere

The human brain contains over 10^8 magnetic nanoparticles of magnetite-maghemite per gram of tissue that may be responsible for a variety of biological effects (Kirschvink et al. 1992). The human mind struggles with complex applications involving image processing or data classification and mining and has recently discovered an underlying similarity between superparamagnetism and data clustering, that allows methods of statistical physics developed for superparamagnetism to be applied to great advantage in information handling (Rose 1990, Domany 1999, Domany et al. 1999). This same information is stored on magnetic media composed of magnetic nanoparticles and the need for larger and larger storage densities drives yet more advanced theoretical models of the supermoment and its fluctuations and field driven reversals. Experimentalists, in turn, devise more and more clever synthetic model nanoparticle systems to test and challenge theory and force more and more realistic features into the calculations (see below).

Meanwhile, Earth scientists, planetary scientists, environmental scientists, and biologists keep finding more and more unusual magnetic nanoparticles in the strangest places: as geomagnetic navigational aids in bacteria, eukaryotic algae, and the bodies of higher animals (Kirschvink et al. 1985, Kirschvink 1989, Wiltschko and Wiltschko 1995) such as homing pigeons (e.g., Hanzlik et al. 2000), migratory birds, ants, bees, salmon, tuna, sharks, rays, salamanders, newts, mice, cetaceans, etc., as the ferrihydrite-like mineral cores of the most common iron storage protein ferritin (e.g., St-Pierre et al. 1989), present in almost every cell of plants and animals including humans, as keystone crystals in the cells of hornet combs (Stokroos et al. 2001), as bacterial micro-fossils (e.g., Chang and Kirschvink 1985, Petersen et al. 1986), precipitated to bacterial cell walls (e.g., Ferris 1997, Fortin et al. 1997, Watson et al. 2000), in lunar samples and as common products of space weathering (e.g., Pieters et al. 2000), in Martian meteorites where they may be of biogenic or inorganic origin (e.g., Bradley et al. 1998, Golden et al. 2001), in Martian soil and its analogues (e.g., Morris et al. 1998, 2001), in interstellar space (Goodman and Whittet 1995), at the Cretaceous/Tertiary (K/T) boundary on Earth where they can be either produced in molten impact droplets or oxidized remnants of the meteoritic projectile itself (e.g., Kyte and Bohor 1995, Kyte and Bostwik 1995, Robin 1996, Gayraud et al. 1996, Kyte 1998), at the oxic/anoxic boundary in lacustrine sediments (e.g., Tarduno 1995), etc. And if these researchers become ill from overwork and the medical diagnosis becomes difficult, chances are they will be injected with magnetic nanoparticles as magnetic resonance imaging (MRI) contrast agents (e.g., Roch et al. 1999, Grüttner and Teller 1999, Bonnemain 1998). If these patients are among the few to develop side effects (e.g., Sharma et al. 1999) and have the occasion to take some time off, they may notice while gazing at the stars one night (with polarizing sun glasses!) a slight polarization of the background starlight that may be due to superparamagnetic (SP) particles (Goodman and Whittet 1995).

Applications of magnetic nanoparticles

Back on Earth, in nature, most magnetic nanoparticles are iron oxides and oxyhydroxides. Pankhurst and Pollard (1993) have reviewed iron oxide nanoparticles and some of their applications. The applications range from model systems to study stochastic resonance (Raikher and Stepanov 1995a, Ricci and Scherer 1997), to synthetic industrial catalysts (e.g., Lopez et al. 1997), to magnetic colloids and ferrofluids for seals, bearings, and dampers, such as the ones in our cars (Rosensweig 1985, Cabuil 2000, Popplewell and Sakhnini 1995), to magneto-optic recording devices (Suzuki 1996), to magnetic force microscopy (MFM) tips (Liou et al. 1997, Hopkins et al. 1996), to giant magneto-resistive devices (Lucinski et al. 1996, Wiser 1996, Xu et al. 1997, Altbir et al. 1998), to field sensing technology (Cowburn et al. 2000), to molecular biology (Grüttner and Teller 1999), to cell biology and immunomagnetic methods (Yeh et al. 1993, Sestier et al. 1998, Sestier and Sabolovic 1998), to cell separation (e.g., Honda et al. 1998), to advanced medical applications (Tiefenauer et al. 1993, Jung et al. 1999), to environmental remediation via synthetic magnetically separable sorbents (e.g., Safarik and Safarikova 1997, Broomberg et al. 1999), in addition to the areas mentioned above. There are also associated technologies, such as magnetic separation of nanoparticles (Zarutskaya and Shapiro 2000). And, of course, one must not leave out the largest single client of magnetic nanoparticle use: the magnetic recording industry (Lodder 1995, Brug et al. 1996, Kryder 1996, Onodera et al. 1996). Here, corporate giants have taken charge of the problem, with claims like "The superparamagnetism limit and what IBM is going to do about it" (e.g., Comello 1998, Soltis 2001).

Since the time of Stoner and Wohlfarth (1948), we have known that the first great application advantage of magnetic nanoparticles is that they are single domain and therefore have large coercivities, allowing them to individually retain their magnetization directions. And since the time of Néel (1949a,b) we have known that, as the particle size is decreased, every particle eventually becomes SP and looses its capacity to retain a remanence magnetization. Higher and higher information storage densities, that have doubled every year since the late 1990s, mean smaller and smaller particles, hence is born the superparamagnetism problem or limit, presently estimated at ~100 Gbits/in^2 (Comello 1998, Soltis 2001). Engineers want to suppress it or avoid it while natural scientists want simply to use it as a means to learn about the particles, hence is born mineral magnetism, with its first client that is rock magnetism.

Towards function and mechanisms

There must be at least as many applications and natural phenomena related to magnetic nanoparticles left to be discovered. The mechanisms of magnetic biosensitivity are mostly unknown (Deutschlander et al. 1999, Wiltschko and Wiltschko 1995). The possibility of magnetically sensitive biological chemical reactions has only recently been demonstrated (Weaver et al. 2000) and such reactions may, in turn, interact with biogenic nanoparticle assemblies. Function is as much a puzzle in environmental science where bacteria-mineral interactions are just beginning to be explored and where most reactive authigenic, biogenic, pedogenic, and diagenetic solid phases are nanoparticles and nanomaterials. Beyond observations of particles, uncovering function is the goal. Elucidation of function requires detailed characterization that, in turn, requires advanced characterization tools that are adapted to the subject. Mineral magnetism, coupled with a fundamental understanding of both the measurement process and nanomagnetic phenomena, is such a tool that offers great promise. It has already given remarkably intricate views of these complex beasts that are magnetic nanomaterials.

MAGNETISM OF THE CRUST AND SURFACE ENVIRONMENTS

Diamagnetic and paramagnetic ions

In terms of both abundance in the Earth's crust (and on planetary surfaces) and numbers of species, most minerals are ionic and covalent in character, rather than metallic. Their magnetism, therefore, is appropriately described in terms of the magnetism of their cations and anions, rather than in terms of band magnetism of conduction electrons. Prominent exceptions are the Fe-Ni phases found in meteorites and that are relevant to planetary cores. Even in metallic minerals, however, the magnetism of the closed shell cation cores can, to a good first approximation, be treated independently from the conduction electron magnetism.

The magnetism of constituent ions in solids is mostly due to electron spin and may have an electron orbital component as well (Ashcroft and Mermin 1976). Closed shell ions have paired spin up and spin down electrons in filled orbitals and zero net orbital angular momentum. As a result, closed shell ions (most ions in the Earth's crust) are strictly non-magnetic, in that their net spontaneous (i.e., in the absence of an applied magnetic field) ionic magnetic moments are strictly zero. Such ions and substances that contain only such ions are said to be diamagnetic (DM). When a magnetic field, H, is applied to a DM ion, a relatively small magnetic moment, μ, is induced, in proportion to the magnitude of and in a direction opposite to the applied field. This negative magnetic susceptibility ($\chi \sim \partial\mu/\partial H < 0$) is taken to be a diagnostic feature of non-metallic diamagnetism. The only other known type of diamagnetism is the strong (Meisner effect) diamagnetism associated with superconductivity. This feature is considered an experimental proof of the superconducting nature of a material.

Ions having partially filled orbitals will have net electron spin magnetic moments and may, in addition, have net electron orbital magnetic moments. Such ions are referred to as paramagnetic (PM). These are the moment-bearing atomic entities of ionic and covalent magnetic minerals. Materials that contain PM ions and in which the PM ions do not interact magnetically, other than via the usual classical and relatively weak dipole-dipole interactions, are also referred to as PM. The corresponding thermally induced disordered state, in which the vector orientations of the PM ionic moments in a given solid phase fluctuate randomly such as to produce zero time averages of the local moments on all the ionic PM centres, except to the extent that an applied field would induce a non-zero value, is referred to as the PM state or phase and any material that is in a PM state at a given temperature of interest can also be referred to as PM. An applied magnetic field will tend to align the PM ionic moments in its direction (as is the case with classical magnetic dipole moments), leading to a positive PM susceptibility that is much larger in magnitude than ionic DM susceptibilities. Strong inter-moment quantum mechanical interactions between ionic PM moments give rise to a large array of possible spontaneous ordered magnetic structures, in which the local time average moments are not zero in zero applied field, that are highly sensitive to nanofeatures of the material and that have larger or smaller than PM susceptibilities, as described below.

Magnetism from crustal ions in surface minerals

Table 1 gives the usual elemental abundances of the Earth's crust (Klein and Hurlbut 1999), where I have added the various common ionic valence states, corresponding electron configurations, and resulting expected net spin moments (Ashcroft and Mermin 1976), in units of Bohr magnetons (μ_B). The great majority of abundant ionic species are DM, with zero net moments, and Fe is the main moment-bearing element in crustal rocks. For this reason, magnetic measurements can be considered a means to specifically examine the iron mineralogy of a given natural sample, much as would be the case with

[57]Fe Mössbauer spectroscopy applied to a whole rock sample. On the other hand, a sample that would have the elemental abundances given in Table 1 but in which all of the Fe were in PM mineral species could have its magnetic response to an applied field dominated by Mn if the Mn was in mineral species that have certain ordered magnetic structures. This is relevant to early diagenesis in marine and lacustrine environments where authigenic nanophase Mn oxyhydroxides play an important role. Similarly, particular mineral assemblages that involve V, Cr, or the magnetic rare earth elements (mostly not shown in Table 1) could exhibit magnetic responses that are due to those elements rather than Fe. In addition, even in the most common cases where the magnetic susceptibility is dominated by Fe signals from several Fe-bearing fractions, magnetic phase transitions, between different ordered magnetic structures or between an ordered phase and the PM phase, can be observed, as temperature and field are varied, that are characteristic of specific majority and minority mineral species, thereby allowing their quantification and characterization.

Table 1. Electronic magnetism of crustal ions.

element	weight % of crust	ion	electrons	spin magnetic moment, μ_B
O	46.60	O^{2-}	[Ne] (=$1s^2 2s^2 2p^6$)	0
Si	27.72	Si^{4+}	[Ne]	0
Al	8.13	Al^{3+}	[Ne]	0
Fe	5.00	Fe^{2+}	[Ar]$3d^6$	4
		Fe^{3+}	[Ar]$3d^5$	5
Ca	3.63	Ca^{2+}	[Ar]	0
Na	2.83	Na^+	[Ne]	0
K	2.59	K^+	[Ar]	0
Mg	2.09	Mg^{2+}	[Ne]	0
Ti	0.44	Ti^{4+}	[Ar]	0
H	0.14	H^+	0	0
P	0.1	P^{5+}	[Ne]	0
Mn	0.09	Mn^{2+}	[Ar]$3d^5$	5
		Mn^{3+}	[Ar]$3d^4$	4
		Mn^{4+}	[Ar]$3d^3$	3
Ba	0.04	Ba^{2+}	[Xe]	0
F	625 ppm	F^-	[Ne]	0
Sr	375 ppm	Sr^{2+}	[Kr]	0
S	260 ppm	S^{6+}	[Ne]	0
C	200 ppm	C^{4+}	[He]	0
Zr	165 ppm	Zr^{4+}	[Kr]	0
V	135 ppm	V^{2+}	[Ar]$3d^3$	3
		V^{3+}	[Ar]$3d^2$	2
		V^{4+}	[Ar]$3d^1$	1
Cl	130 ppm	Cl^-	[Ar]	0
Cr	100 ppm	Cr^{2+}	[Ar]$3d^4$	4
		Cr^{3+}	[Ar]$3d^3$	3
Rb	90 ppm	Rb^+	[Kr]	0
Ni	75 ppm	Ni^{2+}	[Ar]$3d^8$	2
Zn	70 ppm	Zn^{2+}	[Ar]$3d^{10}$	0
Ce	60 ppm	Ce^{3+}	[Xe]$4f^1$	1
Cu	55 ppm	Cu^{2+}	[Ar]$3d^9$	1

Magnetism from crustal and surface mineralogy

This brings us to examine crustal magnetism from the perspective of crustal mineralogy, which is an application of reverse magnetic petrology (Frost 1991). The plagioclase feldspars, the alkali feldspars, and quartz, which together make up 63% of the volume of the crust (Klein and Hurlbut 1999), contain no Fe and consist only of DM minerals containing only DM ions. Clearly, magnetic measurements will not contribute to the study of these most common rock forming minerals, although high resolution magnetometry of DM response can be used to investigate fine aspects of bonding and electronic structure (e.g., Uyeda 1993). The other large classes of abundant minerals (pyroxenes, micas, amphiboles, clay minerals and chlorites, garnets, olivines, carbonates, oxides) generally contain Fe and other PM cations and have important representative end-member species that are Fe-rich. In particular, the next most abundant group, the pyroxenes, with 11% of the crustal volume, represent a large compartment of crustal Fe, predominantly in the form of the enstatite-ferrosilite solid solution, $(Mg,Fe)SiO_3$, and augite, $(Ca,Na)(Mg,Fe,Al)(Si,Al)_2O_6$. The amphiboles and micas represent the next two largest compartments of crustal and petrogenic Fe. Together, the pyroxenes, amphiboles, micas, olivines, and garnets make up 29% of the crustal volume (Ronov and Yaroshevsky 1969) and contain ~90% of the crustal Fe that is tied to petrogenic mineral species. All of the latter Fe is contained in minerals that are PM at room temperature (RT = 22°C) and that generally remain PM down to liquid nitrogen temperature (LNT = 77 K). The remaining ~10% of crustal Fe tied to petrogenic minerals is mostly contained in spinel group Fe oxides, such as magnetite, Fe_3O_4, that comprise 1.5% of the crustal volume. The bulk Fe-rich spinels (magnetite-titanomagnetite-maghemite system) have magnetic ordering temperatures (below which spontaneous ordered magnetic structures occur) that are well above RT and they occur in a broad range of crystallite sizes. As a result, despite the relatively small size of this petrogenic compartment for Fe, the name of the game in rock magnetism is magnetite and its size-dependent magnetic properties (Dunlop 1990). Only a substance with a sufficiently high magnetic ordering temperature can effectively register and preserve remanent geosignals and only a mineral with a magnetic ordering temperature larger than RT can be detected above the PM signals of the rock or sediment matrix, by the usual RT and high temperature measurement protocols.

But rock magnetism and magnetic petrology are not our only concerns here. Approximately as much Fe as is contained in the petrogenic spinel compartment occurs in non-petrogenic minerals and solid phases that reside in the surface environments (soils and sediments). The Fe-bearing phases can be authigenic, biogenic, pedogenic, diagenetic, etc., and have acquired their Fe by weathering and dissolution of the petrogenic Fe phases discussed above, including magnetite. As a result, the magnetism of surface samples is often not dominated by petrogenic magnetite but is instead largely determined by various abiotic and biotic (Banfield and Nealson 1997, Ferris 1997) precipitation reactions that invariably produce nanophase Fe oxides and oxyhydroxides, such as ferrihydrite (Jambor and Dutrizac 1998, Cornell and Schwertmann 1996), in addition to a broad range of nanophase and poorly crystalline materials that are Fe-poor or DM, such as allophane and amorphous silica (Dixon and Weed 1989). Pedogenic and early diagenetic processes also often create and maintain well defined horizons of magnetic (Fe-rich or Mn-rich) phases, such that specific sections of a depth profile can have a magnetism that is overwhelmingly determined by these processes, rather than the geologic nature of the parent material.

Given the importance of spontaneous magnetic order in allowing rock magnetism applications and in determining magnetic susceptibility magnitudes, I give some magnetic ordering and transition temperatures of bulk end-member materials in Table 2.

Table 2. Magnetic ordering and transition temperatures of some bulk end-members.

Material	Transition	Temperature[a] (K)		Comments
magnetite	FI/PM	T_C	853(5)	Table 37, Krupicka & Novak (1982)
	Verwey	T_V	119(1)	p. 264, Krupicka & Novak (1982)
hematite	WF/PM	T_N	948	p. 172, O'Reilly (1984)
	Morin	T_M	260	Rancourt et al (1998)
ilmenite	AF/PM	T_N	55	p. 179, O'Reilly (1984)
ferrihydrite[b]	AF/PM	T_N	350(2)	Seehra et al (2000)
annite[c]	meta/PM	T_N	58(1)	Rancourt et al (1994)

a – C, Curie point; V, Verwey transition; N, Néel temperature; M, Morin transition
b – synthetic two-line ferrihydrite
c – synthetic annite, Fe-end-member of phlogopite-biotite-annite series

Having described the ionic and mineral magnetic species that one should expect to encounter on Earth and the interplay between chemistry and mineralogy that determines the strength of a magnetic response (in the sequence DM << PM << magnetically ordered), we end this section by a few observations that bring us back to our main theme of mineral magnetism. First, as mentioned above, applying mineral magnetic methods (next section) to bulk natural samples or separated fractions of bulk samples should be a powerful tool in elucidating the Fe mineralogy, and in some cases the Mn mineralogy. It has surprised me, as a relative newcomer to the Earth sciences, that this has not been developed as a systematic and widespread approach. Hopefully this chapter will catalyze work along these lines. Second, the cations that are magnetic (i.e., PM rather than DM) are also those, in general, that have multiple valence states (Table 1), for obvious chemical reasons. Such multiple valence states are important in the Earth sciences. They allow various surface reactions such as oxidative precipitation and reductive dissolution in sediment profiles, and several biomediated reactions. They record redox conditions of the melt during petrogenesis. They cause characteristic rare earth element (REE) anomalies that are diagnostic of weathering and pedogenic activity. For these and other reasons, it is important to be able to accurately quantify valence state populations in minerals of interest. Table 1 suggests that magnetic measurements may be an accurate and convenient way to do this. This is indeed the case and it has been exploited in magneto-chemistry (Carlin 1986) but not in the Earth sciences.

MEASUREMENT METHODS FOR MINERAL MAGNETISM

Several methods either directly measure the spontaneous or field-induced macroscopic magnetic moment on a sample or the magnitudes and orientations of microscopic local ionic magnetic moments or are particularly sensitive to various properties of moment-bearing cations or provide some physical property that has a strong interplay with a sample's magnetism. These methods can be classified under the usual categories of microscopy, spectroscopy, diffraction, and bulk properties and are far too numerous to even name here. See for example the various monographs on measurement methods for solid materials (American Society for Metals 1986, Flewitt and Wild 1994, Hawthorne 1988, Lifshin 1992, 1994; Cahn and Lifshin 1993, Sibilia 1996), a recent series of articles on specifically magnetic methods (McVitie and Chapman 1995, Qiu and Bader 1995, Smith and Padmore 1995), and the recent article by Pietzsch et al. (2001) who describe the most advanced magnetic nanoscopic imaging methods. New methods are being devised continuously, involving both large facilities providing synchrotron radiation and

specialized table top apparatus. I will concentrate only on the main well established methods that are likely to be used in most materials magnetism laboratories and that are applicable to broad classes of materials and to various sample types. As is often the case, the usefulness of the latter methods is limited more by the researcher's mastery of the underlying theory than by access to the instruments.

Constant field (dc) magnetometry

The first measurement method that is the main tool in mineral and materials magnetism is constant (dc) field magnetometry. The constant field magnetometer allows one to measure the net magnetic moment on a powder or oriented single crystal or oriented textured sample, at a given measurement temperature and at a given value of a constant and uniform applied magnetic field. The measured magnetization, M, is the sample moment divided by the sample volume. One can also define a measured moment per weight by dividing M by the sample's mass density, ρ. Two popular and comparable instruments for bulk samples of nanomaterials are the vibrating sample magnetometer (VSM) and the superconducting quantum interference device (SQUID) magnetometer. Typically, the measurement temperature can be varied between 4.2 K (or as low as 1.5 K by pumping on the liquid helium reservoir) and RT (or up to ~1000°C with a furnace attachment). The field can be varied through both polarities up to some maximum magnitude that is typically 1 T (10 kG) for an electromagnet or up to 10 T or more for a superconducting magnet. Measurement programs usually involve temperature cycles at fixed field values and field cycles at fixed temperatures. The most common fixed temperatures for field cycles (called hysteresis cycles) are liquid helium temperature (LHT = 4.2 K), LNT, and RT.

The measurements are often sensitive to the magnetic and thermal history of the sample. Remanence may be induced by quenching in a large field, followed by turning off the field and measurement as a function of increasing temperature, at some set heating rate. The resulting curve is called a thermoremanent magnetization (TRM) curve. In rock magnetism, one typically starts at RT, from the natural remanence or from an applied field induced remanence, and one measures as the sample is heated. A common cycle in materials science is to first perform a zero field quench (ZFQ), followed by turning on the applied field to then measure the field warming (FW) curve as a function of increasing temperature, followed by a field cooling (FC) curve back down to the initial cryogenic temperature. In all such measurement cycles, it is important to remember that the measurement in general depends on the heating and cooling rates, waiting times during actual measurements, and any waiting times during magnetic field applications. The latter effects arise from all the physical processes that occur on time scales that are comparable to or larger than the measurement time. Another important measurement schedule is to measure the sample's magnetic moment as a function of time, at fixed temperature and applied field, either following a specific treatment or not. Such measurements performed as functions of time are referred to as relaxation measurements and allow one to obtain the magnetic viscosity, S, defined as $S(T,H) = dM(T,H)/d\ln(t)$, the logarithmic time derivative of M. S is often a constant, as predicted by domain wall motion theory (Street and Woolley 1949) and under common assumptions for ensembles of SP particles (Néel 1949a), but also often depends on time, especially with interacting small particle systems (see below).

The measured sample's magnetic moment is the net spontaneous or induced moment arising from a vector sum of all the microscopic DM, PM, electronic, and nuclear contributions. Nuclei can have permanent magnetic moments, although they are much smaller than electronic moments, $\mu_N/\mu_B \sim 10^{-3}$, and have much weaker interactions with each other and with electronic moments. For our purposes, the sample's magnetic

moment is essentially a vector sum of all the PM moments of moment-bearing cations in the sample, since the nuclear and DM contributions are much smaller and can be reliably accounted for and we are ignoring metallic and superconducting samples. The vector sum of interest is actually a vector sum of local thermal averages of cation moments, since each cation moment has rapid fluctuations in orientation and an average orientation and value that depend both on its local environment and the local field that it is subjected to. We must therefore distinguish between the cation moment magnitude, μ_i, of cation at site-i in the material and the local thermal average moment at site-i, $<\mu_i>_T$, where $< >_a$ signifies averaging of type-a and bold face type is used to represent a vector quantity. Table 1 gives nominal values of the spin component of the ionic moment magnitude, that can also contain an electronic orbital component and, in general, a component from the local polarization of conduction electrons.

With measurements that have characteristic measurement times that are comparable to or shorter than the characteristic cation moment fluctuation time (typically, 10^{-6} to 10^{-12} seconds, depending on the system), the local average cation moments are not directly relevant in interpreting the measurements. This is clearly not the case with classic magnetometry, where the measurement time (per sample moment evaluation) is typically 10 to 0.1 seconds. The power of magnetometry comes from the fact that the individual average moments and their vector sums in a given sample of known structure can be calculated from first principles (quantum mechanics and statistical mechanics) and compared to the intricate field and temperature dependent curves that are collected. As it turns out, various sample features (type of inter-moment interactions, domain structure, size, shape, chemical order, etc.) give rise to dramatically different and often characteristic features in the measured and calculated curves. We will therefore spend some time developing the underlying theoretical framework.

Recent examples of key theoretical and laboratory studies of constant field magnetometry applied to nanoparticles can be divided into the following categories: M(T) temperature cycles (El-Hilo et al. 1992a, Vincent et al. 1996, Sappey et al. 1997a, Friedman et al. 1997, Vaz et al. 1997, Spinu and Stancu 1998, Stancu and Spinu 1998, Ezzir et al. 1999, Chantrell et al. 1999, 2000; Bodker et al. 2000), M(H) field hysteresis cycles (Jiles and Atherton 1984, Victora 1989, Ignatchenko and Mironov 1991, Roberts et al. 1995, Zhu 1995, Tauxe et al. 1996, Vaz et al. 1997, Spinu and Stancu 1998, Stancu and Spinu 1998, Nowak and Hinzke 1999, Basso et al. 2000, Schmidt and Ram 2001), and M(t) viscosity or relaxation measurements (Mullins and Tite 1973, Aharoni 1992, Barbara et al. 1994, Balcells et al. 1997, Basso et al. 2000). In all cases, the starting point should be the remarkable early work of Néel (1949a).

Alternating field magnetometry (ac susceptometry)

The other most used classic magnetic measurement method is alternating field (ac) magnetometry. The derivative of a measured sample moment with respect to applied field magnitude, H, divided by the sample volume, is called the susceptibility ($\chi = \partial M/\partial H$) and it is called the initial susceptibility (χ_o) when evaluated at zero applied field. Alternating field magnetometry is, under certain circumstances, a method of directly measuring the susceptibility. One applies a sinusoidally varying small amplitude field (the driving field) to the sample held at some constant measuring temperature and in a constant and uniform field (often zero or unscreened Earth's field). One then measures the amplitude of the resulting sinusoidally varying component of the sample moment that is induced by the driving field and its phase shift with respect to the driving field. This measurement is particularly easy to implement experimentally, using lock-in amplifier technology. At ambient temperatures and without applied constant fields, it is the basis of many routine laboratory and in the field measurements in rock and environmental magnetism. In

advanced mineral magnetism applications, the experimenter not only controls measurement temperature and the magnitude of the applied constant field (typical ranges 1.5-1500 K and 0-10 T, as in constant field magnetometry) but also: the orientation of the driving field with respect to the constant field, the amplitude of the driving field (typically 10^{-3} to 1 mT), and, most importantly, the frequency of the driving field (typically 1 to 10^4 Hz). In many applications, the measurement frequency is slow compared to the internal equilibration times such that there is no phase shift and the induced moment instantaneously follows the driving field. In this case, the susceptibility is given by dividing the volume normalized induced moment amplitude by the driving field amplitude and is the same as would be obtained from the slope of the M versus H curve. In many other applications, the measurement time is comparable to or shorter than a relevant characteristic time in the sample, a phase shift is observed, and one must treat the measurement as a spectroscopic measurement of response versus probing frequency. This gives much information about the sample and its magnetism that cannot be obtained by constant field magnetometry or easily by any other method. For example, one can extract the distribution of magnetic particle sizes or the distribution of excitation volumes related to domain wall motion or the temperature and field dependencies of supermoment fluctuation times, etc., depending on the system.

The susceptibility described above is also called the linear susceptibility because, in a Taylor expansion of M(H) about the applied field value, it is the coefficient of the term that is linear in H. In this way, higher order susceptibilities can be defined and measured. The higher order (non-linear) susceptibilities can provide information that is not contained in the linear term alone. This information has turned out to be vital in systems of interacting clusters or particles, such as ensembles of magnetic nanoparticles, canonical spin glasses and cluster spin glass systems (see below).

Examples of key theoretical and laboratory studies of alternating field magnetometry applied to nanoparticles are provided by Néel (1949a), Mullins and Tite (1973), Gittleman et al. (1974), Raikher and Shliomis (1975), Aharoni (1992), Sadykov and Isavnin (1996), Djurberg et al. (1997), Garcia-Palacios and Lazaro (1997), Jonsson et al. (1997), Raikher and Stepanov (1997), and Svedlindh et al. (1997). Much of the theory applies equivalently to electron spin resonance (see below) which is an ac susceptibility measurement at much higher driving frequency in which electronic transitions between spin levels are also probed. Néel (1949a) gives a particularly lucid description of alternating field measurements of nanoparticles and of the theoretical relationships with constant field magnetometry measurements.

Neutron diffraction

The next most important method has played a pivotal role in the development of our understanding of magnetism in materials. It has been as important in magnetism as X-ray crystallography has been in mineralogy. Neutron diffraction not only probes nuclear positions but also magnetic structures, by virtue of the neutron's intrinsic spin magnetic moment and its interaction with the atomic magnetic moments of materials. The magnetic Bragg peaks can be analysed to give both the magnitudes and orientations of the cationic moments in the magnetic unit cell. Such measurements provided the first experimental proofs of Néel's proposal of unusual magnetic structures, now well known as antiferromagnetic (AF) and ferrimagnetic (FI) structures (next section). Neutron diffraction is the main method for obtaining magnetic structures and these structures are as diverse as are crystal structures in X-ray diffraction.

Because the measurement time in neutron diffraction (the time that an individual neutron interacts with the diffracting region) is very short ($\sim 10^{-13}$ s), the measurement is

faster that most SP reversal events such that a true intra-particle average magnetization can be measured. In this way, the true magnetic ordering temperature of superparramagnetic ferrihydrite was recently measured for the first time and its AF magnetic structure was demonstrated (Seehra et al. 2000). In another study, Lin et al. (1995) used polarized neutrons to demonstrate the presence of noncollinear surface moment disorder in synthetic colloidal $CoFe_2O_4$ particles. Small angle neutron scattering (SANS) allows one to probe magnetic correlations on length scales in the range 1 to 10^3 nm, which is ideal for nanomaterials (Bacri et al. 1993, Upadhyay et al. 1993). One can also perform magnetic inelastic neutron scattering (INS) which probes the densities of state of the magnetic excitations, much as nuclear INS probes the phonon densities of state. Using quasi-elastic neutron scattering, Gazeau et al. (1997) were recently able to resolve the magnetic ion and supermoment excitations in 4 nm synthetic maghemite nanoparticles.

Mössbauer spectroscopy

Another important magnetic measurement method, that is particularly relevant to the Earth sciences because of the importance of Fe, is ^{57}Fe Mössbauer spectroscopy (Rancourt 1998). This hyperfine nuclear spectroscopy is a probe of atomic magnetism by virtue of the fact that the nuclear hyperfine magnetic field has a large component that is strongly coupled to the local cationic moment on the probe nucleus. Indeed, normally its largest component is the contact electron spin term, that arises and is proportional to the total s-electron spin polarization at the nucleus, which, in turn, in insulators, is predominantly caused by s-d spin-spin interactions between the filled s shells and the partially filled 3d shell (or net cation moment). Other hyperfine parameters are also measured that give local structural and chemical information related to the immediate coordinating environment of the probe. In the Earth sciences, the method is commonly used to measure crystallographic or coordination site populations of Fe^{2+} and Fe^{3+} or site- and valence-state-specific distributions of local distortion environments, in Fe-bearing minerals (Rancourt 1994a,b; Rancourt et al. 1994, Lalonde et al. 1998).

The measurement time in ^{57}Fe Mössbauer spectroscopy is the time during which the γ-ray interacts with the ^{57}Fe nucleus to cause a transition between the ground state and the first excited state. This time is equal to the life time of the first excited state, $\sim 10^{-8}$ seconds. The so-called static limit, in which the usual multiplets (singlets, doublets, sextets, and octets) of Lorentzian lines are observed, occurs when all the characteristic fluctuation times of the relevant hyperfine interactions are much smaller or much larger than the measurement time. Since the usual fluctuations in bulk materials (electron residence times << atomic vibrational times << atomic magnetic moment orientation fluctuation time) are much faster than the measurement time, the static limit is quite common. The so-called dynamic or relaxation case, on the other hand, is not uncommon. Characteristic fluctuation times in a broad range centered on $\sim 10^{-8}$ seconds occur in many circumstances, including: at temperatures near structural or magnetic or other phase transition temperatures, when atomic diffusion hopping times are in this range, when valence fluctuations ($Fe^{3+} + e^- = Fe^{2+}$) occur with these characteristic times, and many cases where structural constraints, such as reduced dimensionality of the bonding network or a particular microstructure, are associated with relatively slow magnetic excitations. This is particularly true with nanophase materials and nanoparticles, where (non-Lorentzian) relaxation lineshapes are as common as their bulk Lorentzian multiplet counterparts. One must therefore analyse the data in the context of a general lineshape model that allows the full continuum of possible characteristic times. This can directly give measured microscopic times (in the range 10^{-6} to 10^{-10} seconds) that cannot easily be obtained by other methods (Rancourt 1988, 1998).

Mössbauer spectroscopy is also able to give local moment orientations, with respect to the crystalline lattice, or the correlations between moment orientations and local distortion axis orientations in a chemically disordered or amorphous material. This arises from the interplay between the structural (electric field gradient) hyperfine parameters and the magnetic hyperfine parameters. In this way, the spin flop Morin transition of hematite, for example, is easily detected and characterized (e.g., Dang et al. 1998). The noncollinear magnetic structures of nanoparticles can also be characterized.

Finally, because of the complexity of magnetic nanomaterials and because of the intrinsic difficulties related to spectral modeling, there are probably many incorrect interpretations of the Mössbauer spectra of nanoparticles (as there already are of bulk complex minerals). I discuss this further below where I argue that Mössbauer spectroscopy will not attain its full potential in this area until a significant shift in paradigm is achieved.

Electron spin resonance

One final method that is worth mentioning in this brief and selective overview is electron spin resonance (ESR). This is a resonance absorption spectroscopy, involving transitions between the applied-field Zeeman split ground state level of a PM center. Selection rules are such that not all cation species of a given PM element (e.g., Fe, Mn, V, Cr, Table 1) are detected, thereby providing a sensitive probe of valence state. Again, thanks to hyperfine and fine structure (here on electronic energy levels rather than on nuclear levels), the various ESR active cations and their local bonding environments can be resolved and quantified. The method is characterized by a remarkable sensitivity, easily allowing dilute solutions and rare impurities to be studied. For example, PM centers corresponding to electrons trapped in radiation-induced defects in quartz are routinely used to date sand (Grun 2000) and a similar method allows one to date fossil teeth (Oka et al. 1997).

The sensitivity of ESR is, in a sense, a weakness because in samples with large concentrations of PM cations (whether ESR active or not) inter-moment interactions cause resonance line broadening and associated loss of hyperfine and fine structures. On the other hand, the latter broadening can be used to study concentrated magnetic materials since it has a large dependence on the degree and type of spontaneous magnetic order. It is also sensitive to the superparamagnetism of magnetic nanoparticles (Dubowik and Baszynski 1968, Sharma and Waldner 1977, de Biasi and Devezas 1978, Griscom et al. 1979, Sharma and Baiker 1981, Raikher and Stepanov 1995b, Berger et al. 1997, 1998; Gazeau et al. 1998). In a natural sample that combines concentrated and dilute magnetic materials, the resulting ESR signal is a simple linear superposition of all material-specific signals, thereby allowing each to be studied and quantified separately. I expect ESR to be rediscovered in the near future, as a valuable probe in environmental science.

TYPES OF MAGNETIC ORDER AND
UNDERLYING MICROSCOPIC INTERACTIONS

Intra-atomic interactions and moment formation

Strong intra-atomic electron-electron interactions, in the presence of the central forces due to the charged nucleus and as perturbed by the crystalline environment, are such that a certain net atomic (i.e., cationic) magnetic moment will result, depending on the total number of atomic electrons. This leads to the DM and PM cations discussed above in the context of Table 1. For a given number of atomic electrons, these intra-atomic forces are sufficiently strong to establish a permanent magnetic moment

magnitude having a value that is little affected by either applied magnetic fields, up to the largest fields that are present in nature or the laboratory, or ambient temperatures, to far beyond melting and vaporization temperatures. As a result, we treat the cationic moments as permanent vector magnetic dipole moments having fixed magnitudes (represented by vector operators in quantum descriptions of solid state magnetism). On the other hand, nothing intra-atomic imposes a preferred orientation of the cationic moment. Therefore, in the absence of extra-atomic aligning influences the cationic moment experiences random fluctuations in orientations, induced by the ambient bath of relevant thermal excitations, leading to a thermal or time average of exactly zero ($<\mu_i>_T = <\mu_i>_t = 0$). This is the PM state of a material having non-interacting PM moments. An instantaneous snap shot of the PM state (in zero applied field) would have each cationic moment frozen in some random direction, such that the spatial average over all instantaneous moment vectors in the large sample is also zero ($<\mu>_s = (1/N) \Sigma_i \mu_i = 0$).

Inter-atomic exchange interactions

The atoms touch and participate in bonding. As a result, there will often be inter-moment interactions that tend to align neighboring cationic moments. These interactions are of quantum mechanical origin and are much stronger that the classical dipole-dipole interactions that must act between all moments (and bar magnets). They are called magnetic exchange interactions and they are said to be ferromagnetic (FM) if they tend to make the interacting moments parallel ($\uparrow\uparrow$) and AF if they tend to make the interacting moments antiparallel ($\downarrow\uparrow$). Because they arise from orbital overlap and electron sharing, they tend to be short range, unlike the long range dipole-dipole forces that are a direct consequence of electromagnetism. Exchange interactions are sufficiently strong to align cationic moments against the randomizing influence of temperature and are the cause of magnetic order and the spontaneous magnetic structures mentioned in the previous sections.

When the exchange directly arises from the overlap of nearest neighbor (NN) atoms it is called direct exchange. The exchange interaction between moment-bearing (PM) cations can also be propagated via a shared coordinating (DM) anion, such as O^{2-}, OH^-, Cl^-, and F^-. This is called superexchange and is the relevant exchange interaction in oxides, hydroxides, and silicates. Note that one consequence of superexchange is that the magnetism of a mineral can be dramatically affected by its anion chemistry, without changing anything else. In metals, the exchange interaction can be propagated via the conduction electrons. This type of exchange is usually referred to as Ruderman-Kittel-Kasuya-Yosida (RKKY) exchange and it can be of longer range than just NN. The exchange interactions in meteoritic Fe-Ni alloys (e.g., kamacite, taenite) are visualized as a combination of direct and conduction electron mediated exchange.

Magnetic order-disorder transitions

The magnetic structures (or spin structures or moment configurations) that are caused by the exchange interactions and, to a lesser extent, by dipole-dipole interactions and spin-orbit coupling effects that I describe below, are remarkably varied and can involve magnetic unit cells many times larger than the crystallographic unit cells or magnetic structures that are incommensurate with the underlying crystalline frameworks. I next describe the more common magnetic structures, including those relevant to magnetic minerals and nanoparticles. Examples are illustrated in Figure 1. These structures typically occur at low temperatures and persist up to some magnetic ordering temperature that is characteristic of the material (but is affected by particle size), above which the system is in a PM state (Table 2). As temperature is increased towards the magnetic ordering temperature, the magnetic structure is usually preserved (or a
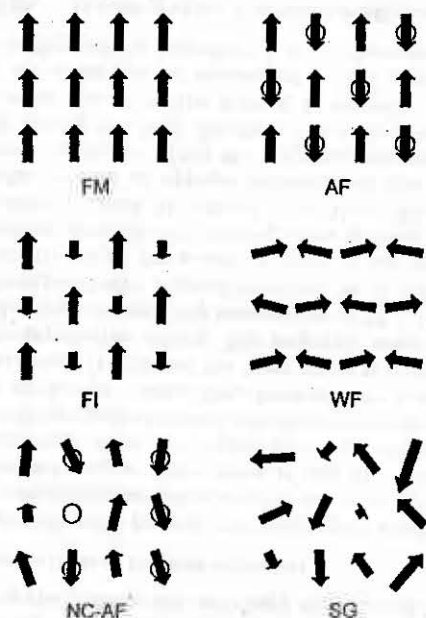
Figure 1.

Classic spin structures corresponding to:

    ferromagnetic (FM)
    anti-ferromagnetic (AF)
    ferrimagnetic (FI)
    weak ferromagnetic (WF)
    noncollinear antiferromagnetic (NC-AF)
    spin glass (SG)

arrangements of the thermal average cation magnetic moments. In the AF and NC-AF structures, the down sublattices are identified by open circles. Only the simplest two-sublattice cases are illustrated. In the NC-AF example, a cation vacancy (or substitution with a DM cation) on the down sublattice is illustrated, which gives rise to a net uncompensated sample moment.

transition to another magnetic structure can occur at a magnetic structure transition temperature) and each local average moment generally decreases continuously, while maintaining its orientation, up to the magnetic ordering temperature, above which it is zero, in the absence of an applied field.

Collinear and noncollinear ferromagnetism

When the magnetic structure corresponds to all the moments being aligned in the same direction, the ordered magnetic structure is said to be FM and we speak of ferromagnetism (Fig. 1). The magnetic ordering temperature in this case is called the Curie point or Curie temperature. This is the magnetic structure of the FM first row transition metals: body centered cubic (BCC) α-Fe, hexagonal Co, and face centered cubic (FCC) Ni. In a FM material, all moment-bearing cations need not be the same but all moments (of different magnitudes and different local thermal averages) must point in the same direction, to within allowed small site to site deviations of the average direction. When there are no such deviations, one can explicitly refer to a collinear ferromagnet. Or, if one wishes to stress the importance of small deviations that occur in a particular material, one can use the term noncollinear (NC) ferromagnetism. NC-FM structures occur in the presence of substitutional (chemical) disorder and positional (strain or structural) disorder. They appear to be common magnetic structures in FM alloys, especially amorphous FM alloys (Coey and Readman 1973a, Coey 1978, Ferchmin and Kobe 1983). An important defect that can lead to NC magnetic structures is the surface of a nanoparticle, via the mechanism of surface pinning that I describe below. Also, some FM alloys have a relatively small population of cationic moments that point opposite to the main FM direction. This is the case with the well known (synthetic and natural) Fe-rich FCC Fe-Ni alloys (e.g., Invar, taenite), where it has been referred to as latent antiferromagnetism.

Collinear and noncollinear antiferromagnetism

The magnetic structure that is most common in the oxides arises from the fact that the superexchange bonds are AF in these materials and is referred to as the AF structure (Fig. 1). Here, the identical moment-bearing cations are typically divided into two interpenetrating sublattices that have opposite moment orientations. In Figure 1 the lattice sites of the sublattice with down moments are identified by open circles in the AF structure. The other sublattice is populated with up moments. As a result of this arrangement, the net spontaneous macroscopic moment on the sample and the corresponding magnetization are zero, just as they would be in DM or PM materials. Historically, this made the recognition of antiferromagnetism difficult. The magnetic ordering temperature of an AF material is called the Néel temperature.

As is the case with the FM state, the ideal AF structure that occurs in bulk ordered crystalline compounds has perfectly collinear moments, all aligned along the same axis, but NC-AF structures typically occur in nanophase, chemically disordered, and poorly crystalline materials. The NC-AF structure is illustrated in Figure 1. The down sublattice is again identified by open circles. The thermal average moment sizes (lengths of arrows, Fig. 1) vary from site to site, as does the degree of noncollinearity. In this example (NC-AF, Fig. 1), a vacancy of one of the down sublattice moments is also illustrated. Such a magnetic vacancy, can either be due to a true cation vacancy or to a chemical substitution of a PM cation by a DM cation (e.g., Al^{3+} for Fe^{3+}). The type of NC-AF structure illustrated in Figure 1 is the relevant starting point for describing important environmental nanomaterials such as the hydrous ferric oxides (HFOs) and the manganese hydroxides. It is a key feature of nanophase AF materials that the two magnetic sublattices on a given particle are not usually equally populated. This gives rise to a residual net magnetic moment per particle (i.e., the supermoment) that is much larger than one would expect from an AF structure.

Ferrimagnetism

The magnetic structure of the most prominent natural magnetically ordered material, magnetite, is a ferrimagnetic (FI) structure (Fig. 1). FI magnetic structures are similar to AF structures except that the moments on the different sublattices do not cancel each other completely. For example, one of the two sublattices (the down sublattice in Fig. 1) is populated by a cation species having a smaller moment magnitude than the moment magnitude of the cation species on the other sublattice. As a result, there is a large net magnetic moment per sample and large corresponding magnetization, in the direction of the moments of the dominant sublattice. Only FM and FI materials are "magnetic" in the sense that only these two magnetic structures give rise to net magnetizations that are sufficiently large for the material to be noticeably affected by an ordinary bar magnet and only these materials are used to make permanent magnets for various applications.

Whereas in ideal FM and AF compounds having only one type of magnetic cation on one type of crystal site the evolution with changing temperature of the average local moment is the same for all moments, in FI materials the temperature dependence of one sublattice magnetization (i.e., net average magnetic moment on a given sublattice divided by sample volume) can be quite different from that on the another sublattice. As a result, compensation points can occur at temperatures where a dominant sublattice becomes subordinate and vice versa (Néel 1955, Kahn 1999). In magnetometry experiments, this can lead to unusual situations where large measured sample moments occur in the direction opposite to the applied field, as temperature is varied.

As with FM and AF materials, the FI structure can be noncollinear and can include imperfections such as vacancies, chemical disorder of the magnetic cations, exchange

bond disorder from superexchange anion substitutions, and distributions of exchange values from strain distributions of inter-ionic distances. This, in particular, is the case with natural magnetite-titanomagnetite-maghemite materials.

Weak ferromagnetism, canted antiferromagnetism

At ambient temperature, the stable surface environment end-product of Fe dissolution and oxidation and the principle iron ore, hematite, α-Fe_2O_3, has a magnetic structure of the weak ferromagnetic (WF) or canted antiferromagnetic type that is illustrated in Figure 1. This structure consists of an AF starting point, with exact cancellation of the two sublattice magnetizations, in which a small moment canting of both sublattices leads to a small non-compensated net residual moment. In Figure 1, the underlying AF structure has horizontal moments pointing to the left in one sublattice and to the right in the other and the canting involves counter rotations of the two sublattice magnetizations such that a net up-pointing vertical moment results.

From the perspective of the microscopic theory of magnetism, WF magnetic structures are quite unusual in that the canting arises from the combined effects of superexchange and spin-orbit coupling to the crystalline lattice (Dzyaloshinsky 1958, Moriya 1960). This coherent canting must be distinguished from the local noncollinear effects that arise from disorder. In following the magnetization versus temperature and applied field, it is expected that both the local average moment value and the canting (of the average moment) change.

A material such as hematite, that can host a WF magnetic structure, also is able to host a classic AF structure with magnetic sublattices along a different crystalline axis. A spin flop transition, known as the Morin transition in hematite, can occur where the AF axis abruptly changes from one crystal orientation to another, at a certain transition temperature. Such spin flop transitions are sensitive to sample features such as impurity chemistry and particle size and shape, as discussed below (Dang et al. 1998).

Metamagnetism of layered materials

Materials with layered crystallographic structures, such as layer silicates, layered double hydroxides, layered chlorides, and graphite intercalation compounds (GICs), often have layered magnetic structures arising from intra-layer exchange interactions being much stronger than inter-layer exchange interactions. Indeed, often there are no superexchange paths between the moment-bearing cations in different layers and there are no exchange interactions between the layers. In many cases the intra-layer superexchange is FM and the layer plane is a magnetic easy plane, as determined by magneto-crystalline effects. The magnetic structure that then results is that of annite below its magnetic ordering temperature of 58 K (Rancourt et al. 1994), in which planes of ferromagnetically aligned moments lie in the ab-plane and are stacked antiferro-magnetically along the c-axis. In general, the in-plane ferromagnetism is due to FM superexchange and the AF stacking is due to some combination of dipole-dipole coupling and a relatively weak AF inter-plane exchange. Because the inter-plane coupling is weak, there often occurs an applied field-induced spin flop transition, at attainable in-plane laboratory fields, in which the magnetic structure changes from AF stacking to FM stacking, along the field direction. The term metamagnetism is used in relation to the existence of this spin flop feature, in materials that have in-plane ferromagnetically aligned moments and AF stacking of the FM planes in zero field. In Fe-rich biotites, the LHT spin flop field is typically 0.1–0.2 T (Rancourt et al. 1994).

Spin glasses, cluster glasses, and multi-configuration states

There are many other magnetic structures, in addition to the above described

classical FM, AF, FI, WF, and metamagnetic structures, that include: decoupled sub-lattices having various relative sublattice magnetization orientations and different sublattice-specific magnetic ordering temperatures, helical spin structures, and static spin density waves. Elemental Cr, for example, has a particularly complicated ordered magnetism and helical structures are common in rare earth element compounds. Non-classical magnetic structures may also be present in many important Fe-bearing rock forming minerals that have not been extensively studied to low temperatures. At present, such structures can be considered rare in Earth materials. One exotic magnetic structure, however, has often been suggested to occur at low temperatures in minerals and should be considered here: the spin glass (SG) magnetic structure (Binder and Young 1986, Chowdhury 1986, Fischer and Hertz 1991).

I stress that this magnetic structure represents a theoretical end-point that, in my opinion, has never been conclusively observed in a real material, synthetic or natural. The SG state is represented in Figure 1 and has the following defining ingredients: (1) random orientations of the average local moment vectors, and (2) some statistical distribution of average local moment values. That is, the SG state is a static configuration of average moments that is similar to an instantaneous snap shot of the ideal PM state, except that in a crystalline PM compound with only one moment-bearing cation species all local moments have equal values. The SG state can equally well be postulated to occur in amorphous or crystalline materials. It is believed to be the result of magnetic frustration, in which the moment configuration is established by competing exchange interactions. The required frustration has been described as occurring either from a distribution of exchange values, including both negative (AF) and positive (FM) values, or from a geometric effect called magnetic topological frustration whereby the exchange bond preferences cannot all be satisfied simultaneously because of the particular exchange bond network architecture.

Crystalline and amorphous materials that contain small concentrations of one or several moment-bearing cations, such as Fe-poor silicates, normally display a low temperature alternating field magnetometry peak or cusp having a magnitude and position that are sensitive to the driving field frequency and to the size of the constant applied field. An analogous cusp occurs in the low-field ZFQ-FW constant field magnetization curve, having a magnitude and position that is sensitive to the applied field magnitude. These systems are generally believed to have SG order below the cusp temperature and the cusp temperature is often associated with a SG transition temperature, at which the system is assumed to become PM on increasing the temperature. It is also possible to interpret these phenomena in terms of the response of correlated clusters of moments, without reference to SG formalism (e.g., Continento and Malozemoff 1986). Indeed, systems of FM, AF, and FI nanoparticles display very similar alternating and constant field responses (discussed below).

The SG picture has a life of its own and when disordered multi-component FM materials are observed to have unusual features at temperatures below their Curie points, researchers often attempt to describe their observations in terms of a reentrant SG phase. Such interpretations should be considered tentative and have not provided much insight into the mechanism(s) for the unusual behaviors. A true understanding will emerge as microscopic models include more and more realistic features and directly deal with simulating the actual measurements, rather than via attempts to map an enticing simple theoretical picture onto complex real materials. Realistic features that are not usually taken into account include: the effects of dipolar interactions (last subsection), domain wall motion, chemical clustering on several length scales, coexistence of several moment-bearing cation species, and coexisting correlated distributions of local ionic

anisotropy (next subsection), exchange strengths and signs, and cation species and positions. Nonetheless, the extensive theoretical musings related to SG magnetism seem to have had applications in several other areas, such as biology, neural networks, and machine learning (e.g., Chowdhury 1986, Fischer and Hertz 1991, Stein 1992). This stems from an underlying theoretical difficulty of dealing with systems that have large numbers of energetically equivalent state configurations.

Systems of randomly oriented magnetic nanoparticles randomly dispersed in a supporting medium or matrix and that interact via dipole-dipole forces (last subsection) are systems having several energetically equivalent supermoment orientational states, at given temperatures and applied fields. As such, it is relevant to compare their magnetic behaviors with both the observed behaviors of canonical SG systems (dilute magnetic alloys such as MnCu) and the theoretical predictions from overly simple SG models. This has lead to a productive examination of the effects of dipolar and other inter-particle interactions in synthetic nanoparticle model systems that is reviewed below. Hopefully, this will in turn motivate the development of more realistic theoretical models of disordered dipolar systems.

Spin-orbit coupling and magneto-crystalline energy

Spin-orbit coupling is the intra-ionic coupling between an ionic shell's electronic spin angular momentum and its electronic orbital angular momentum. Since the ionic moment is largely due to electronic spin and since the orbitals participate in bonding, the spin-orbit interaction effectively couples the ionic magnetic moment to the underlying crystalline lattice or amorphous structure. For this reason, there can be preferred or easy directions along which the moments prefer to align. These directions have the symmetry of the crystallographic site or local bonding environment such that they cannot be the cause of magnetic order in a given vector direction but only define easy and hard magnetic axes. The energy required to turn an ionic moment from an easy direction to a hard direction is called the local magneto-crystalline energy or magneto-crystalline constant, K. This is the phenomenon that binds a given magnetic structure to the underlying crystal structure.

In most cases of interest K is much smaller than the NN magnetic exchange constant, J, such that an applied field will typically cause coherent rotations of exchange correlated moments rather than moment flips that would break exchange bonds. For example, when a sufficiently large field is applied to a classic AF structure along the easy axis of sublattice magnetizations, the system responds by a spin flop in which both sublattices go to a hard direction, perpendicular to the field, while preserving their AF relation and allowing a small WF rotation to produce an induced moment along the field. The field at which this occurs is called the spin flop field. It is determined by K, J, and the magnitude of the ionic moment, and it is temperature dependent. In a fixed sample of FM material, K determines how easy it is for an applied field to cause a coherent rotation of the FM magnetization along the field direction. K also plays a key role in determining the domain wall width and the ease with which domain walls can be moved by a driving applied field (next subsection). FM materials with small K are called shoft (Permalloys are good examples) and FM materials with large K are called hard. Hard materials are required for permanent magnets. Soft materials are required for transformer cores.

Electronic shells that have all orbitals equally populated, such as filled and half filled shells, have zero net total angular momentum. As a result, they have no spin-orbit coupling of the moment to the underlying crystal structure. This is a major difference between ferric and ferrous cations: Fe^{3+} ($3d^5$) has K ~ 0 whereas Fe^{2+} has a significant K, that in the flattened octahedral environment of micas, for example, causes a net

preference for in-plane alignment and a larger in-plane PM susceptibility. In nanophase materials, near-surface distortions can cause deviant magneto-crystalline axes and altered K values, leading to surface moment pinning and noncollinearity.

Dipole-dipole interactions and magnetic domains

Any two magnetic dipole moments, μ_1 and μ_2, whether macroscopic or microscopic, have a dipole-dipole interaction energy that is given by the classical electromagnetic expression:

$$U_{dd} = (1/r^3) [\mu_1 \cdot \mu_2 - 3 (\mu_1 \cdot u_r) (\mu_2 \cdot u_r)] \qquad (1)$$

where r is the distance between the two moments and u_r is a unit vector that points along the straight line joining the two moments. The strength of this interaction falls off as $1/r^3$ and it does not have a limited range as is the case with exchange interactions. In astrophysics, for example, these forces may play a significant role in plantesimal accretion (Nuth and Wilkinson 1995). For ionic moments and typical inter-ionic separations in solids, U_{dd} is much smaller than typical exchange bond energies. As a result, dipole-dipole interactions play a minor role in establishing the magnetic structures described above. However, dipolar interactions occur between all pairs of moments and extend over large distances such that the dipolar fields due to large regions of ordered moments do become quite large. The dipolar field of a bar magnet is an example of this phenomenon.

Because of the first term in Equation (1), dipolar forces tend to advantage antiparallel configurations but in a FM or FI material, for example, the stronger exchange forces must prevail at short distances. The compromise (i.e., the situation that minimizes the system's total free energy) involves large regions of ordered moments that organize their respective magnetization directions in antiparallel and canted arrangements that mostly cancel any net sample moment. The regions of given directions of magnetic order are called domains and a macroscopic sample in the absence of an applied field will have a domain structure that results in no net sample moment, as is the case with a piece of demagnetized iron. The magnetic structures (FM, AF, FI, etc.) described above are intra-domain structures whereas the sample also has a magnetic microstructure or domain structure.

The boundaries between domains are called domain walls. These walls must involve a rotation of ionic moments from one domain orientation to the other and therefore constitute high energy defects. The domain wall thickness is also determined by free energy minimization and arises from a balance between exchange energy J and magneto-crystalline energy K. The domain structure of a macroscopic sample is difficult to calculate because of the long range nature of dipole-dipole forces and it depends on the size and shape of the sample. It is also sensitive to any applied field, including stray fields from nearby FM or FI samples.

In magnetizing a FM or FI material, it is initially easier, as applied field is increased, to move domain walls in such a way as to favor domains that are more aligned with the applied field. In a bulk material, this will generally be the dominant process in the initial rise of a hysteresis curve. Only domain wall pinning by inclusions and defects retards this process. The next step is typically to work against the magneto-crystalline energy in order to coherently rotate the magnetization of the surviving domain along the field direction, until saturation is reached. In a FI material, a spin flop with continued further rotation or a spin flip of the subordinate sublattice can occur at higher fields.

An AF sample may also have domains, that are defined in terms of how the up and

down sublattices are assigned to the two underlying crystallographic sublattices: as up/down = A/B or as down/up = A/B, for example. In one dimension, this situation with one domain wall in the middle would be ↑↓↑↓↓↑↓↑. Alternatively, AF domains can be defined with the AF sublattices in a given domain along any of the equivalent n-fold magnetic easy axes. These domain walls in AF materials are not imposed by dipole-dipole forces and do not represent equilibrium situations. Instead, they can be considered quenched-in defects that increase the free energy. In small AF particles, this type of domain wall can cause significant residual sample moments or can participate in reducing residual moments. Analogous domain walls tend not to occur in FI materials, unless they are accompanied by chemical ordering domain walls, of the two moment-bearing cation species on the underlying crystallographic lattice sites, as: XOXOOXOX = ABABABAB.

FM and FI nanoparticles are always single domain particles because calculated domain sizes (and indeed even domain wall widths, often) are larger than the nanoscale (Stoner and Wohlfarth 1948). Microcrystals, however, can be multi-domain and it is of great concern in rock magnetism whether magnetite particles are single or multi-domain because this dramatically changes their relevant magnetic characteristics (Dunlop 1990). With single-domain particles, the magnetic and crystallographic domains are defined by the particle itself, although particles can also be polycrystalline. In any case, dipole-dipole forces will be an important inter-particle interaction that affects the applied field response of an ensemble of magnetic particles. The other main inter-particle interaction consists of exchange bridges, via inter-particle chemical bond bridges. I review this aspect of magnetic nanoparticle systems below.

FROM BULK TO NANOPARTICLE VIA SUPERPARRAMAGNETISM

Phenomena induced by small size and sequence of critical particle sizes

Having described the exchange, magneto-crystalline, and dipole-dipole interactions and their roles in determining the magnetic nanoscale and mesoscale structures and magnetic responses to applied fields of bulk samples, I now examine how particle size affects magnetic phenomena. What happens to a sample's magnetism as one continuously decreases the sample size, from macroscopic bulk dimensions down to an individual PM cation with its inner sphere coordination shell in solution?

Magnetic domain structure. Let us start with a bulk single crystal sample of FM or FI or AF material and let us consider that we are at a temperature, T, that is much lower than the magnetic ordering temperature, T_{oB}, of the bulk material (e.g., RT in magnetite or hematite is such a temperature, Table 1). Initially, we also assume that we are in thermodynamic equilibrium at each step in the size reduction process. The system first finds itself with an ordered magnetic structure, with well defined average moments on each PM cation site. The FM and FI varieties also have equilibrium domain structures, that are consistent with any applied field and the sample's shape and orientation in the applied field. As the particle size decreases and becomes compable to equilibrium domain sizes of the bulk material (10^6 to 1 nm, depending on the intrinsic material properties), the domain configuration or domain microstructure must significantly modify and adjust itself to the new equilibrium configuration of each new size. Here particle shape also plays an important role and the surface acts as a significant perturbation. Domain wall pinning by various intra-particle and surface defects will play an important role in that domain walls will take advantage of regions that are comparable in size to or larger than the domain wall thickness (10^2 to 10^{-1} nm, depending on the material) and that lower their energies.

Multi-domain/single-domain transition. At a first critical size, $d_{SD} \sim$ equilibrium domain size, as particle size continues to decrease, the particle will become single domain (SD), rather than multi-domain (MD). This is an important boundary that dramatically affects the particle's magnetic properties. The particle no longer sustains a domain wall and now consists of an essentially uniformly magnetized grain carrying a net magnetic supermoment frozen along one of its magneto-crystalline easy directions. At $d > d_{SD}$, one could magnetize or demagnetize the particle under changing applied field simply by moving the domain wall(s), a relatively low barrier energy process. Now, the only way, at constant temperature, to change the magnetization of a sample of fixed SD particles is for the applied field to work against the magneto-crystalline barrier by causing a uniform rotation of the strongly exchange coupled moments, that is, of the supermoment. This is of course a simplified picture (the magnetization and the rotation are never perfectly uniform, as discussed below) but one that is often close enough to reality to be extremely useful. It is due to Stoner and Wohlfarth (1948).

Single-domain/superparamagnetic transition. As we continue to decrease the particle size, the SD state is stable down to the next critical size, d_{SP}, the size below which the particle becomes SP. This critical size depends strongly on both temperature and the measurement or observation time, τ_m. It is the size below which spontaneous thermally driven fluctuations of the supermoment between the particle's easy directions occur with a large enough probability to be observed within a chosen measurement or observation time. In the limit of an infinite observation time, all SD particles are SP and $d_{SP} = d_{SD}$. That is, all SD particles have true equilibrium thermal average moments of exactly zero, in zero applied field. This is an academic point but one that has large consequences in terms of how the theoretical calculations are done: one cannot simply use the methods of equilibrium thermodynamics and statistical mechanics. In rock magnetism, d_{SP} is normally given for RT and assuming the measurement time of constant field magnetometry. It is adjusted for the relevant measurement time when using alternating field magnetometry.

There has been much theoretical work, starting with Néel (1949a,b) and reviewed below, in developing valid expressions for the characteristic SP fluctuation time, τ. This is the average time one must wait before the supermoment spontaneously jumps from an initial easy direction orientation to a different easy direction orientation. The energy barrier that the supermoment must cross in doing this is denoted E_b. The simplest case of uniaxial magneto-crystalline anisotropy has been treated most frequently. In this case $E_b = nK$, where n is the number of PM cations in the particle and K is the ionic anisotropy constant. There can also be a dipolar contribution to E_b that depends on the sample shape and its magnetization. For uniaxial anisotropy and in zero applied field, the theoretical consenssus is that τ is given by:

$$1/\tau = f_o \exp(-E_b/k_BT) \tag{2}$$

where k_B is Boltzmann's constant and f_o is called the pre-exponential factor or attempt frequency. Temperature of course is in Kelvin. Various calculations obtain similar but different expressions for f_o which depends somewhat on temperature and on various material properties of the particle. Typical calculated, measured, and estimated values of the attempt frequency are in the range 10^6 to 10^{13} Hz. As I discuss below, the validity of Equation (2), first developed by Néel, has now been amply demonstrated experimentally on individual nanoparticles, not just macroscopic ensembles of particles.

One notes that d_{SP} is, in cases where Equation (2) applies, given by satisfying the equation $1/\tau_m = f_o \exp(-E_b/k_BT)$, where both f_o and E_b depend on the particle size. To a good approximation, f_o can be taken as a constant and $E_b = vK_v$ where v is the particle

volume and $K_v = nK/v$ is the (known) total anisotropy energy constant per unit volume of the material. This gives:

$$v_{SP} = (\pi/6)d_{SP}^3 = (k_B T/K_v) \ln(f_o \tau_m) \qquad (3)$$

which leaves the most difficult task of correctly evaluating the attempt frequency f_o in order to predict a correct d_{SP}. Clearly, however, temperature plays the dominant role and it is possible to block all SP fluctuations by going to sufficiently low temperatures. This is one reason that advanced mineral magnetic methods include variable temperature measurements over broad ranges from cryogenic to high temperatures. In such measurements, the concept of a SP blocking temperature, T_{SP}, is a useful one. Below this temperature, the SP supermoment fluctuations are observed to be blocked on the timescale of the measurement. T_{SP} is obtained by solving Equation (3) for temperature, given the particle volume: $T_{SP} = (E_b/k_B) \ln(f_o \tau_m)$.

Surface region size. Now, let us continue decreasing the particle size. One will next encounter a third characteristic size, d_{SR}, the surface region (SR) thermal local moment size. At this point, the particle size is equal to the SR thickness of the disorder size. At this point, the particle size is equal to the SR thickness of the equilibrium surface layer that has thermal average local ionic moments that are significantly affected (usually decreased but can be increased) by the surface in a semi-infinite slab of the material. This SR of modified average moments arises because the moment-bearing cations are coordinated via exchange interactions to fewer neighbors when at the surface than when in the bulk. That is, the magnetic interaction coordination is smaller at the surface than in the bulk. The ideal SR thickness depends on temperature, the strengths of the exchange interactions, and the crystallographic orientation of the surface (Hohenburg et al. 1975). In real particles, the SR thickness is also sensitive to: particle shape, surface roughness, surface complexed impurities, surface chemical bond relaxation and reconstruction, surface defects such as vacancies, SR compositional inhomogeneities, and particle shape orientation on the underlying crystal lattice. To understand this SR effect, consider that magnetic order is, in general, very sensitive to the degree of magnetic interaction coordination. Indeed, it can be rigorously proven that, with the usual isotropic short range exchange interactions, magnetic order cannot be sustained at any non-zero temperature in one or two dimensions, irrespective of the finite exchange strength (Mermin and Wagner 1966, Hohenburg 1967). In a finite one dimensional system (an extreme case of an elongated magnetic nanoparticle), magnetic order cannot be sustained at any temperature, irrespective of the exchange and magneto-crystalline anisotropy strengths (de Jongh and Miedema 1974, Steiner et al. 1976). When $d < d_{SR}$, the concept of a well defined supermoment breaks down, as does that of SP fluctuations. One is back to modelling individual ionic moments using equilibrium statistical physics methods (on finite systems), a task that is considerably simpler than dealing with superparamagnetism. Reviews of SR effects and their importance in dealing with real SP particles have recently been given by Kodama (1999) and Berkowitz et al. (1999). Monodisperse synthetic nanoparticles are now sufficiently small for these effects to become important (see below).

Quantum tunnelling. If we continue to decrease the particle size, we encounter a fourth characteristic size, d_{QT}, the quantum tunnelling size, that is relevant at low temperatures where thermal fluctuations become negligible. This is the size at which, at zero or near zero temperatures, the quantum tunnelling barrier is low or narrow enough to allow macroscopic quantum tunnelling (MQT) of the supermoment between its easy axis orientations, within a set measurement or observation time. Such tunnelling has recently been reported in, for example, molecular clusters of twelve PM cations (Friedman et al. 1996) and magnetic proteins (Awschalom et al. 1992). We review some of the evidence for MQT below.

Molecular clusters and N-mers. One eventually reaches the smallest sizes, where it may be more relevant to speak of polynuclear molecules and small polymer networks than of nanoparticles. Here we think of molecular clusters of only ten or so PM cations, down to the bi-nuclear molecule. Crystals of molecular clusters can be elegant model systems of identical magnetic nanoparticles (e.g., Barra et al. 1996). When one reaches these sizes, any change in cluster size (i.e., by as little as one PM cation or one coordinating anion) can cause dramatic changes in the magnetic properties. For example, with AF coupling, clusters with odd numbers of PM cations have large residual supermoments whereas clusters with even numbers of PM cations do not. Similarly, substitution of a single coordinating (i.e., superexchange) anion can change a key magnetic exchange bond from being AF to being FM or vice versa. Also, with such small clusters, the magnetic exchange bond topology becomes critical and, as with low dimensional materials, the concept of a bulk magnetic ordering temperature becomes irrelevant. This is because soliton and single-ion magnetic excitations become the energetically preferred excitations, even at the lowest temperatures, relative to cooperative magnetic excitations such as supermoment and SP fluctuations (e.g., Rancourt 1986). In this limit, therefore, depending on temperature, magneto-crystalline anisotropy, exchange strength, and exchange bond topology, the concept of a supermoment looses its usefulness because fluctuations in the supermoment magnitude become comparable to the fluctuations in supermoment direction. Often, the magnetism of molecular clusters is better described in terms of exchange-modified paramagnetism than in term of superparamagnetism (Carlin 1986).

Single coordinated cation. The smallest size of interest is the single PM cation and its inner sphere coordination shell of anions. These are the $Fe^{3+}(OH_2,OH^-)_6$ and $Fe^{2+}(OH_2,OH^-)_6$ octahedral cations of aqueous chemistry, for example. One encounters the usual crystal field stabilisation energetics and a PM fluid that has an ideal Curie law paramagnetism. Frozen and unfrozen solutions have been studied by ESR, magnetometry, and Mössbauer spectroscopy. These ionic clusters are mainly of interest to us here because they are the relevant starting points in various synthesis reactions of magnetic nanoparticles and they are the precursor forms that will surface complex to nanoparticles of interest. In this regard, it is important to note that geochemists often incorrectly assume the free metal ion model; that the equilibrium cation species in solution will be the only species that surface complex or that participate in nucleation and growth of new nanoparticles and that, therefore, the solution conditions (pH, Eh) completely determine the valence states and coordinations of intra-particle and surface cations. In fact, the valence states and coordinations of intra-particle and surface cations must be consistent with intra-particle and surface stereochemical constraints and can be quite different from those predicted by the free metal ion model, as they are near cell membranes (Simkiss and Taylor 2001). For example, tridentate complexation of a surface phosphate group can stabilize a surface ferrous cation on a hydrous ferric oxide nanoparticle, via a crystal field stabilization energy that is greater than the electron transfer energy from the environment, under conditions where only a ferric oxide solid phase is thermodynamically stable (Rancourt et al. 1999a, 2001a).

The above sequence of characteristic sizes is meant as a representative scenario only, not a rigorous path that all materials must follow when particle size is decreased. The same is true of the thermal path from high temperatures, above T_{oB}, to 0 K where zero point motion and quantum tunnelling persist. For example, goethite has a T_{oB} just above RT and nanoparticles of goethite probably have SP fluctuations starting at T_{oB} itself, where the single ion and supermoment excitations coexist and cannot be treated separately as with most other Fe oxide nanoparticles. This is probably the reason that goethite exhibits such unusual Mössbauer spectra compared to other Fe oxide

nanoparticle systems (Morup et al. 1983, Bocquet 1996).

Magneto-sensitive features of magnetic nanoparticles

In this subsection, I describe the features of real nanoparticle systems that need to be added to the ideal starting point of a uniform magnetization on a regular crystal lattice, both the magnetization and the lattice being unperturbed by the particle surface, relative to the magnetism and structure of the bulk material. These crystal-chemical features significantly affect the magnetism and are therefore probed by magnetic measurements. Most of these effects were anticipated and described by Néel (1949a, 1953, 1954, 1961a,b,c,d).

SR thermal effects. I have already described the SR average thermal local moment effect that was characterized by d_{SR}. If the bulk magnetic bond structure is such that there is some degree of exchange bond frustration, where, for example, NN bonds would be AF whereas next or second nearest neighbor (2NN) bonds would be FM, and if the surface preferentially removes, for example, more 2NN bonds than NN bonds, then some or all of the local thermal average ionic moments in the SR can be larger than the local thermal average ionic moments in the middle region of the particle. The different local thermal average ionic moments will also have different applied field responses or local susceptibilities. To some extent, all moments in a particle are affected by this phenomenon and the magnetic ordering transition itself is affected compared to its occurrence at T_{oB} in the bulk material. Indeed, the normally sharp transition is affected by what are known as finite size effects. The transition does not exhibit the usual divergences of thermodynamic properties at T_{oB} and critical exponents of the transition region are different (e.g., Fisher and Privman 1985). For sufficiently small particles ($d \sim d_{SR}$) the perturbation extends to temperatures far below T_{oB} and the entire intrinsic magnetization curve is affected down to 0 K.

Surface magneto-crystalline anisotropy and SR anisotropy disorder. Regarding the surface, another important effect is that the local ionic magneto-crystalline anisotropies (K) in the SR can be significantly different in magnitude (including sign), symmetry, and orientation, compared to their values in the middle regions of particles. This is due to the different ionic coordination environments near the surface and was first described by Néel (1954a,b). Indeed, using a classical approach and the continuum limit, Néel showed that a surface magneto-crystalline anisotropy, distinct from the dipolar anisotropy described below, must occur that produces a local easy direction that is either perpendicular to the surface or in the plane tangent to the surface, depending on the sign of the surface anisotropy density k_S (in J/m²). The density k_S was shown to depend on the crystal chemistry of the material and the crystalline orientation of the surface and to be significant for nanoparticles. Modern ab initio electronic structure calculations are now able to calculate such effects at the atomic and intra-atomic levels (e.g., Pastor et al. 1995, Nordström and Singh 1996). In discrete atomic models, the local anisotropy is not simply related to the surface normal but instead depends on the local coordination environment. A similar effect arises from chemical disorder in an alloy or solid solution, where K is locally defined by the chemical environment at a cation site. This means that, in addition to the above described d_{SR} thermal effect, the local thermal average moments in the SR will not only have different magnitudes than in the middle region but may also have different local easy directions and local orientations. The surface moment orientations (i.e., misalignments or non-collinearities) will result from an interplay and compromise between thermal agitation, exchange interactions, and local magneto-crystalline anisotropies. Such misaligned moments have been called surface pinned spins. They contribute to the particle's overall supermoment, have temperature and field dependent misalignments, and represent a main mechanism for large residual high field

susceptibilities, above the saturation fields that give technical saturations in which all supermoments and middle region local moments are aligned at low temperatures. These phenomena have recently been elegantly modelled and described by Kodama and co-workers (Kodama 1999, Kodama and Berkowitz 1999, Berkowitz et al. 1999). These researchers also point out that the associated phenomena have probably been frequently misinterpreted as quantum tunnelling effects.

Incomplete sublattice cancellation and residual moments. Another important finite size effect, again first described theoretically by Néel (1961a), is relevant with AF and FI nanoparticles: In a two sublattice material, there probably will not be equal numbers of cations on each sublattice. This implies that not all moments will be compensated, as they would be in the AF or FI bulk materials. With AF nanoparticles, this will usually be the main mechanism to create a large supermoment, as is the case with ferrihydrite, ferritin, and hematite nanoparticles (Rancourt et al. 1985, Makhlouf et al. 1997a, Dang et al. 1998, Rancourt et al. 2001b). An elegant example of this effect, where exchange bond frustration also plays an important role, is provided in the case of a synthetic two dimensional nanoparticle system (Rancourt et al. 1986). The resulting residual super-moment that resides on an AF nanoparticle does not have a simple dependence on particle size and depends on the details of the material, including: vacancies, cation substitutions, shape, surface complexation, etc. Néel (1961a) proposed simple situations where the residual moment would go as $n^{1/2}$ or $n^{1/3}$ or $n^{2/3}$, depending on the underlying conditions.

Dipolar shape anisotropy barrier. Given the nature of dipole-dipole forces (Eqn. 1), a uniformly magnetized FM or FI SD particle having a non-spherical shape will tend to be magnetized along the particle's axis of greatest elongation. That is, the dipolar contribution to the energy is minimized for a magnetization axis that is parallel to the main elongation axis. It is simple to see that one consequence of Equation (1) is that, for the same local ionic moments having the same inter-ionic separations, the FM configuration $\rightarrow \rightarrow$ (or $\rightarrow \rightarrow \rightarrow$, etc.) has a smaller dipole-dipole interaction energy than that of the FM configuration $\uparrow \uparrow$ (or $\uparrow \uparrow \uparrow$, etc.). Elongated or acicular SD particles are common so this is an important effect and the shape dependent dipolar contribution to E_b can be significant. For AF particles that have vanishingly small supermoments, this effect is relatively negligible because many of the long range terms in the total energy sum cancel. It is important to note that the magneto-crystalline anisotropy easy axis is coupled to the underlying crystal lattice and that it may not, therefore, be aligned with the elongation axis. The resulting easy axis directions will represent a compromise between the middle region (bulk) K axes, the SR K axes, and the dipolar anisotropy. For a uniformly magnetized particle of magnetization $M = m\mu/v = \mu_S/v$, where m is the net number of cationic moments μ per supermoment μ_S, having the shape of an ellipsoid of revolution with long (rotation) semi-axis a, short semi-axis b, and small eccentricity e, the dipolar anisotropy energy is given by (Néel 1954):

$$E_d = -(16\pi^2/30)\, a\, b^2\, e^2\, M^2 \cos^2\theta_{\mu a} = -(4\pi e^2/10)\, (\mu_S^2/v) \cos^2\theta_{\mu a} \qquad (4)$$

where $\theta_{\mu a}$ is the angle between the supermoment and and the long axis. This continuum limit result applies irrespective of the underlying crystalline orientation. By comparison, the net surface magneto-crystalline anisotropy energy for such a particle is given by (Néel 1954):

$$E_s = -(16\pi/15)\, a\, b\, e^2\, k_S \cos^2\theta_{\mu a}. \qquad (5)$$

For nanoparticles, these two shape and size dependent energies are significant and comparable in magnitude. Depending on the sign of k_S, they can add or partially cancel.

They are independent of and in addition to the net volume magneto-crystalline energy, E_v, which, for the uniaxial case, is given by:

$$E_v = -nK \cos^2\theta_{\mu K} \qquad (6)$$

where $\theta_{\mu K}$ is the angle between the supermoment and the crystalline K axis. K, like k_S, can also be positive or negative. In the simple case where the K axis and the ellipsoid long axis a are parallel, the total uniaxial barrier energy of Equation (2) is

$$E_b = E_d + E_s + E_v.$$

Of course, in general, the magnetization is not uniform, the particle is not an ellipsoid of rotation, the volume magneto-crystalline anisotropy is not uniaxial nor is it aligned with the particle shape, there are local orientational and magnitude variations of both SR and middle region magneto-crystalline anisotropies, etc.

Intrinsic and quenched-in nanoparticle defects. Even if a nanoparticle could be made by simply cutting out a piece of desired shape and size from a perfect single crystal of material, it would then relax and spontaneously change itself to lower its free energy, via all mechanisms available to it within its life or annealing time. First and foremost, an ionic nanoparticle will not generally be stoichiometric and this problem will require significant SR adjustments to achieve electrical and valence stability. In additon, the SR bond lengths relax, relative to the bond lengths in the bulk, as a direct consequence of lower surface atom coordinations. Indeed, there is a continuous radial distribution of bond lengths, from bulk-like middle region values to SR values. This distribution is affected by the surface conditions. Surface modifications will include: reconstruction, complexation of impurities from the environment, adsorption of neutral molecules such as water molecules that complete ligand field stabilized inner shell coordinations of surface cations, and loss or gain of protons depending on solution pH. The changes in bond length are small (10^{-2} to 10^{-4} nm or less) but magnetic exchange interactions are very sensitive to bond lengths and bond angles and can even change signs under moderate structural perturbations. As a result, magnetic probes can often uncover changes, relative to the bulk material, that are difficult to detect by any other method. For example, the particle size dependent moment rotations seen by ^{57}Fe Mössbauer spectroscopy in the WF state of hematite (Dang et al. 1998, and references therein).

The intrinsic size-induced changes in bond lengths are accompanied by changes in atomic vibrational amplitudes, such that vibrational entropy per atom and effective Debye or Einstein temperatures will be different than those of the bulk. The Debye-Waller factors of measurements that are affected by lattice vibrations (e.g., X-ray diffraction, Mössbauer spectroscopy) will also be different than in the bulk. In addition, the surface will cause atomic vibrations of atoms near the surface of the particle to be anisotropic, even if they were isotropic in the bulk, typically with larger vibrational amplitudes perpendicular to the surface. With magneto-volume coupling, the surface-perturbed magnetic structure also contributes to changing the vibrational characteristics, relative to those of the bulk material.

Regarding both vibrational (phonon) and magnetic (magnon) excitations, the finite particle size imposes an upper wavelength limit. This can be detected in measurements that probe the excitation spectra up to large wavelengths (e.g., inelastic neutron scattering) and it affects the thermodynamic properties of the nanoparticles.

On the other hand, natural nanoparticles are usually nothing like clean crystalline surfaces that simply relax their structure and admit complexing cations on well defined bonding sites. They are often formed by rapid precipitation and represent metastable

phases with high densities of quenched-in defects. These defects include: vacancies, often charged balanced by O^{2-}/OH^- substitutions, cation substitutions such as Al^{3+} for Fe^{3+} and substitutions of cations with different valences using various charge balancing schemes, strong surface complexation involving ubiquitous elements such as C and Si, an interface region with a supporting material or matrix phase, and crystal grain boundaries both between grains of the same phase and between grains of different phases.

Exchange anisotropy in multi-phase particles. An example of the latter situation is a metal nanoparticle that has a metal oxide layer or a magnetite nanoparticle that has an oxidized maghemite layer. The interfaces between phases can be disordered or crystallographically continuous or some combination of these situations. The interfaces can also be atomically sharp or continuous. For example, a magnetite/maghemite particle could have a continuous radial gradient of oxidation, from the middle region to the SR. When both phases of a two-phase particle are magnetic, such as the case of magnetite/maghemite particles, there may be continuous magnetic exchange interactions across the phase boundary. In this case, at temperatures between the blocking temperatures of the two phases, a phenomenon known as exchange anisotropy occurs, whereby the blocked component exerts a significant exchange force on the supermoment of the unblocked phase. This exchange force can be represented as a mean magnetic field that is applied to the SP component, thereby polarizing it in some preferred direction. This direction will have established itself at the higher blocking temperature where the blocked phased became blocked, depending on the ambient applied or interaction fields present at that time.

Inter-particle interactions. The various forms of magnetic and non-magnetic inter-particle interactions, in an ensemble of, say, identical nanoparticles, can dramatically affect the magnetic behavior of the macroscopic ensemble or sample. It has only recently become possible to study individual isolated nanoparticles (see below) so that most studies have had to struggle with resolving individual particle properties and properties that arise from inter-particle interactions. In a given sample, such as a rock or a consolidated or frozen sediment or a frozen ferrofluid, etc., there will be inter-particle interactions that depend on such factors as: the concentration of magnetic particles, the spatial distribution of particles, the nature of the matrix phase, and the nature of the particles. These factors have recently been given significant attention in controlled synthetic model systems (see below). If the particles make contact, there may be chemical bonds between them and relatively strong inter-particle exchange interactions via exchange bond bridges. The geometry of these bridges will predominantly determine the strength of the corresponding inter-particle exchange interactions (Rancourt 1987, p. 91-92). If the particles are not connected via exchange interactions, then the remaining relevant magnetic inter-particle interaction is the dipolar interaction: Equation (1) where each supermoment is considered a fundamental interacting moment and the interaction sum is carried out on all pairs of magnetic particles in the sample. As a result of these long range interactions, the magnetic properties depend on the shape of the macroscopic sample, assumed to contain a uniform distribution of particles. For this reason experimenters must take special precautions to make proper demagnetizing field corrections or calculations.

I have already mentioned that inter-ionic exchange interactions depend on inter-ionic separation (bond length). This gives rise to magneto-volume effects, where bond lengths adjust to the degree of local magnetic order, that is, to the magnitudes of local average ionic moments and to their relative orientations (Grossmann and Rancourt 1996). In addition, spin-orbit coupling induces a phenomenon known as magneto-elastic effects, where inter-ionic separation (bond length) is affected by the angle that an average local

ionic moment makes with its local magneto-crystalline easy axis. That is, the effective ionic radius is a function of the angle between the local moment and the local magneto-crystalline axis. These magneto-volume and magneto-elastic effects are generally small in terms of the bond length changes but their influence on the magnetic properties can be large. In particular, if the particles are imbedded in a rigid matrix, then strain mediated interactions can become important (Jones and Srivastava 1989). Unlike the exchange and dipolar inter-particle interactions (and unlike exchange anisotropy described above), the later strain mediated inter-particle interactions cannot be modelled by mean interaction fields (i.e., by effective magnetic fields arising from the interactions) because they cannot induce a local preferred direction, although they could, for example, change the orientations of easy axes. Here one must distinguish the direction of a vector from the orientation of an axis. This has important consequences in interpreting measurements because an external or effective applied field will induce different SP dwell times on a given particle (τ_+ and τ_- given by an equation similar to Equation (2), that has a field dependence, more below) whereas magneto-crystalline and strain effects cannot.

More on magneto-elastic and magneto-volume effects. The SP supermoment fluctuations themselves arise from thermal lattice vibrations via magneto-elastic coupling (Néel 1949a,b). The supermoment fluctuations are intimately tied to lattice vibrations, contractions, and expansions. This is the source of the matrix mediated strain interactions described above but it also implies that, even in an isolated SP particle, there will be whole-particle volume fluctuations occurring in phase with the SP supermoment fluctuations that will have the same characteristic time τ, given by Equation (2). It should be possible to detect a sound of characteristic SP frequency $1/\tau$ emitted from a suitably prepared sample of imbedded nanoparticles and this may have applications as a means to characterize ensembles of nanoparticles where the acoustic noise spectrum would contain information about the distributions of τ values and their field and temperature dependencies. Gunther and Mohie-Eldin (1994) have suggested that such magneto-strictive SP lattice fluctuations should produce measurable effects in the Mössbauer spectra of SP nanoparticles.

Distributions of everything. The latter comment on distributions of τ values brings us to our next topic, the fact that most samples containing nanoparticles contain many different nanoparticles, with entire distributions of particle sizes and shapes, particle compositions and structures, matrix media, etc. Natural and synthetic assemblies of nanoparticles are complex, mainly because there are correlated distributions of all the physico-chemical properties of the nanoparticles themselves, not to mention the supporting medium or matrix. As a result, most measured properties cannot be understood on the basis of the properties of individual nanoparticles alone. For example, Equation (2) leads to a predicted exponential time dependence of the sample magnetization, at constant temperature and applied field, of the form

$$M(t) = M(\infty) + [M(0) - M(\infty)] \exp(-t/\tau) \tag{7}$$

whereas measured time dependences are most often logarithmic, with near-constant viscosities. This striking discrepancy can be shown to arise from the distribution of nanoparticle volumes, via the volume's effect on both τ and the supermoment magnitude (Néel 1949a). Indeed, the distribution of particle volumes or sizes is most often the single most important distribution to affect macroscopic sample properties, mainly because of the particle volume effect on τ, via the barrier energy E_b (Eqn. 2). As a result, magnetic measurements allow detailed quantitative determinations of particle size distributions. On the other hand, the barrier energy has significant contributions that are not simply proportional to particle volume (e.g., Eqns. 4-5) and have strong dependencies on particle shape and supermoment formation mechanism. The pre-exponential factor in Equation

(2), f_o, also has a complex dependence on particle properties and its value will be strongly correlated to the value of E_b.

The above discussion assumes non-interacting (well dispersed) nanoparticles but, in non-dilute samples of nanoparticles, interactions are the other major complicating factor, in addition to the particle volume distribution. Because of inter-particle interactions (both dipolar and exchange bridges), the distributions of spatial positions and orientations of the particles can significantly affect the measured properties. For example, the nano-particles may form aggregates or clusters, with exchange interaction bridges between the nanoparticles in a cluster and dipolar interactions within and between clusters. The distributions of cluster sizes and structures and their separations then become important. Such clusters may act as large magnetic particles and dramatically affect the observed behavior.

As a result of magnetic inter-particle interactions, each nanoparticle will feel a net local interaction field that can be modelled by a time-dependent local applied field, $H_{int}(t)$. If the time variation of the local interaction field is either very fast or very slow compared to the relevant characteristic times (e.g., τ) of the particle, then $H_{int}(t)$ can in turn be modelled as a static local field, that will, of course, depend on temperature and macroscopic applied field. The distributions of particle positions, orientations, and supermoments will determine the distribution of local interaction fields. These interaction fields are present in zero applied field and dramatically affect the behaviors of the individual nanoparticles and, consequently, of the sample as a whole. They achieve this in two important ways. First, they change the equilibrium magnetic properties of the sample, giving rise, for example, to superferromagnetic ordering or interaction Curie-Weiss behaviors (see below). Second, and possibly more importantly, they affect dynamic response, via their influence on SP dwell times.

The latter point has not been sufficiently recognized, despite Néel's (1949a) clear original exposition, and deserves more explanation. Equation (2) is valid only in zero applied field. At $T = 0$ K, a critical applied field, H_o, equal to the coercivity at this temperature for our uniaxial particle, is given by

$$H_o = 2 E_b/\mu_S = 2 E_b/m\mu. \tag{8}$$

where $E_b = E_d + E_s + E_v$ (Eqns. 4-6). Applied fields greater than this magnitude will remove the barrier and completely saturate the sample magnetization, within the limits of equilibrium thermal averaging at the given temperature. At smaller fields, $H < H_o$, a barrier between the two easy directions persists but it is of different heights depending on whether the supermoment is predominantly parallel or antiparallel to the field direction. As a result, one defines two different SP dwell times: τ_+ is the average time one must wait for the supermoment to spontaneously flip to the other (i.e., minus) easy direction if it is initially in the plus easy direction (i.e., the easy direction that is predominantly aligned with H, for a given orientation of the particle) and τ_- is the average time one must wait for the supermoment to spontaneously flip to the plus easy direction if it is initially in the minus easy direction. The action of the field is such that $\tau_+ > \tau_-$. Both are field-dependent and one defines the field-independent (for $H << H_o$) average dwell time, τ, as

$$1/\tau = 1/\tau_+(H) + 1/\tau_-(H) \tag{9}$$

which, to first order in H, is given by Equation (2). Derivations of correct microscopic expressions, analogous to Equation (2), for $\tau_+(H)$ and $\tau_-(H)$ in an ideal uniaxial particle are non-trivial and have involved much fundamental work (see below). For example, the expressions of Néel, Brown, and recent workers differ somewhat, depending on details of the assumptions and approximations made.

The main points are that there are at least two characteristic microscopic dwell times, at the level of a single nanoparticle, that they are field dependent, and that they are distributed, at the level of the sample, by two mechanisms: via the distributions of particle properties (E_b, μ_S) and via the distribution of interaction fields (H_{int}). Such is the added complexity due to inter-particle interactions.

Measurement time complexity. Yet another level of issues must be addressed when one considers whether the microscopic dwell times introduced above are much smaller than, comparable to, or much larger than the measurement time, that, in turn, is highly dependent on the type of measurement (see above). The simplest situation arises when all the microscopic dwell times are much smaller than the measurement time. In this case, one observes equilibrium values. For example, the average supermoment on a given particle is

$$<\mu_S>(T, H) = ([\tau_+(T,H) - \tau_-(T,H)]/[\tau_+(T,H) + \tau_-(T,H)]) \, m <\mu>(T,H) \qquad (10)$$

where $<A>(T,H)$ denotes the equilibrium thermal average of A, evaluated at temperature T and field $H = H_{applied} + H_{int}$. For a sample with N magnetic particles and of volume V, one then has, a sample magnetization given by

$$M(T,H) = (N/V) \int P(m,E_b,H_{int}...) <\mu_S>(T, H) \, dm \, dE_b \, dH_{int} ... \qquad (11)$$

where the integral is over all distributed parameters and $P(m,E_b,H_{int},...)$ is the joint probability distribution of all distributed parameters. An expression such as Equation (11) is relatively simple to evaluate and interpret.

If the microscopic dwell times are all much larger than the measurement time, then one probes the system as a static distribution of its parameters in order to deduce the state in which the system was prepared, by its previous temperature, applied field, and structuro-chemical history. For example, this would correspond to a remanence magnetization measurement, in the absence of time or relaxation effects. Alternatively, one can consider that all the particles in the sample that have microscopic dwell times much larger than the measurement time form a subgroup or subsystem that has reliably preserved a subsystem-specific remanence signal. Since dwell times are highly temperature dependent (Eqn. 2), partial thermoremanence measurements are a powerful tool to reconstruct a rock's thermomagnetic history.

If the sample contains very broad distributions of microscopic dwell times, arising from broad distributions of E_b, H_{int}, etc., with many dwell times that are much larger than and much smaller than the measurement time, and if the measurement is one that is similarly sensitive to all signals from the sample, then one can ignore those particles having dwell times that are comparable to the measurement time and simply divide the sample into two groups having $\tau > \tau_m$ and $\tau < \tau_m$, in the spirit of Equation (3). One then proceeds to use static configuration calculations on the first group and equilibrium calculations on the second group. This approximation was first introduced by Néel (1949a) and is widely used in many fields related to magnetic nanoparticles. It is often a very good approximation for constant field magnetometry with natural geologic or environmental samples, where very broad distributions of magnetic particle sizes do occur. Its validity depends on both the nature of the sample and the characteristics of the measurement technique, since different measurement methods have different measurement response time windows (centered on τ_m).

If all of the particles or a significant fraction of all the particles in the sample have dwell times that are comparable to the measurement time, then one has the most complex situation. In particular, we stress that the measurement may be very sensitive to the fact

that $\tau_+ \neq \tau_-$ and to the actual values of both τ_+ and τ_-, not just the average τ. Mössbauer spectroscopy is an example of a measurement method where this is important and has not generally been recognized (Rancourt and Daniels 1984). We discuss this in more depth below.

More measurement complexity. In addition to the problem of measurement time, each measurement method normally has a non-flat response or sensitivity function. By this I mean that the measurement of a macroscopic sample of nanoparticles will, for example, often involve a higher sensitivity to a particular subgroup of particles in the sample. Examples are as follows: alternating field susceptibility resonance damping (phase shift) being predominantly caused by those particles having $1/\tau$ comparable to the probing field frequency, Mössbauer recoilless fractions being smaller for the smaller loosely bound particles, high frequency alternating field susceptibility being predominantly sensitive to supermoment fluctuations about a given easy axis rather than to SP fluctuations, magnetometry being more sensitive to those particles with larger supermoments, ESR not detecting contributions that are broader than the experimental field (i.e., resonance) range, etc. One must guard against assuming a flat response function and assigning the observed behavior from the given measurement method to an "average particle" that has a behavior representative of all the particles in the sample.

Size and shape versus crystal chemical effects. Another aspect of the complexity of real nanoparticles is that there can often be strong correlations between quite different structuro-chemical features of the nanoparticles, thereby leading the experimenter to identify incorrect causal relationships between measured characteristics (e.g., size, shape, composition) and measured behaviors (e.g., phase transitions, changes in physical properties). The strong correlations between different particle characteristics arise because, for a given suite of natural or synthetic samples, the main relevant synthesis or treatment parameters (temperature, pH, oxygen fugacity, kinetic supply of reactants, bulk composition, annealing or aging time, etc.) simultaneously control several resulting nanoparticle characteristics (size, shape, composition, degree of agglomeration or sintering, degree of oxidation, surface conditions, degree of chemical order, etc.) and their distributions. This is very important because the goal of much research on nanoparticles is often to identify the role of particle size, as a key controlling parameter. There is an unfortunate tendency for assigning causal relationships between those particular particle characteristics and sample behaviors that the experimenter has happened to measure, although the causal link may actually be with characteristics that were not measured. The best defences against such errors is to measure as many different sample characteristics as possible on the same samples (Waychunas, this volume). We treat one classic example below, where many authors have attributed changes in the Morin transition of hematite to particle size in cases where these changes are due to chemically induced lattice deformations.

Ferrofluids. Ferrofluids are an important class of magnetic nanomaterials that is not of primary interest in this chapter. Nonetheless, it is useful to point out some key differences between magnetic fluids and solid phase magnetic nanomaterials. There are three main differences regarding microscopic magnetic phenomena: (1) regarding supermoment relaxation, ferrofluids have a Brownian relaxation component in addition to Néel superparamagnetism, (2) in relation to applied field response, in a ferrofluid the particle itself can rotate, thereby providing an independent induced magnetization mechanism that depends on fluid viscosity, particle surface properties, and magneto-crystalline coupling strength, and (3) particle aggregation and spatial correlations are largely determined by magnetic inter-particle interactions and change in response to applied fields. Some of these features are relevant to aquatic sediments, industrial sedimentation

and holding pools, and to the filtering or separation of magnetic precipitates in environmental and industrial applications.

MICROSCOPIC AND MESOSCOPIC CALCULATIONS OF MAGNETISM IN MATERIALS

The remarkable situation in which we find ourselves in modern materials science is that physics has for some time been sufficiently developed, in terms of fundamental quantum mechanics and statistical mechanics, that complete and exact *ab initio* calculations of materials properties can, in principle, be performed for any property and any material. The term "*ab initio*" in this context means without any adjustable or phenomenological or calibration parameters being required or provided. One simply puts the required nuclei and electrons in a box and one applies theory to obtain the outcome of a specified measurement. The recipe for doing this is known but the execution can be tedious to the point of being impossible. The name of the game, therefore, has been to devise approximations and methods that make the actual calculations doable with limited computer resources. Thanks to increased computer power, the various approximations can be tested and surpassed and more and more complex materials can be modelled. This section provides a brief overview of the theoretical methods of solid state magnetism and of nanomaterial magnetism in particular.

Methods of calculation in solid state magnetism

Electronic structure calculations. The most fundamental approach is *ab initio* electron structure calculations (ESCs) (e.g., Sutton 1993, Szabo and Ostlund 1996). In this method, one specifies the nuclei and their positions and one uses quantum mechanics to deduce how the electrons will organize themselves about these nuclei. All the properties due to electrons, including chemical bonding, valence states of ions, and magnetism, are calculated from first principles. Such calculations are normally performed assuming a temperature of T = 0 K. The characteristic temperature at which electronic structure deviates from its T = 0 K configuration, known as the Fermi temperature, is normally very high ($\sim 10^4$ K) such that calculated ESCs are normally valid at all temperatures of interest, in terms of the electron distributions (i.e., bonding configurations, bond strengths, bond types, relative bond lengths, ionic magnetic moment magnitudes, magnetic exchange bond strengths, fine and hyperfine parameters, etc.). ESCs represent the methods of choice for understanding crystal chemistry at a fundamental level and for predicting the structures of unknown materials of given compositions and subjected to any pressure. They can be used to investigate dramatic changes in electronic structure and the associated magnetism that can occur as one varies the composition and/or the lattice parameters. A good example of the latter application is provided by the study of low-moment (LM) and high-moment (HM) meteoritic and synthetic taenite phases (Rancourt et al. 1999b, Lagarec et al. 2001). They can equally well be used on bulk materials, molecules, clusters, and nanomaterials.

At present, there has been only limited success at developing ESCs for non-zero temperatures. This means that ESCs can only be used for obtaining ground state configurations (e.g., T = 0 K magnetic moment structure or T = 0 K chemical ordering energy) and the T = 0 K properties of imposed structures that may only be stable at non-zero temperatures. ESCs are not presently available for treating non-zero temperature behavior, including magnetic and chemical order-disorder transitions and vibrational, electronic, and magnetic excitations. One can perform ESCs for any set of nuclear positions and, since electron density equilibrium times ($\sim 10^{-18}$ s) are much shorter than any other relevant time such as that associated with nuclear motion, thereby examine

chemical reactions, atomic diffusion, precipitation and coagulation, etc., but always from a perspective that ignores the low energy excitations, compared to chemical bond energies. The low energy excitations that are ignored are: atomic and collective vibrations, valence fluctuations, magnetic moment orientation excitations (including ionic and SP varieties), entropic defect generation and diffusion, etc. When chemical bonding is a given and it is the latter phenomena that are of interest, then present ESCs need to be abandoned for more phenomenological calculations that take the electronic structure as fixed and treat the excitations of interest, to various degrees of exactness.

Magnetic subsystem. Next we briefly describe the most common such methods that are used in magnetism, to specifically study magnetic phenomena that are due to the responses of and interactions between permanent ionic moments in solids, to the extent that the magnetic subsystem can be decoupled from the underlying chemical, electronic, vibrational, etc. subsystems. As it turns out, the magnetic subsystem of a solid can usually be conveniently decoupled from the other degrees of freedom for calculation, thanks to significantly different time scales for the different excitation subsystems (e.g., Grossmann and Rancourt 1996). In these calculations, the ionic magnetic moments of the PM cations become the fundamental microscopic entities that replace the electrons of ESCs. The latter ionic moments are taken to be "permanent" in that their magnitudes are assumed not to vary with temperature. That is, ground state ionic configurations are assumed with set dimensionless total ionic angular momentum and spin quantum operators, L and S, respectively. Inter-moment exchange interactions, J_{ij}, between PM cations i and j, are also assumed to be fixed and given, as are the local ionic magneto-crystalline anisotropy constants, K_i, for cations i. The reader now appreciates that the cation-specific physical parameters L, S, J_{ij}, and K_i are determined by the electronic structure and normally have temperature variations, to the extent that the electronic structure itself does. The operational link between ESCs and the methods described below is that ESCs can be used to calculate the T = 0 K values of L, S, J_{ij}, and K_i rather than treating the latter as adjustable phenomenological parameters.

Exact analytic solutions. As usual in solid state magnetism, the recipe for a formally exact solution to the magnetic subsystem problem described above is known. For simplicity, we take the angular momenta to be quenched (L = 0), as often occurs from bonding, and the Hamiltonian of the magnetic subsystem is written

$$\mathcal{H} = -\sum_{ij} J_{ij}\, \mathbf{S}_i \cdot \mathbf{S}_j + \sum_i K_i\, (\mathbf{u}_i \cdot \mathbf{S}_i)^2 + g\mu_B \sum_i \mathbf{S}_i \cdot \mathbf{H} \qquad (12)$$

where bold symbols are vectors or vector operators. The first sum is over all interaction pairs of PM cations in the sample and represents the total exchange bond energy. The negative sign in front of the first term is such that positive exchange constants correspond to FM exchange bonds whereas negative constants correspond to AF bonds. The second sum is over all cations and represents the total magneto-crystalline energy for an assumed local uniaxial symmetry where $\mathbf{u}_i$ is a dimensionless unit vector parallel to the local symmetry axis. The third term is also over all cations and represents the total energy of interaction between an applied field and the cation moments. A given cation moment has magnitude $\mu_i = g\mu_B S_i$, where g is the electronic g-factor and S_i is a dimensionless half integer quantum number (in Table 1, g = 2). The quantum operator $\mathcal{H}$ acts on a $(2S+1)^N$ dimensional state space, where N is the total number of cations in the sample. One solves the associated eigenvalue problem for the $(2S+1)^N$ energy eigenvalues, E_n, and eigenstates, $|n\rangle$, and one uses these in the usual Boltzmann statistics to calculate the equilibrium value of any physical property A as

$$\langle A \rangle (T,H) = (1/Z) \sum_n \langle n|A|n\rangle \exp(-E_n/k_B T) \qquad (13)$$

where $Z = \sum_n \exp(-E_n/k_BT)$ is the partition function and the sums are over all eigenstates. Non-equilibrium properties and transition probabilities can also be calculated.

One notes that the problem is separated into two parts: a purely quantum part of obtaining the energy eigenvalues and eigenfunctions and matrix elements $\langle n|A|n\rangle$ and a purely statistical mechanics part of evaluating the Boltzmann sum and partition function. The problem is solved, in principle. In practice, exact analytic solutions have been obtained in only a few cases corresponding to simplified (low dimensional) bulk materials with simplified exchange and magneto-crystalline interactions. Nonetheless, this has represented a fruitful area of interaction between theory and synthetic low dimensional model systems. Most importantly in the present context, available computers now allow one to treat clusters and small nanoparticles directly by these exact methods and to add realistic additional features such as magneto-elastic and magneto-volume coupling to the underlying lattice or chemical effects.

Other analytic methods. Several analytic methods have been developed to treat the statistical mechanical part of the above exact problem, since the quantum part is often known (Van Vleck 1959). These include: near-critical point renormalization group methods, temperature expansion methods for limited temperature regions, and various rigorous proofs relating to ground state or high temperature properties and to relations between critical exponents, near magnetic phase transitions. These results have often been extensively verified experimentally. Each such new result or method is considered a milestone in statistical physics, and magnetism is one of the major model system testing grounds used by statistical physicists.

Approximate analytic methods. If one is willing to make certain physically reasonable approximations, one can often obtain powerful and elegant closed form analytic solutions to the problem of evaluating expressions such as Equation (13). Historically, the most important of these methods is called mean field theory (MFT), as first developed by Weiss (1948, Pathria 1988) and used to great advantage by Néel and others. The basic simplifying assumption consists in replacing the cation moments that interact with a given central moment with their thermal averages in Equation (12). That is, we replace the operator S_j in Equation (12) by the scalar $\langle S_j\rangle(T,H)$, given by Equation (13) where $A = S_j$. If all thermal average local moments are equal, as in an all-sites-equivalent ferromagnet for example, then the inter-cation terms in the interaction sum drop out and the problem goes from being a $(2S+1)^N$ dimensional one to being $2S+1$ dimensional. The relevant Hamiltonian becomes

$$\mathcal{H}_i = -\sum_j J_{ij} S_i \cdot \langle S_j\rangle + K_i (u_i \cdot S_i)^2 + g\mu_B S_i \cdot H \tag{14}$$

and the problem is reduced to a single ion problem. The local interaction sum is over all j-cations that interact with the central i-cation. We denote the single ion eigenenergies as ε_n and, in the case of the all-sites-equivalent ferromagnet, one has

$$\langle S\rangle(T,H) = (1/Z) \sum_n \langle n|S|n\rangle \exp(-\varepsilon_n/k_BT) \tag{15}$$

where the sum has only $2S+1$ terms (e.g., for Fe^{3+}, $S = 5/2$, Table 1) and all the eigen-values, eigenstates, and matrix elements are known. Equation (15) is solved self-consistently for $\langle S\rangle(T,H)$ and the sample magnetization density is simply $M(T,H) = (N/V) \langle S\rangle(T,H)$. For $K_i = 0$, the calculation predicts a Curie point occurring at

$$T_C = [S(S+1)/3k_B] \sum_j J_{ij} \tag{16}$$

where the sum is over all pair-wise exchange bonds with the central i-cation. For

example, with NN only exchange bonds and z NNs in the structure, $T_C = zJ_{NN}S(S+1)/3k_B$. Otherwise, T_C depends on the non-zero value of K_i and the induced magnetization depends on the relative orientations of H and u_i. The calculation also predicts the usual high temperature $(T > T_C)$ Curie-Weiss behavior of the initial susceptibility:

$$\chi_o = C/(T - \theta_{CW}) \tag{17}$$

with Curie constant $C = (N/V) (g\mu_B)^2 S(S+1)/3k_B$, as given by an exact calculation for a paramagnet where $\chi_o = C/T$, and Curie-Weiss temperature $\theta_{CW} = T_C$. In reality, one normally has $\theta_{CW} \sim T_C$. These are remarkably good predictions for such a simple model.

For a two-sublattice antiferromagnet, one simply has two coupled single-ion equations such as Equation (15) that are simultaneously solved selfconsistently for the two sublattice average moments. A p-sublattice material gives rise to p coupled equations and presents no special difficulty. The MFT method has been generalized to random, disordered, and amorphous magnetic materials by Rancourt et al. (1993).

MFT can also be made as exact as computer resources permit by applying a Bethe-Peierls cluster approach (Pathria 1988). In this adaptation of the model, one considers an entire cluster of PM cations around a central cation of interest in the bulk material and one exactly solves the intra-cluster system, using the exact analytic approach described above, by replacing all extra-cluster cation moments that have exchange interactions with intra-cluster moments by their respective thermal averages. This calculation for the entire bulk material becomes more and more exact as the assumed cluster size is increased. In practice, it is often found that using relatively small clusters with only 1NN or 2NN cations provides a remarkably good approximation that is significantly better than MFT alone in its simplest form (e.g., Chamberlin 2000).

The relevance of MFT and related methods to magnetic nanoparticles is twofold. First, MFT provides valuable insight regarding the depth-wise profile of thermal average moments starting at the surface of a semi-infinite solid. In this application, each successive surface layer is treated as a separate sublattice. This allows a fair estimate of the SR depth, d_{SR}, defined above and its temperature, surface structure, and applied field dependencies. Second, although MFT is not well suited to describing the magnetism of a given nanoparticle compared to the recommended exact analytic method, it is a valuable method for treating inter-particle interactions. In this application of MFT (e.g., Rancourt 1985), one treats each supermoment as an elementary cation moment in a bulk magnetic material. That is, one models the interactions of a given supermoment (on a given nanoparticle) with all other supermoments in the sample by replacing the supermoments of interaction by their thermal averages. In this way, the central supermoment of interest sees an effective interaction field of interaction that is due to the thermal averages of all the other supermoments. This mean field is the H_{int} field introduced above in the case where it is not time dependent. The same is true in the application of MFT to bulk magnetic materials. The mean field or molecular field of MFT does not need to be calculated explicitly in obtaining the various thermal average properties but it is a useful representation of the average effects of interactions. For a bulk magnetic material, the vector mean field at site-i is given by

$$H_{int}(1) = (1/g\mu_B) \sum_j J_{ij} \langle S_j\rangle \tag{18}$$

where the sum is over all interaction pairs with the central cation. In a sample of nanoparticles interacting by dipolar interactions (Eqn. 1), the static vector mean field of

interaction seen by particle-i at position vector r_i is given by

$$H_{int}(r_i) = \sum_j (1/r_{ij})^3 \left[<\mu_j> - 3 (<\mu_j> \cdot u_{ij}) u_{ij} \right] \qquad (19)$$

where r_{ij} is the distance between central supermoment-i and supermoment-j, u_{ij} is a dimensionless unit vector pointing in a direction parallel to the straight line separating supermoment-i and supermoment-j, and the sum is over all $j \neq i$, to include all supermoments interacting with supermoment-i. One notes that the interaction mean field depends on relative positions of particles, position of the particle considered within the sample, orientations and magnitudes of all the average supermoments of interacting particles, number density of nanoparticles, etc. These factors give rise to the distributions of interaction fields described above.

Numerical simulation methods. The two most widespread numerical simulation methods in materials science are Monte Carlo (MC) simulation and molecular dynamics (MD). MC simulation consists in evaluating the integrals and sum of statistical mechanics, such as the sums in Equation (13) for a given equilibrium physical property, by a trial and error statistical method using computer generated random trials rather than analytically or by direct summation (Binder and Heermann 1992). It has been used extensively to evaluate the properties of both ferrofluids and solid nanoparticle systems, including inter-particle interactions and particle aggregation effects (e.g., Menear et al. 1984, Ferré et al. 1995, Dimitrov and Wysin 1996, Ribas and Labarta 1996a,b; Kechrakos and Trohidou 1998a,b; Chantrell et al. 1999, 2000; Psenichnikov and Mekhonoshin 2000). Cluster MC algorithms (Wang and Swendsen 1990) are particularly relevant to magnetic nanoparticles. MC simulation has also recently been extended to be applicable to the problem of SP fluctuations on a single nanoparticle (Nowak et al. 2000). In the latter work, a time step calibration allows one to go beyond the usual extraction of equilibrium properties only and to model the microscopic SP fluctuations themselves. It can also be used to study the SP rotation mechanism on a single particle (Nowak and Hinzke 1999), beyond the simple uniform coherent rotation picture of Stoner and Wohlfath (1948) that most workers assume.

MD consists in modelling the atomic vibrations and movements using Newton's classical laws of motion, by including the relevant microscopic inter-atomic interactions. MC can also be used to model atomic displacements but only by discontinuous discrete steps and only to obtain equilibrium average positions and without including kinetic or real time effects or true vibrational effects, as is done with MD. MD is useful when one is primarily concerned with atomic motion and vibrational energy, such as to model chemical intercalation reactions, chemical mixing and reactions, surface adsorption phenomena, diffusion through micro- and nanopores, chemical order-disorder phenomena, phase separation, solid-liquid-gas phase transitions, etc. The chemical binding forces can be modelled via phenomenological microscopic forces or full ESCs can be performed at discrete times, since the electronic structure response time is much smaller than the MD atomic displacement times. MD has not been used to model the atomic vibrational part of magnetic nanoparticles and has not been applied to solid state magnetism in general, until recently. SP fluctuations themselves are due to thermal atomic vibrations and magneto-elastic, magneto-volume, and magneto-shape couplings, such that it would be important to use MD as part of complete and realistic simulations of magnetic nanoparticles. Grossmann and Rancourt (1996) have made a first step along these lines by showing how MD and MC can be combined to model the atomic motion and magnetic components, respectively, of a magneto-volume active bulk material. The method relies on the fact that, most often, atomic vibrational times ($\sim 10^{-13}$ s) are much shorter than ionic magnetic moment fluctuation times ($\sim 10^{-6}$ to 10^{-12} s) such that average atomic

positions can be used to calculate magnetic exchange strengths and equilibrium spin structures and instantaneous moment configurations can be used to calculate inter-atomic potentials. Supermoment fluctuations are in turn much slower than ionic moment fluctuations such that a similar approach should be fruitful in modelling magnetic nanoparticles.

Calculations of superparamagnetism and inter-particle interactions

Uniaxial particles and fixed supermoment magnitudes. Starting with Néel (1949a,b) and Brown (1963), the great majority of researchers who have developed our theoretical understanding of SP fluctuations have treated only the simplest and most common case of uniaxial particles having well defined supermoments of fixed magnitudes. That is, particles having axial symmetries of their barrier energy profiles, such as those predicted for axial magneto-crystalline anisotropy (Eqn. 6), surface magneto-crystalline anisotropy of an ellipsoid of revolution (Eqn. 5), and dipolar anisotropy of a uniformly magnetized ellipsoid of revolution (Eqn. 4), and in which the supermoments have robust magnitudes arising from strong inter-cation exchange interactions. All researchers agree that the SP fluctuation time of an isolated uniaxial nanoparticle in zero applied field is given by an expression analogous to Equation (2) but there are several different expressions for the pre-exponential factor f_o, depending on the physical couplings that are included and the particular approximations that are used. In this regard, Yelon and Movaghar (1990) have made some interesting general comments. There are also important variations in the expressions obtained by various authors for $\tau_+(H)$ and $\tau_-(H)$ of Equation (9). It is beyond the scope of this chapter to review the details of these developments but the reader should know that much recent fundamental work has been done in this very active area and that the early results have been but in a broader context that allows one to understand the different approaches and approximations. Key papers and reviews addressing the underlying theory and calculations of τ, $\tau_+(H)$, and $\tau_-(H)$ include those of: Aharony (1969, 1992), Bessais et al. (1992), Coffey et al. (1993, 1994a,b,c, 1995a,b,c, 1996, 1998a,b), Cregg et al. (1994), Garanin (1996, 1997), Garanin et al. (2000), Garcia-Palacios and Svedlindh (2001), Jones and Srivastava (1989), Kalmykov and Titov (1999), Kalmykov (2000), Nowak et al. (2000), Pfannes et al. (2000), Popkov et al. (1999), Raikher and Stepanov (1995a), and Srivastava and Jones (1988). It is a non-trivial problem that consists in calculating the kinetics of a complex magnetic system, not just equilibrium properties.

Beyond isolated uniaxial particles. Several researchers have attempted to extend the fundamental envelope beyond isolated uniaxial particles with pre-defined supermoments. Raikher and Shliomis (1994) have reviewed the application of fundamental results to magnetic fluids. In addition to the important MC work cited above, other researchers have also attempted to calculate inter-particle interactions effects. Examples are provided by Kneller (1968) and by Song and Roshko (2000). Kalmykov and Titov (2000) and Coffey et al. (1998a) have treated non-axially symmetric particles. Chang et al. (1997) have described a way to go beyond the fixed supermoment two-level approximation. Victora (1989) has made an important link to measured properties by developing the concept of the time-dependent switching field. This is along the lines of Garanin's (1999) integrated relaxation time. Some authors have made first important steps in going beyond the coherent supermoment rotation model. New effects include domain wall nucleation (Broz et al. 1990) and non-uniform rotation (Braun 1993, Nowak and Hinzke 1999). Dormann et al. (1987) described the field dependence of the blocking temperature, thereby making another useful link to measurements.

Towards natural nanoparticle systems. I have already described the main physico-chemical features of real nanoparticle systems. Much theoretical work is still needed to

bring the kind of fundamental understanding that has been achieved for the uniaxial fixed-magnitude supermoment model towards including these real features. Ongoing theoretical work is needed in three areas of active present research. First, as described above, to continue expanding from the uniaxial fixed-magnitude supermoment picture towards piece-wise additions of more and more real features. Second, to continue developing our theoretical understanding of the measurement methods themselves, as discussed further above and below. Third, to develop methods that combine the various results from the latter two areas, using known approaches, in order to model and analyse the behaviors of real samples. I review advances in the third area, that attempts to make links between fundamental theoretical results and observed behaviors, below.

INTERPLAYS BETWEEN MAGNETISM AND OTHER SAMPLE FEATURES

In this brief section I attempt to make a list of the main physico-chemical features of a material that can have strong interplays with the magnetism of the material. With nanoparticles, the strength and nature of such an interplay or coupling may vary dramatically with size. The size itself, independently of anything else, is such a feature because of the SR and finite size effects on magnetic order already described above. Simply put, spontaneous magnetic order (i.e., spontaneous existence of some array of non-zero thermal average local ionic magnetic moments) is more difficult to establish in a small particle than in a bulk, effectively infinite, material. With nanoparticles, shape itself, independently of any other factor, is also such a feature because of the dipolar (Eqn. 4) and surface anisotropy (Eqn. 5) effects described above. Shape can also play a role in producing sample texture (i.e., non-randomness of particle orientations) which in turn affects inter-particle magnetic interactions.

Chemistry and structure via $\{\mu_i, K_i, J_{ij}(r_{ij})\}$

The other main features that couple strongly with magnetism, excluding exotic effects involving superconductivity, all fall into two categories: chemistry and structure. Indeed, mineral magnetic studies are geared towards extracting crystal chemical information from magnetic measurements and therefore rely on the following coupling mechanisms. In terms of its magnetism, a local moment system is completely specified by: the set $\{r_i\}$ of the vector positions of the PM cations, the set $\{\mu_i\}$ of local magnetic moment magnitudes on each of the PM cations, the set $\{K_i\}$ of local magneto-crystalline anisotropy constants and directions, and the set $\{J_{ij}\}$ of all inter-cation pair-wise magnetic exchange bonds. The electronic origins of these parameters are such that J_{ij} has a small dependence on inter-cation distance as $J_{ij}(r_{ij})$ and K_i has a small dependence on the positions and identities of neighboring cations. Indeed, excluding the relatively weak inter-cation dipolar interactions, the only dependence on $\{r_i\}$ is via $J_{ij}(r_{ij})$ and K_i. In the present context, one therefore asks how structure and chemistry affect or determine the set $\{\mu_i, K_i, J_{ij}(r_{ij})\}$ and how this in turn determines all the magnetic properties. The identity of cation-i is the main factor determining both μ_i and K_i and the identities of the interacting cations (i and j) and of the related superexchange anions are the main factors determining J_{ij}.

Chemical coupling to magnetism in nanoparticles

Bond and site disorder. Thermodynamic aspects of the interplay between chemical order and magnetism have been reviewed by Burton (1991), without consideration of size effects. Changing the degree of chemical order in a material changes the magnetic exchange bond topology of the network of interacting PM cations, thereby directly affecting the magnetism. For example, in a MFT description, the degree of chemical order determines the set $\{J_{ij}\}$, the sums in Equations (16) and (18), and all the magnetic

properties. With complete solid solution randomness, one has a random set $\{J_{ij}\}$ and one speaks of magnetic exchange bond disorder. If the exchange bonds are superexchange bonds, then the degree of anion order (or substitution) does indeed directly control the bond set $\{J_{ij}\}$ and the degree of exchange bond disorder. If, on the other hand, it is the cations that are distributed (or substituted), then in addition to exchange bond disorder there is also cation site disorder. That is, the magnetism is affected by correlated distributions of both exchange bonds and cation species that may have different magnetic moments and different local magneto-crystalline anisotropies. Pure site dilution occurs when one type of PM cation is substituted by a DM cation species (the magnetic equivalent of a vacancy), without any change in the anion network. Pure bond dilution is said to occur when exchange bonds are removed, without removing moment-bearing cations.

Magnetism affects chemistry. Given that chemical bond energies are much larger ($U_{ij} \sim 10^4$ K) than magnetic exchange bond energies ($J_{ij} \sim 1$ to 10^3 K), one might expect that chemical order can affect magnetic properties but not vice versa. In fact, the chemical bond differences that drive chemical order are comparable to magnetic exchange bond energies such that magnetic degrees of freedom can significantly affect chemical order-disorder effects and even induce chemical order in situations where chemical bonds alone would lead to randomness or even phase separation (Dang and Rancourt 1996). This, in turn, implies that the magnetic SR effect could induce a radial gradient of chemical order in a magnetic nanoparticles, in addition to the surface-induced purely chemical effects that could produce such gradients. In general, we must expect radial gradients of chemical order, defect densities, and composition that must have strong interplays with magnetic radial gradients. This is true of both equilibrium properties and quenched-in defects and configurations that do not evolve because of the slowness of diffusion at the temperatures of interest.

Surface diffusion faster than bulk diffusion. In the latter regard, it is important to keep in mind that lateral surface diffusion times are typically two orders of magnitude smaller than bulk inter-site diffusion or hopping times. This implies that when a particle is annealed it will repair its surface before it can repair its middle region. Since magnetism is very sensitive to surface conditions, one can observe significant changes in magnetic response as a function of annealing temperature (or annealing time) at temperatures far below chemical reaction or sintering temperatures.

Structural coupling to magnetism in nanoparticles

Low magnetic dimensionality effects. Magnetic dimensionality of a bulk material was described above, in the context of SR effects, as a structural feature that dramatically affects magnetism. By low dimensionality we mean that the J_{ij}s are such that they form chains or ribbons or planes instead of three-dimensional frameworks. Indeed, low dimensionality can suppress the occurrence of magnetic order, even with exchange strengths that would normally give large Curie or Néel points. This is because the interactive feedback provided by fewer interacting neighbors is not enough to counter thermal agitation and because novel excitations occur that are not quenched by low temperatures. In addition, the behavior of finite low dimensional systems can be significantly different from the behaviors of their infinite low dimensional counterparts. For example, a short AF chain with an odd number of PM cations gives rise to a large initial susceptibility at low temperatures whereas the infinite chain does not. For these reasons, nanoparticles made of materials that have low dimensional exchange bond networks have magnetic properties that are particularly sensitive to particle size (e.g., Rancourt et al. 1986).

Magnetic frustration effects. A phenomenon known as magnetic frustration can effectively lower the dimensionality or connectedness of an exchange bond network. For example, consider a chain of moments that interact via 1NN and 2NN exchange interactions only. Each cation has two 1NN bonds and two 2NN bonds and if the 1NN exchange bonds are FM whereas the 2NN bonds are AF and of equal magnitude ($J_{1NN} = -J_{2NN}$) then each cation is completely frustrated regarding its orientation that would minimize the magnetic energy. As a result, the cations respond to applied magnetic fields much as isolated cations would in a PM material, despite the presence of strong exchange interactions. In this example, the dimensionality has been effectively reduced from 1 to 0. If a nanoparticle is made of such a material that has magnetic frustration in its bulk structure, then the magnetism of the particle can be very sensitive to size because cations at or near the surface will have missing bonds and may be less frustrated than they would be in the bulk. As a result, the SR can be more strongly magnetic than the bulk of the particle. That is, thermal average cation moments near the surface can be larger than in the middle region of the particle. Similarly, chains and planes of cations that were frustration isolated in the bulk may become exchange coupled via an uncompensated edge effect in the nanoparticle. In the above discussion, frustration referred to the local moment experiencing a mean field of interaction of zero and not receiving conclusive instructions from its neighbors regarding the orientation that it should adopt. I call this site frustration. Frustration can also refer to magnetic exchange bonds that are not energetically satisfied (i.e., do not participate in lowering the energy of the system) in a magnetically ordered structure because the orientations of the relevant moments are determined by other exchange bonds. I call this exchange bond frustration.

Chemical origin of positional disorder. The degree of positional disorder or the degree of crystallinity or amorphousness, for a given composition or fixed compositional distribution, in a nanoparticle is an important structural feature that couples to the magnetism via $\{K_i, J_{ij}\}$. Much of the cation positional disorder comes from quenched-in disordered anion substitutions, such as (OH^-, OH_2) in authigenic oxyhydroxides. Much position disorder must also arise from cation chemical disorder, such as $(Fe,Al)^{3+}$ in alumino-oxides, in compliance with cation-anion bond length constraints and associated local anion types. Of course, positional disorder does not occur alone and the combination of several chemical and positional effects will lead to such striking nanoparticle phenomena as anticipated by Néel and recently described by Kodama (1999) and Berkowitz et al. (1999).

MAGNETIC AND RELATED TRANSITIONS AFFECTED BY PARTICLE SIZE

In this section, I briefly survey the different kinds of magnetic and related transitions that should or may be affected by particle size and shape. Transitions occur at special compensation or cooperative build-up points (critical temperatures, fields, compositions, or pressures, and at multi-critical points) where several factors conspire to give an abrupt change in physical state of the system. As such, it is expected that transitions will be particularly sensitive to particle size, not to mention intra-particle and surface conditions...

Defining the size effect question

When we ask whether a certain transition or property is affected by particle size, we generally mean "Would reducing the size of a bulk sample, without otherwise changing the material, eventually produces changes that are directly attributable to size?" The problem with this question is that it cannot be answered by experiment, for two main reasons. First, even with a pure and initially undisturbed piece of bulk material, the bond structure, chemical distributions, particle shape and size, etc., will relax, anneal,

reconstruct, redistribute, etc., to best minimize the free energy of the particle in its environment within the time available to it. Second, nanoparticles are not produced by cutting out perfect pieces of bulk material and are often nothing like their closest bulk counterparts, as amply discussed above. The classic examples are ferrihydrites, ferritin cores, and hydrous ferric oxides (HFOs) that exist only as nanoparticles and do not have known bulk counterparts. On the other hand, the question can be posed and answered by theoretical calculations or simulations and such studies can be useful in interpreting the results of experiments. It is in this context and perspective that I pose the question.

Classic order-disorder, spin flops, electronic localization, and percolation

The classic magnetic order-disorder transitions at which a PM cation-bearing material goes from a PM state to a FM or FI or AF or WF state, etc., at associated Curie or Néel or equivalent transition points, as temperature is decreased, are affected by particle size as already described above. Spin flop transitions, such as the Morin transition of hematite, should also be affected by particle size for sufficiently small sizes and this is reviewed below for the case of hematite. Electron localization or cooperative valence fluctuation transitions, such as the Verwey transition of magnetite, should be affected by particle size for sufficiently small particle sizes but there have been no systematic studies of this or theoretical estimates of the size effect. Magnetic percolation transitions refer to the percolation of infinite clusters of exchange coupled cations in bulk dilute magnetic materials. The concept of percolation (Essam 1980) has relevance to the Verwey transition in impurity-bearing magnetite (Marin et al. 1990, Aragon et al. 1993) and to dynamic and relaxation effects in solid solution magnetic materials (e.g., Chamberlin and Haines 1990). In small particles the concept must be revised in that the effective critical composition becomes the composition at which the mean cluster size of the bulk analogue becomes equal to the largest cluster that the particle can sustain. One should expect, therefore, that all properties that critically depend on percolation will be significantly affected by particle size and will exhibit a critical size anomaly or saturation point.

Frustration and magneto-strain effects

I have already described how magnetic frustration that directly results from the geometrical arrangements of exchange bonds, such as three equal AF exchange bonds between identical PM cations at the corners of an equilateral triangle that cannot all be simultaneously satisfied, can suppress a magnetic ordering temperature that would otherwise occur given the large magnitudes of the exchange interactions. It is easy to see how the surface of a nanoparticle could reduce frustration in the SR, thereby effectively allowing a higher degree of magnetic order to occur than would occur in the bulk. Another factor must be considered also. Perfect site frustration does not normally persist to low temperatures because the inter-cation separation dependence of J_{ij}, explicitly expressed as $J_{ij}(r_{ij})$, often will drive a spontaneous distortion of the lattice that will remove the site frustration and allow establishment of magnetic order, in the presence of residual bond frustration. Such cooperative magneto-strain transitions are expected to be sensitive to particle size since both strain and magnetic order exhibit surface-induced intrinsic radial distributions.

Magneto-volume effects

Magneto-volume effects refer to the balance between chemical bond energy inter-atomic separation dependence and magnetic exchange energy inter-moment separation dependence that, along with vibrational energy inter-atomic separation dependence, produces a resulting equilibrium distribution of inter-atomic separations in the material. Rancourt and Dang (1996) and Lagarec and Rancourt (2000) have developed the theory

of magneto-volume effects in local moment systems with some magnetic exchange bond frustration and varying degrees of chemical order. Clearly, all relevant aspects of the problem (i.e., nature of the chemical bonds, separation dependence of the exchange parameters, vibrational amplitudes and energies, presence of exchange bond frustration, degree of chemical order, etc.) and their interrelations are affected by particle size and the presence of the surface. As a result, a nanoparticle can be significantly expanded or contracted relative to its bulk counterpart and in a non-uniform way, depending on the details of the inter-atomic interactions and the size and shape of the particle. Matrix effects, including differential thermal expansion, can also play an important role via positive or negative effective pressures on the nanoparticle.

Exotic effects and transitions

Other important transitions and cooperative solid state effects that have a coupling to magnetism and that would be sensitive to particle size include: superconductivity, Jahn-Teller effects, photo-magnetic effects as in magnetic semiconductors, radiation-induced defect susceptibility and associated PM centres, and magnetic moment formation or stabilization effects. In the latter case, one departs from our simple ionic picture of fixed cation magnetic moment magnitudes and covalent-type superexchange interactions to venture into the metallic domain where conduction electrons may or may not form local magnetic moments corresponding to non-integer values of electron spins. Some metals, such as body centered cubic iron (α-Fe, $\mu_{Fe} \sim 2.2 \mu_B$, $T_C = 1043$ K), have stable and constant moment magnitudes up to and far beyond their magnetic ordering temperatures (Pindor et al. 1983) whereas others have weak local moments on the verge of stability or exhibit moment loss/formation transitions. Such exotic phenomena have recently been discovered in synthetic Fe-Ni alloys (Lagarec et al. 2001) and are relevant to meteoritic Fe-Ni phases where the nanoscale microstructure probably plays an important role (Rancourt et al. 1999b), as described below. They may also be relevant to geomagnetism?

OVERVIEW OF RECENT DEVELOPMENTS

Main recent developments in magnetic nanoparticle systems

Fundamentals of SP fluctuations. In the calculation methods section, I described the recent and ongoing flurry of activity in the area of fundamental calculations of the SP supermoment reversal fluctuations themselves and their dependencies on applied field, underlying magneto-crystalline anisotropy, etc. Such work is vital in that it links the main microscopic fluctuations that determine sample response and its time evolution to their fundamental causes and the associated particle features and material properties. All areas of science and technology that involve magnetic nanoparticles can only benefit from these fundamental advances.

Addressing inter-particle interactions. Another important recent development has been the explicit considerations of inter-particle dipolar interactions. In solid state magnetism as a whole, dipolar interactions have been largely ignored except for their acknowledged role in causing magnetic domain structures in bulk materials. This is because in bulk materials inter-cation dipole-dipole interactions are several orders of magnitude smaller than typical inter-cation exchange interactions. In nanoparticle systems, however, dipolar interactions are often the main inter-particle interactions and they are amplified by the presence of supermoments.

Detailed analyses using synthetic model systems. A third significant recent development, in terms of moving towards complete understanding of natural magnetic nanoparticle systems, has been the study of synthetic magnetic nanoparticle systems having controlled nanoparticle characteristics and controlled nanoparticle dilution or

number density in an inert matrix phase. Typically, such samples are frozen synthetic ferrofluids. These studies have often pushed the limit of analysis by including most needed realistic features, such as the dipolar interactions mentioned above, to model several different types of magnetic measurements and have provided interesting debates and clever insights.

Other continued recent advances include the explicit recognition and analysis of intra-particle complexity (e.g., Kodama 1999, Berkowitz et al. 1999) and the development of the measurement methods themselves and their underlying theoretical understanding (e.g., Victora 1989, Kodama and Berkowitz 1999, Pfannes et al. 2000). I present the above main areas of development and other key advances in the sections that follow. Readers should also note the comprehensive review by Dormann et al. (1997), in comparison with an earlier review (Dormann 1981).

Measurements on single magnetic nanoparticles

Some remarkable recent experiments involve measurements of SP fluctuations and time-resolved supermoment dynamics on single magnetic nanoparticles. Probably the first measurements on individual magnetic nanoparticles were performed by Awschalom et al. (1990) where a scanning tunneling microscope was used to deposit nanoparticles directly into the micro pickup coil of a SQUID alternating field susceptometer. The measurements were performed at ultra-low temperatures (~20 mK) where SP fluctuations are quenched out and MQT of the supermoment can occur. The results were found to be "difficult to reconcile ... with the current theoretical picture of magnetic MQT". This first work lead to several more studies using either magnetic force microscopy (MFM) or micro-SQUID methods.

Wernsdorfer et al. (1997a) performed the first magnetization measurements of single nanoparticles in a range of low temperatures, thereby providing direct observations of SP supermoment reversals and quantitative verifications of the Néel-Brown SP model (Eqn. 2) and the Stoner-Wohlfarth reversal mechanism. Measured hysteresis curves and switching fields were like theoretical textbook examples of the predictions arising from Equation (2) and its underlying assumptions. This study provided a first direct evaluation of the attempt frequency pre-factor of Equation (2) which was found to be $1/f_o \sim 4 \times 10^{-9}$ s for an ellipsoidal single-crystal face centered cubic Co particle having a mean diameter 25 ± 5 nm.

At the lowest temperatures, Wernsdorfer et al. (1997b) found that deviations from the Néel-Brown model of SP fluctuations were in quantitative agreement with magnetic MQT models in the low dissipation regime. They briefly reviewed past attempts to measure magnetic MQT phenomena on individual nanoparticles and discussed the various processes that have been pointed out to cause MQT-like effects. In particular, MQT-like artefacts are more likely in many-particle systems such that MQT observations in bulk or many-particle samples (Awschalom et al. 1992, Gider et al. 1995, 1996; Ibrahim et al. 1995, Tejada et al. 1996, Sappey et al. 1997b) must be analysed with care (Kodama and Berkowitz 1999), although single-crystal samples of molecular clusters (Thomas et al. 1996, Friedman et al. 1996) may not suffer from these difficulties. Theoretical developments in the area on magnetic MQT phenomena are ongoing (e.g., Barbara and Chudnovsky 1990, Stamp 1991, Politi et al. 1995, Hartmann-Boutron et al. 1996, Pfannes 1997).

Bonet et al. (1999) performed the first three dimensional switching field measurements on individual magnetic nanoparticles of barium ferrite in the size range 10-20 nm. They showed conclusively that the total anisotropy energies of such particles of hexagonal symmetry could not be modelled as uniaxial but that a hexagonal anisotropy

term needed to be added to the principle uniaxial term. These authors indicated the possibility of exploring the underlying physics of the pre-exponential factor f_0 and its relation to the total anisotropy energy function in individual particles, thereby opening the way to quantitatively test the most recent models of SP fluctuations described above, without the almost unbearable complexities associated with ensembles of nanoparticles and their distributions of properties and inter-particle interactions.

Acremann et al. (2000; Miltat 2000) recently reported picosecond time-resolved imaging of the precessional motion of individual supermoments, in response to sudden applied field changes, measured using a vectorial Kerr effect laser system. Such measurements allow one to compare the classical motion of the supermoment to well established classical models of its dynamics. In this way, the validities, necessities, and magnitudes of various damping and noise terms in the classical equations can be evaluated by comparing predicted and measured time evolutions.

Synthetic model systems of magnetic nanoparticles

Synthesis methods. Synthetic nanoparticles can be made by several quite different methods including: scanning tunnelling microscopy deposition, evaporative deposition and masking, molecular beam epitaxy, arc discharge, electron beam evaporation, gas phase condensation, laser annealing, mechanical alloying methods such as ball milling, particle irradiation-induced phase separation, nuclear implantation methods, and a great variety of wet chemical methods such as those involving ion exchange, molecular intercalation, precipitation, Langmuir-Blodgett films, micelle and reverse micelle syntheses, etc. Other fabrication methods involve growing organisms, in controlled growth media, that produce biogenic particles or, for example, using organic components such as the ferritin polymer shell as templates for particle growth. The wet chemical methods are generally those most accessible to large numbers of researchers and they often more closely mimic natural synthesis routes, in aquatic environments in any case.

Simplified model systems. Wet chemical methods have been developed that provide single crystals or polycrystals of identical nanoparticles or molecular clusters. Organometallic clusters (e.g., Van Ruitenbeek et al. 1994) constitute one example where identical individual euhedral nanocrystals of metallic atoms (typically $10-10^3$ atoms per nanocrystal) are surrounded by organic ligands and assembled into macrocrystals or polycrystalline powders. These are ideal for studying size and surface effects in metallic nanosystems. Molecular clusters (e.g., Gatteschi and Sessoli 1996) tend to be smaller (typically 2-20 cations per cluster) and are systems where the metal cation centers are covalently bonded via coordinating anions or organic groups that propagate inter-cation magnetic exchange interactions. Molecular clusters have the remarkable attributes that all clusters in a sample are identical and that they can form single crystals where the relative positions and orientation of the clusters are known. One the other hand, they are unlike many natural systems that have larger nanoparticles, distributions of particle sizes, shapes, and types, and distributions of particle positions and orientations. Reverse micelle synthesis appears to provide the possibility of continuously varying the the particle size in the 4-15 nm range with narrow size distribution widths of ~9% (Liu et al. 2000). Intercalation or ion exchange into zeolites, clay minerals, layered hydroxides, and graphite offer many other possibilities for nanoparticle synthesis.

Model systems of Fe oxides and oxyhydroxides. From an environmental and magnetic nanoparticle perspective and given the importance of Fe (Table 1), it is the Fe oxides and oxyhydroxides that are of greatest interest to us here and, fortunately, these systems have been at the center of much recent work, mainly involving precipitation syntheses, directly aimed at understanding the magnetic properties of realistic model

systems. Examples of magnetic nanoparticle studies and reviews involving specific Fe oxides or oxyhydroxides (synthetic, natural, and biogenic) are as follows: (1) magnetite, Fe_3O_4 (Sharma and Waldner 1977, Kirschvink et al. 1989, 1992; Luo et al. 1991, El-Hilo et al. 1992a,b; Popplewell and Sakhnini 1995, Balcells et al. 1997, Hayashi et al. 1997, Malaescu and Marin 2000, Golden et al. 2001, van Lierop and Ryan 2001, Morris et al. 2001), (2) maghemite, γ-Fe_2O_3 (Bacri et al. 1993, Chaput et al. 1993, Parker et al. 1993, Morup and Tronc 1994, Dormann and Fiorani 1995, Jonsson et al. 1995a, 1997, 1998, 2000; Morup et al. 1995, Dormann et al. 1996, 1998a,b; Gazeau et al. 1997, Moskowitz et al. 1997, Sappey et al. 1997a, Svedlindh et al. 1997, Vaz et al. 1997, Fiorani et al. 1999), (3) hematite, α-Fe_2O_3 (Kundig et al. 1966, van der Kraan 1971, Rancourt et al. 1985, Amin and Arajs 1987, Ibrahim et al. 1992, Morup 1994a, Hansen et al. 1997, Dang et al. 1998, Suber et al. 1998, 1999; Vasquez-Mansilla et al. 1999, Bodker and Morup 2000, Bodker et al. 2000, Hansen and Morup 2000, Zysler et al. 2001), (4) ferrihydrite or hydrous ferric oxide (Van der Giessen 1967, Coey and Redman 1973b, Madsen et al. 1986, Lear 1987, Quin et al. 1988, Murad et al. 1988, Cianchi et al. 1992, Pankhurst and Pollard 1992, Pollard et al. 1992, Ibrahim et al. 1994, 1995; Zhao et al. 1996, Mira et 1997, Prozorov et al. 1999, Seehra et al. 2000, Rancourt et al. 2001b), and (5) ferritin cores (Bauminger and Nowik 1989, St-Pierre et al. 1989, 1996; Awschalom 1992, Dickson et al. 1993, Hawkins et al. 1994, Tajada and Zhang 1994, Gider et al. 1995, 1996; Friedman et al. 1997, Makhlouf et al. 1997b, Moskowitz et al, 1997, Sappey et al. 1997b, Tajada et al. 1997, Allen et al. 1998, Gilles et al. 2000). Key aspects of these studies are described below.

Inter-particle interactions and collective behavior

Phenomenological models. The recognition of the importance of inter-particle interactions in describing the field-induced responses of magnetic nanostructured materials and their theoretical description by Preisach (1935) predate the discovery of superparamagnetism. The status of such early mean field models of inter-particle interactions was reviewed by Wohlfarth (1964) and by Kneller and Puschert (1966). Phenomenological Preisach models still form the basis of powerful current approaches for handling the effects of inter-particle interactions (e.g., Spinu and Stancu 1998, Stancu and Spinu 1998, Song and Roshko 2000). These calculations are mainly concerned with modelling measured relaxation and response behaviors using phenomenological parameters, without much concern for the nature of the collective ordered state that can be induced by interactions or the nature of a possible phase transition to such a collective state.

Dipolar interactions and SG behavior. Given the significant progress described above in dealing with the disordered interacting magnetic systems known as SGs, many researches have recently examined inter-particle interaction effects with this perspective, based on classic SG results (e.g., Chalupa 1977, Omari et al. 1983), using synthetic model systems. Several authors have written critical reviews of this recent approach (Morup 1994b, Dormann et al. 1997, Hansen and Morup 1998, Fiorani et al. 1999). Luo et al. (1991) were among the first to take this modern perspective, in describing the behavior of their ferrofluid of 5.0 ± 1.6 nm shielded magnetite particles. This launched significant activity along these lines, using carefully prepared synthetic model systems in which inter-particle interactions were varied by controlling particle dilution and type (El-Hilo et al. 1992a, Morup and Tronc 1994, Morup 1994a, Dormann and Fiorani 1995, Jonsson et al. 1995b, 1998a,b; Ligenza et al. 1995, Morup et al. 1995, Bitoh et al. 1996, Dormann et al. 1996, 1998a,b; Scheinfein 1996, Vincent et al. 1996, Djurberg et al. 1997, Hansen and Morup 1998, Mamiya et al. 1998, Fiorani et al. 1999, Prozorov et al. 1999, Garcia-Palacios and Svedlindh 2000, Kleemann et al. 2001), that had been anticipated by

Morup et al. (1983), Fiorani et al. (1986), Dormann et al. (1988), Rancourt et al. (1990a,b), and others.

The above examinations from the SG perspective have lead to a consensus that dipolar coupled nanoparticles with disordered spatial arrangements have several characteristics in their non-equilibrium responses to applied fields that directly stem from the dipolar interactions and that are typical of multi-state free energy structures. On the other hand, it seems that there may be significant differences with canonical SGs in that divergences associated with a SG transitions do not occur (e.g., Dormann et al. 1988). The latter point is one of debate, as it was with the alloy SG systems. The next question is "What happens if there are inter-particle exchange bridges, in the common cases of dense arrays of nanoparticles?" Kleemann et al. (2001) interpret the behavior of their dense particle system in terms of a superferromagnetic (SF) transition, driven by inter-particle exchange interactions, followed by a reentrant super-SG transition as temperature is lowered and weaker dipolar interactions become relevant.

Exchange bridges and superferromagnetism. This brings us to the concept of superferromagnetism. The effects of inter-particle interactions are clearly seen in the Mössbauer spectra of magnetic nanoparticles, although the actual spectral analysis and interpretation is complicated (more below). Certain Mössbauer spectral features were first attributed to inter-particle interactions and associated phenomena first termed "superferromagnetism" independently by Morup et al. (1983) and by Rancourt and Daniels (1984). Morup et al. attributed variations in hyperfine field distributions (HFDs) to mean interaction fields and proposed the existence of a spontaneous ordered supermoment state, the SF state. Rancourt and Daniels used the term to mean any effect, such as inter-particle interactions and exchange anisotropy, that could locally cause $\tau_+ \neq \tau_-$ (Eqn. 9), thereby changing the fluctuation-dependent lineshape. Both Rancourt (1988) and Morup (1994b) have further explained their positions. Both authors agree that the term superparamagnetism should be reserved for magnetic effects resulting from inter-particle interactions, specifically, a spontaneous ordered state called the SF state. Explicit theoretical calculations of exchange bridge coupled SF systems and quantitative comparisons with magnetic measurements on synthetic model systems were provided by Rancourt (1985, 1987) and Rancourt et al. (1986).

Noteworthy attempts at dealing with nanoparticle complexity

In this section, I describe some classic and recent examples of studies in which the authors have made noteworthy attempts to deal with the complexities of real nanoparticle systems. The difficulties have been outlined above. In these examples, the authors have provided in depth quantitative analyses of data from several types of measurements on several samples, in an effort to identify or demonstrate key needed physico-chemical characteristics of the samples and to show how these affect measured properties. The selection of works is only meant as an illustration of promising approaches. I also include some examples of theoretical work aimed at understanding particular measurements themselves in application to magnetic nanoparticles.

Early classics. I must first emphasise that the early comprehensive studies of Stoner and Wohlfarth (1948) and Néel (1949a) have retained their validity and remarkable insight. Their rigorous and lucid theoretical developments are recommended to anyone wishing to understand the magnetic properties of environmental materials. They lay the foundations for modeling time, temperature, and field dependent magnetic measurements of small particle systems with broad distributions of particle sizes. Another such classic paper is that of Gittleman et al. (1974) who showed how the initial and alternating field susceptibilities could be modeled. The following examples are a subset of the many high

quality papers published in the last 10 years or so, excluding the important works already mentioned in the sections above and below.

Molecular cluster system. Barra et al. (1996) studied an eight Fe atom molecular cluster systems by ESR, alternating field susceptometry, and Mössbauer spectroscopy. The system has the great advantages of molecular cluster model systems: There is only one particle size and type, the particles are arranged on a known regular lattice, and the particle or molecular structure is known. Combining alternating field susceptometry with Mössbauer spectroscopy allowed the SP relaxation time to be followed over six orders of magnitude in frequency as temperature was varied. A value of the pre-exponential frequency factor (Eqn. 2) could thereby be obtained as $1/f_o = 1.9 \times 10^{-7}$ s. This may be the first such combination of alternating field susceptometry and Mössbauer spectroscopy to obtain dynamic information in a nanoparticle system but the procedure is well known (e.g., as discussed and reviewed by Rancourt 1987) in one dimensional magnetic soliton systems, that can be considered one dimensional nanoparticle systems. The first use of Mössbauer spectroscopy to measure SP fluctuation frequencies in a nanoparticle system by dynamic lineshape analysis was made by Rancourt et al. (1983, 1985) and described by Rancourt and Daniels (1984).

Magnetic viscosity and distributions. Barbara et al. (1994) made an in depth study of the field and temperature dependencies of the magnetic viscosity S(T,H) of well characterized Ba-ferrite nanoparticles. They expressed $S(T,H) = dM(T,H)/d\ln(t)$ in terms of the distributions of particles sizes, P(v), and of switching fields, $P(H_o)$, (H_o given by Eqn. 8) and showed that these were the main required distributions. P(v) was imposed by detailed transmission electron microscopy measurements and $P(H_o)$ was obtained from the extrapolated T = 0 K hysteresis cycle. In this way, the intricate behaviors of S(T,H) were quantitatively modeled without any free parameters. This impressive study shows the extent to which the time dependence of the magnetization of non-interacting nanoparticles can be understood in terms of the underlying distributions of relevant particle characteristics.

Alternating field susceptibility and intra-barrier fluctuations. Svedlindh et al. (1997) have presented a comprehensive description of the real and imaginary (i.e., driving frequency linear response and phase shift) parts of the alternating field susceptibilities of non-interacting nanoparticle systems having distributions of axial barrier energies and associated particle size distributions. They have critically reviewed previous work, including the classic paper of Gittleman et al. (1974) and the various methods for obtaining particle size distributions from alternating field susceptometry. They present convincing arguments that the alternating field susceptibility is sensitive to both near anisotropy axis intra-potential well supermoment fluctuations and the SP inter-well reversals described by Equation (2), not just the usual SP fluctuations (Eqn. 2) and an average perpendicular term. They are able to extract the separate frequencies of the two types of fluctuations first described by Néel.

Alternating field susceptibilities and inter-particle interactions. Jönsson et al. (2000) have made an exemplary analysis of the linear and cubic ($M = \chi H + \chi_3 H^3 + \dots$) alternating field susceptibilities of non-interacting and interacting nanoparticles. Inconsistencies between the linear and cubic susceptibilities of non-interacting particles were interpreted as evidence for a more than axial structure of the barrier potential (Garcia-Palacios and Lazaro 1997) or an inadequate description of the intrinsic SP damping constant (that enters in the theoretical determination of f_o in Eqn. 2). The effects of inter-particle dipolar interactions were clearly recognized and characterized. Similarities with the behaviors of canonical SG systems were demonstrated and the key difference of the lack of a SG ordering divergence was again noted (Fiorani et al. 1986,

1999; Dormann et al. 1988). This is in contrast to an earlier paper by Jonsson et al. (1998) who report the first SG divergence transition in a dipolar interacting nanoparticle system. Jönsson et al. (2000) argued against the approach developed by Dormann and co-workers (see review, Dormann et al. 1997, and Dormann et al. 1998a,b) that has the main effect of inter-particle interactions modeled via an average interaction field that shifts the barrier energy distribution to larger energies thereby increasing the SP relaxation times. A similar approach was developed by Morup and Tronc (1994) and further advanced by Hansen and Morup (1998). Jönsson et al. (2000) argue that the low temperature magnetic relaxation of interacting nanoparticles is "dominated by collective particle dynamics" and "cannot be reduced to that of non-interacting particles shifted to longer time scales".

Constant field magnetometry and distributions. Sappey et al. (1997a) have made a thorough analysis of ZFQ-FW-FC and TRM curves for non-interacting nanoparticles with particle size distributions. They demonstrated the dependence of these curves, including the temperature T_{peak} of the peak in a ZFQ-FW curve, on the particle size distribution and showed that anomalous increases in T_{peak} as applied field is increased can arise from an effective field-induced broadening of the energy barrier distribution, rather than from MQT effects as sometimes claimed. The authors introduce a reverse-field TRM measurement procedure that has some advantages over standard methods and provide a lucid discussion of all such constant field magnetometry measurements, in the case of non-interacting (highly dilute) nanoparticles. El-Hilo et al. (1992a) and Vincent et al. (1996) have provided detailed analyses of how inter-particle interactions affect and participate in determining T_{peak} in less dilute systems. See also the review by Dormann et al. (1997) and the tentative mean field discussion by Morup (1994b).

Curie-Weiss behavior and interactions versus barriers. El-Hilo et al. (1992b) have made a thorough examination of the Curie-Weiss behaviors (e.g., Eqn. 17) of the high-temperature ($T > T_{peak}$, θ_{CW}) constant field initial susceptibility of non-interacting and interacting nanoparticles. Extending the works of Gittleman et al. (1974) and others, they find that distributions of barriers arising from distributions of particle sizes in non-interacting systems give rise to negative effective Curie-Weiss temperatures, T_{0B}, and that interacting systems have effective Curie-Weiss temperatures that combine a negative T_{0B} contribution and a positive contribution, T_{0i}, arising from the inter-particle interactions. In systems where the barrier term dominates at the lower temperatures but becomes smaller at the higher temperatures, one obtains breaks in the χ_0^{-1} versus temperature curves, with separate temperature ranges giving different T_{0B} and T_{0i} intercepts. This illustrates the care that must be taken in interpreting high temperature initial susceptibility results. I would add that at still higher temperatures (or not higher is some systems) one must cross over to the true PM behavior of independent ionic moments and an ionic value of θ_{CW} (e.g., Eqns. 16-17).

High-field non-isotropy effects. Gilles et al. (2000) have made a detailed study of artificial ferritin nanoparticles, combining high field and low field constant field magnetometry and Mössbauer spectroscopy. Novel features include an attempt to give a dynamic lineshape interpretation to Mössbauer spectra in the blocking transition region and a thorough analysis of the non-Langevin high-field behavior of the supermoment susceptibility. They show that at high fields it becomes important to treat the SP fluctuations as occurring between the easy directions of the particles rather than as isotropic fluctuations, as assumed in the classic Langevin derivation. This is expected to be important in all studies involving high and moderate applied fields.

Theory of measurements and processes. Finally, a few theoretical studies can be mentioned, in addition to the contributions cited above, in the present context of dealing with the complexities of real nanoparticle systems. Yelon and Movaghar (1990) made

some general deductions, about the relationship between the barrier energy and the pre-exponential factor or attempt frequency in equations of the type of Equation (2), that should be examined further in the context of SP particles. Pfannes et al. (2000) have proposed calculations of the SP fluctuation times that depart from the Néel-Brown coherent rotation picture and explicitly include coupling to the phonon spectrum of the particle. They have made a fundamental link to the Mössbauer spectral interpretation for SP and SF nanoparticles proposed by Rancourt and Daniels (1984) and discussed in the next subsection. Kliava and Berger (1999) have provided an elegant analysis of the ESR spectra of non-interacting nanoparticles with broad distributions of sizes and shapes. As mentioned above, Kodama and Berkowitz (1999) (and as reviewed by Kodama 1999 and Berkowitz et al. 1999) have provided lucid numerical analyses of various intra-particle and SR defects and their effects.

Interpreting the Mössbauer spectra of nanoparticle systems

Pervasiveness of dynamic effects. [57]Fe Mössbauer spectroscopy is potentially one of the most powerful methods for studying Fe-bearing nanoparticles because, in addition to being sensitive to several local crystal chemical and magnetic features, it is also sensitive to fluctuations in the local hyperfine interactions in a broad characteristic time window (10^{-6} to 10^{-10} s, or so) centered around the measurement time (Rancourt 1988). This means that SP supermoment reversal times (τ_+ and τ_- of Eqn. 10) can be measured directly, as functions of temperature and applied field and for different samples. The Mössbauer spectra arising from such dynamic or relaxation effects are quite different from the classical multiplets (singlets, doublets, sextets, and octets) that arise from the static limit (see above discussion) and the relevance of this to nanoparticle applications of Mössbauer spectroscopy has unfortunately generally not been recognized.

Dominant spectral analysis paradigm. Possibly the first suggestion that dynamic spectral effects are important in nanoparticles was made by van der Kraan (1971) who cited the early relaxation lineshape models of van der Woude and Dekker (1965a,b) and Wickman et al. (1966). This idea was not followed up until much later and has only very rarely been effectively applied in the analysis of Mössbauer spectra of nanoparticles. Instead, most authors followed the lead provided by the outstanding early work of Kündig et al. (1966) who divided the Mössbauer spectra of samples having broad distributions of particle sizes into two subspectra: a doublet for those particles in the sample that are SP and a sextet for the larger particles that are blocked. This approach neglects the spectral contribution from intermediate size particles ($v \sim v_{SP}$; Eqn. 3) that have $\tau \sim \tau_m$ and transitional type or relaxation type spectra, the possible effects of dwell time values (τ_+ and τ_-) on the sextet subspectrum, and the possible effects of dwell time (τ) on the doublet subspectrum. Nonetheless, this approximation should be valid for sufficiently broad distributions of barrier energies (E_b in Eqn. 2) and sufficiently large values of f_o (Eqn. 2) for the resulting distributions of SP fluctuation times to mainly contain $\tau \gg \tau_m$ and $\tau \ll \tau_m$ values. It proved to be applicable for many samples and allowed a particle size distribution to be extracted from the temperature dependence of the spectral area ratio of the doublet and sextet subspectra (Kündig et al. 1966). Unfortunately, it also became a spectral interpretation paradigm that until today has not been superseded.

Collective magnetic excitations. In the face of various inadequacies of the above interpretation paradigm, ingenious and physically reasonable additional physical mechanisms were proposed (and widely accepted) to explain the main anomalous features. One anomaly was that the hyperfine magnetic field spitting (see above) at low temperatures was usually found to be somewhat smaller than that of the corresponding bulk material. Morup et al. (1976) proposed that this was due to the thermal reduction of

the average supermoment arising from relatively rapid intra-barrier fluctuations. That is, supermoment fluctuations in orientation within a minimum of the potential energy curve (Eqns. 4-6), occuring during the dwell times between supermoment reversals. This phenomenon was termed collective magnetic excitations (CMEs). This mechanism assumes both that the supermoment intra-barrier fluctuations are coherent fluctuations of the supermoment orientation, rather than arising from single-ion or spin wave excitations (that are assumed to be the same as in the corresponding bulk material), and that the local average ^{57}Fe hyperfine field is effectively static and directly proportional to the CME average. The main problems with the first assumption are (1) that the supermoment fluctuations are not simple coherent fluctuations of orientation but include magnitude fluctuations from the relevant single-ion and spin wave fluctuations and (2) the single-ion and spin wave fluctuations may be significantly different from those in the bulk material and these differences can be the dominant causes of local average hyperfine field reduction. The main problem with the second assumption is that the local fluctuations of the hyperfine field arising from all the relevant collective and single-ion excitations, although expected to be very fast compared to both the measurement time and τ (Eqn. 2), as assumed, may not be the only fluctuations to affect the resulting lineshape. Indeed, Rancourt and Daniels (1984) have shown that relaxation lineshapes with SP characteristic times $\tau_+ \neq \tau_-$ can lead to sextet patterns having reduced hyperfine field splittings under the most common circumstances involving ensembles of nanoparticles. In other words, reduced magnetic hyperfine spittings are often not directly related to fast averaging processes.

Distributions of static hyperfine fields. Another difficulty of the dominant spectral analysis paradigm is that the Mössbauer spectra of nanoparticle samples often have sextet contributions or subspectra that are significantly different from the static sextets expected from blocked particles of the bulk material, having much broader and asymmetric absorption lines. Morup et al. (1983) proposed that this arose from inter-particle interactions, as follows. The interactions in a sample of positionally disordered nanoparticles would give rise to a broad distribution of different average interaction field magnitudes (e.g., Eqn. 19 applied to supermoments) that, in turn, would cause a broad distribution of average supermoments, each supermoment having a thermal average in accordance with the average interaction field that it experiences. The supermoment averages were taken to give rise to a distribution of average local hyperfine fields by assuming an effectively instantaneous coupling of the supermoment and the hyperfine field. Consequently, the sextet components were analysed in terms of distributions of static hyperfine field magnitudes or HFDs. This has become the dominant method for analysing the sextet components of the spectra of nanoparticle samples. The underlying assumptions and the analysis method itself are often referred to as superferromagnetism. The most tenuous underlying assumption here is that all supermoment fluctuations are fast enough for static sextet lineshape components to be used and distributed to account for the observed absorption spectra. The extracted HFDs are extracted to obtain agreement with measured spectra and have not been put on a firm theoretical basis. Indeed, most estimates of f_o (10^6 to 10^{11} Hz) suggest that the usual barrier energy values should give rise to SP fluctuation times that are within the dynamic effect measurement window. Inter-particle interactions are important but they need not give rise to static HFDs.

Anisotropic fluctuation lineshapes. Rancourt and Daniels (1984) showed that the τ_+ and τ_- values that arise from typical interaction fields, with typical values of f_o, give dynamic lineshapes of sextets having broad and asymmetric absorption lines similar to the observed ones in many nanoparticle systems. This suggests that the often extracted HFDs are artefacts of an incorrect spectral analysis. One difficulty that inhibited the

application of dynamic effect lineshapes to nanoparticle systems was that isotropic fluctuation lineshape models (with $\tau_+ = \tau_-$) gave predicted lineshapes that were very different from observed spectra. Rancourt and Daniels (1984) demonstrated that anisotropic fluctuation lineshape models (with $\tau_+ \neq \tau_-$) give dramatically different lineshapes than those predicted by isotropic models and that the window of characteristic times inside of which dynamic spectral effects could be detected was much larger than previously thought. See Rancourt (1988), Rancourt (1998), and section 3 of Rancourt and Ping (1991) for further discussion. Rancourt et al. (1983, 1985) were the first to use dynamic effect lineshapes to directly extract SP fluctuation times and interaction field magnitudes from the Mössbauer spectra of nanoparticle samples.

Other dynamic lineshape attempts. Hansen et al. (2000) used an isotropic fluctuation model for the partially collapsed doublet contributions in their Mössbauer spectra while retaining a HFD analysis for the sextet contributions. I would argue, as above, that the sextet contribution is being incorrectly interpreted. Van Lierop and Ryan (2001) used distributions of various particle properties and isotropic fluctuations to model their spectra. I would argue that their restriction to isotropic fluctuations is not justified. Pfannes (1997) made a theoretical analysis that considered only isotropic fluctuations in describing the Mössbauer spectra. Pfannes et al. (2000) later gave a theoretical analysis that stresses the importance of anisotropic fluctuations and questions the validity of CMEs. Gunther et al. (1994) discussed relevant features related to the isotropic fluctuation effects of non-interacting particles. St-Pierre et al. (1987) and Gilles et al. (2000) used an interpretation model that admits anisotropic fluctuations ($\tau_+ \neq \tau_-$) but that assumes $\tau_+, \tau_- \ll \tau_m$ and an associated absence of dynamic lineshape effects. Such assumptions that are used to justify a static analysis approach should always be substantiated when dealing with nanoparticles. Finally, I have already mentioned the interesting work of Barra et al. (1996) who extracted isotropic fluctuation times, for monodisperse non-interacting molecular clusters, that correlated with those extracted from alternating field susceptibility measurements.

Clearly, there is much room for improvement in the analysis of the Mössbauer spectra of nanoparticle systems. One can only hope that the tendency to adopt unjustified simplifying assumptions, in the face of admittedly somewhat overwhelming complexity, will be gradually overcome. A recommended approach is to insist that the same model produce agreement with many different measurements from several measurement methods, including methods having measurement times that are comparable to the expected characteristic times, and to apply as many rigorously valid theoretical constraints as possible.

Needed areas of development

Intra-particle crystal chemistry. Environmental nanoparticles are expected to have intra-particle radial distributions and inhomogeneities involving various coordinating anion substitutions, cation substitutions, vacancies, surface complexed groups, etc. For example, the Al, Mn, and Fe oxyhydroxides are expected to have significant (O^{2-}, OH^-, OH_2) substitutions with various charge balancing mechanisms involving vacancies, cation substitutions, and surface non-stoichiometry. This chemical disorder is expected to modify the bond lengths, bond angles, and most particle properties more than the purely nanocrystalline effects arising directly from small size alone, yet it is rarely measured directly at the single particle scale. Mineral magnetic properties are expected to be very sensitive to these features and first principles electronic structure calculations can be used to predict the relevant magnetic and intra-particle crystal chemical interplay.

Electronic structure calculations. A promising direction is to use first principles

ESCs that are well suited to dealing with magnetic and finite size clusters. The needed codes are rare because most advanced methods either deal with infinite crystalline inorganic materials using periodic boundary conditions or organic molecules that are DM and do not contain transition metals. Particularly promising methods are the spin-polarized molecular orbital calculations in the local density approximation (Grodzicki 1980, Blaes et al. 1987). For example, this method has been applied to the study of biologically relevant polynuclear clusters where intra-cluster magnetic interactions have a direct bearing on charge transfer functionality (Kröckel et al. 1996). Such methods could be used to predict relative stabilities, surface chemical reactions, spectroscopic properties, microscopic and macroscopic magnetic properties, etc., of environmentally relevant nanoparticles.

Dipolar interactions. Inter-particle interactions are important and are often dipolar in nature. These interactions have, to date, not been modeled correctly. Realistic calculations must include both the spatial distributions of average dipolar interaction fields (Eqn. 19) and the temporal fluctuations of the local dipolar interaction field. The latter fluctuations must have characteristic times that are comparable to the SP fluctuation times of the particles since the interaction field is directly caused by the neighboring times of the particles since the interaction field is directly caused by the neighboring supermoments. Indeed, for this reason, the concept of an interaction field must be replaced by a proper handling of inter-particle spatial and temporal correlations. This will determine the dynamics in assemblies of interacting particles and has not yet been attempted.

Integrated multi-method studies. As is true in many areas of natural science, there is a need for an integrated approach combining several measurement and theoretical methods and involving systematic studies of both natural and synthetic samples. The high resolution TEM, with its associated methods (EDS, CBED, SAED, EELS) goes a long way in this respect but suffers from the small size of the subsample. It must be combined with whole-sample diffraction, spectroscopy, and bulk property measurements, in order to deal with the macroscopic sample distributions. There is a great need for organized groups of experts to share the same samples and, if possible, to provide reference materials to other groups. Magnetism, in particular, is sensitive to several sample features that are not easily detected by other methods.

Development and application of mineral magnetism. Mineral magnetism, including measurements over broad temperature and applied field ranges and using measurement methods with vastly different measurement times, needs to be developed for and applied to environmental, geochemical, geological, and space nanomaterials, as stressed in this chapter. More controlled syntheses that model the materials of interest are needed. Further development of the underlying theory for the various measurement methods is vital. The case of Mössbauer spectroscopy has been described above. Further developments of the fundamental theory of the physical properties of nanoparticles are needed, with continued inclusion of more and more realistic crystal chemical features. Explicit inclusion of interparticle magnetic interactions is of interest.

Diffraction theory of nanoparticles. Bulk nanoparticle sample powder diffraction, including X-ray diffraction, neutron diffraction, synchrotron-based anomalous scattering, and electron diffraction, needs to be developed to explicitly treat nanomaterials. The standard crystallographic approach to work from the infinite crystal limit towards small-particle size effects is not appropriate for nanoparticles, where it is no longer useful or mathematically justified to divide the diffraction pattern into separate Bragg reflections. Instead, a Debye formula approach can be used in which one explicitly includes positional and chemical disorder and site-specific Debye-Waller factors. Here, the term "site" refers to the position in a given cluster rather than to a crystallographic site. This

approach is also valid, using the appropriate ionic magnetic form factors, for modeling the magnetic neutron scattering of nanomaterials.

Mössbauer spectroscopy. The inclusion of anisotropic fluctuations, modeled as $\tau_+ \neq \tau_-$ in uniaxial symmetry, in the presence of applied magnetic fields, exchange anisotropy, or inter-particle interactions, must be used as a starting assumption unless the more restricted assumption that all relevant fluctuations are much faster than the measurement frequency (τ_+, $\tau_- \ll \tau_m$, in uniaxial symmetry) is justified independently. All other relevant realistic features (distributions of characteristics and properties!) must also be included, by applying as many justified theoretical constraints as possible.

EXAMPLES: CLUSTERS, BUGS, METEORITES, AND LOESS

In this section, I give brief descriptions of a few case studies of magnetic nano-materials that I have been involved with, with reference to related works.

Two-dimensional nanomagnetism of layer silicates and layered materials

Two-dimensional magnetic materials have one dimension that is reduced to the nanoscale. That is, magnetic exchange interactions exist only within layers and do not propagate between layers. In-plane chemical inhomogeneity can then cause further subdivision to produce nanoscale two-dimensional magnetic clusters. The layer silicates are such materials where Fe^{2+} and Fe^{3+} are almost the only PM cations that are mainly confined to the octahedral sheet, except Fe^{3+} that can occupy tetrahedral sites (Rancourt et al. 1992). In addition, as clay minerals, layer silicates can also approach nanoparticle sizes and may sometimes form from nanomaterial precursor phases such as Si-bearing HFOs (Rancourt et al. 2001b).

Given their platy habits, layer silicates such as biotite play an important role in determining the magnetic fabrics of rocks, both because of their easy-plane paramagnetism and because they often contain stoichiometric magnetite micro-inclusions. The latter petrogenic micro-inclusions are easily detected and quantified by mineral magnetometry and are found to exhibit Verwey transition temperatures of 119 K, that can only occur in stoichiometric magnetite. Layer silicates also form a major class of diagenetic clay minerals (illite, smectite, etc.) that have important associations with diagenetic Fe oxides (see below).

From early work (Ballet and Coey 1982, Beausoleil et al. 1983, Coey and Ghose 1988) it was concluded that layer silicates would not order magnetically above ~10 K for intrinsic reasons due to the presence of chemical disorder in two dimensions. Rancourt et al. (1994) showed this to be incorrect and found magnetic ordering temperatures of 42 K and 58 K in a natural annite sample and in a synthetic annite end-member sample, respectively. Neutron diffraction showed an AF stacking of in-plane ferromagnetically aligned moments. The AF stacking was attributed to dipolar interactions and can be thought of as part of the domain structure of this layered material. The $^{[4]}Fe^{3+}$ and $^{[6]}Fe^{3+}$ moments were found to be magnetically exchange coupled to the octahedral sheet Fe^{2+} FM backbone but to only acquire significant average values at temperatures far below the magnetic ordering temperatures, as clearly seen in the Mössbauer spectra.

Transition metal di- and tri-chloride ($FeCl_2$, $FeCl_3$, $NiCl_2$, $CoCl_2$, $CrCl_3$, $CuCl_2$) GICs and graphite bi-intercalation compounds (GBICs) are ideal model systems for the study of two-dimensional nanomagnetism because most of these compounds intercalate by forming two-dimensional islands with diameters of ~15 nm and corresponding stabilizing charge transfers arising from island edge non-stoichiometry. The magnetism of such compounds and its relation to microstructural and nanostructural details have

been reviewed (Rancourt et al. 1986, Rancourt 1987). These systems present many classic examples of effects that are relevant to natural systems, such as: inter-particle interactions via exchange bridging, coexisting nanophase materials exhibiting distinct magnetic ordering temperatures, dipole-dipole mediated magnetic nanostructures, supermoment formation by incomplete AF lattice cancellation, frustration-isolated loose end or SR moments giving rise to large low temperature PM Curie signals, etc., and allow direct comparisons with the pristine Van der Waals layered chlorides.

Abiotic and biotic hydrous ferric oxide and sorbed-Fe on bacterial cell walls

Ferrihydrite is possibly the only accepted mineral species that is intrinsically nanophase (d ~ 5 nm), without any known bulk material counterpart. It is an important environmental material that forms by precipitation, in not too acidic pH environments, whenever Fe(2) meets oxidizing conditions. Its less ordered and smaller variety, known as 2-line ferrihydrite or HFO, is believed to play key roles in controlling the cycling of both nutrients (such as P) and heavy metals in aquatic environments. When formed in the presence of bacteria, this material is often found to be attached to the cell walls and to encase bacterial cells. For this reason, it is generally believed that bacteria play an active role in HFO formation in many environments.

It is also observed in laboratory experiments that bacterial cell walls can directly surface complex Fe and it has been proposed that this may be a first step towards biotic HFO formation (Warren and Ferris 1998). I follow Thibault (2001) in referring to such HFO as biotic (b-HFO) rather than as biogenic or bacteriogenic since the mechanism of its formation is not known. In the absence of bacteria, authigenic HFO can be referred to as abiotic (a-HFO). Rancourt (Rancourt et al. 1999a, 2001a; and as cited by Thibault 2001) has described four possible types of mechanisms for b-HFO formation:

(1) heterogeneous nucleation on the bacterial cell wall, the so-called template effect,

(2) homogeneous nucleation and growth in the near-cell chemical environment,

(3) enhanced precipitation from ancillary organic compounds from the bacteria, and

(4) catalytically enhanced nucleation and growth where the bacterial surface functional groups act as catalytic agents.

The first of these is the organic equivalent of epitaxial growth and includes surface nucleation barrier reduction by contact. It is presently the preferred picture in the literature but has not been substantiated by relevant observations.

Thibault (2001) has made comparisons of synthetic a-HFO and b-HFO samples made under identical chemical conditions but in the absence or presence of washed bacteria (*Bacillus subtilis* or *Bacillus licheniformis*), respectively. He combined TEM, Mössbauer spectroscopy, X-ray diffraction, and constant field magnetometry measurements to conclude that there were significant differences between a-HFO and b-HFO. The main differences were:

(1) smaller particle sizes and a less dense colloidal network in b-HFO, as inferred from TEM pictures,

(2) much lower SP blocking temperatures or SF ordering temperatures in b-HFO, as seen in both magnetometry and Mössbauer measurements,

(3) significantly different quadrupole splitting distributions extracted from RT Mössbauer spectra, showing different distributions of local distortion environments, and

(4) the presence of particle-complexed Fe^{2+} in b-HFO samples only, with the amount having a systematic variation with synthesis pH.

Rancourt et al. (1999a, 2001a) have made the first spectroscopic measurements of

surface complexed Fe on bacterial cell walls. They find that sorbed-Fe (s-Fe) is easily resolved from any b-HFO present by cryogenic Mössbauer measurements since the s-Fe does not order magnetically down to 4.2 K where all types of HFO always do. Evidence was found that the phosphate functional groups could form tridentate coordinations that ligand field stabilize the Fe^{2+} cation. This may be part of the mechanism that produces Fe^{2+} in b-HFO samples.

Indeed, P is known to complex strongly to HFO, as does As. In a recent study of natural As-rich and Si and C-bearing a-HFO samples, Rancourt et al. (2001b) showed many interesting phenomena. Si and C were found to compete with As (and presumably P) for surface complexation to the HFO, leading to banding of As-rich (Si and C-poor, yellowish) and As-poor (Si and C-rich, reddish) HFO deposits. The As was found to cause large Fe local environment distortions, directly measured by Mössbauer spectroscopy, that in turn correlated to the colors and related visible band edge positions, thereby directly illustrating the color mechanism involving Fe^{3+} valence orbital transitions. Dramatic differences between the magnetic behaviors of the As-rich and As-poor samples and synthetic a-HFO samples were seen. These were discussed in terms of particle sizes and supermoment formation mechanisms and illustrate the remarkable sensitivity of magnetic properties to the characteristics of surface complexed HFO nanoparticles.

Hydroxyhematite, nanohematite, and the Morin transition

Most authors who have studied small particle hematite have, as a first approximation, considered their samples to be small pieces of the ideal bulk material α-Fe_2O_3, where the changes in physical properties are predominantly controlled by particle size (e.g., Vandenberghe et al. 2000). In contrast, Dang et al. (1998) have stressed that even bulk hematite has a complex crystal chemistry involving the known OH/vacancy substitutional mechanism,

$$2\,Fe^{3+} + 3\,O^{2-} + 3\,H\uparrow\ = Fe^{3+} + \square + 3\,OH^- + Fe\downarrow ,$$
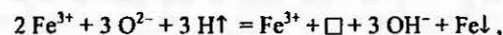
and at least one other crystal chemical mechanism that significantly affects the lattice parameters and that the resulting compositions of nanoparticles will be highly correlated to particle size for a given set of synthesis circumstances. They found that the chemistry of hematite particles predominantly determined the lattice parameters and that the lattice parameters, in turn, predominantly determined the Morin transition. A plot of c versus a for many samples showed a well defined OH/vacancy line and many points above this line that could be made to join the OH/vacancy line by annealing in air to 200°C. Annealing to progressively higher temperatures then caused evolution along the OH/vacancy line towards the stoichiometric hematite end-point. The position on this c-a plot completely determined both the existence of a Morin transition (down to 4.2 K) and the value of the Morin transition temperature for particles with d ~ 30 nm or larger. Continued unpublished work is aimed at: understanding the crystal chemistry of samples having a-c values above the OH/vacancy line, exploring particle size effects in smaller hematite particles, and exploring the effects of different solvating anions used in the hydrothermal syntheses. Dang et al. (1998) also showed that the baseline magnetic susceptibility in the AF state (below the Morin transition temperature) decreased with increasing annealing temperature, in a way that is consistent with a vacancy mechanism for supermoment formation.

Mineral magnetism of loess/paleosol deposits

Loess deposits are wind blown deposits that cover approximately 10% of the terrestrial landmass. Chinese loess deposits may constitute the best land-based records of

paleoclimates for the last several Ma (Kukla 1987, Kukla and An 1989, Liu 1988, 1991; Ding et al. 2001, Zhang et al. 2001). Alternating layers of loess and paleosol record different climates, relatively dry and cold versus wet and warm, respectively, where the main mineralogical differences are due to the varying degrees of pedogenesis and the associated authigenic and biogenic materials that have undergone various degrees of diagenesis since deposition. Magnetic measurements have been used both to provide dating from magnetic reversals (Heller and Evans 1995) and to provide sensitive and high resolution depth profiles that have been correlated to isotopic ratios from deep sea sediments (Evans et al. 1996).

Dang et al. (1999) performed a mineral magnetic and mineralogical study of a loess/paleosol couplet from the Chinese loess plateau in an effort to uncover which climate feature(s) the magnetic signal primarily records, by attempting to determine the magnetic mineralogy. They found the paleosol to contain more hydroxyhematite and maghemite that appeared to have formed at the expense of chlorite and layer silicate phases. Surprisingly, only the loess contained stoichiometric magnetite that displayed a Verwey transition at 119 K (Table 2), although its RT susceptibility was much smaller than that of the paleosol. The latter observation is particularly interesting when compared to observations of Siberian loess/paleosol deposits, that were deposited in arctic conditions. The Siberian susceptibility profiles also match deep sea isotopic ratio profiles but with a reversed sign, compared to the Chinese profiles (Chlachula et al. 1997, 1998). That is, Chinese paleosol units have larger susceptibilities than Chinese loess units whereas Siberian paleosol units have smaller susceptibilities than Siberian loess units.

Sabourin et al. (2001) have undertaken a detailed mineral magnetic and mineralogical study of a Siberian profile, in comparison to Chinese loess. They find that Siberian paleosols have undergone far less pedogenic transformation than Chinese paleosols, as expected, and that the first step relevant to magnetic measurements is the oxidation and transformation of the petrogenic stoichiometric magnetite. It appears that in Chinese paleosols the formation of pedogenic magnetic oxides far outweighs the loss of petrogenic magnetite whereas in Siberian paleosols the loss of petrogenic magnetite is not compensated by sufficient formation of pedogenic magnetic oxides. In both Chinese and Siberian paleosols there are significant fractions of SP magnetic particles that need to be characterized more completely.

Synthetic and meteoritic nanophase Fe-Ni and Earth's geodynamo

The iron meteorites are mostly composed of the Fe-Ni alloy minerals kamacite, taenite, and tetrataenite, and are believed to be remnants of the cores of parent bodies. Grains of Fe-Ni alloys are also common in most other types of meteorites. Because of exceedingly low cooling rates from the melt (typically ~1 K/Ma), the recovered materials are believed to be close to equilibrium structures and are therefore of interest to metallurgists, especially given the importance of industrial Fe-Ni alloys such as Invar ($Fe_{65}Ni_{35}$), Elinvar, and Permalloy.

Rancourt and Scorzelli (1995) recently proposed that the ubiquitous "PM taenite phase" in meteorites was a LM taenite phase, distinct from its HM taenite counterpart and analogous to the LM phase that had been theoretically predicted to occur but never observed or recognized as such. The LM phase was proposed to have low atomic moment magnitudes ($\mu_{Fe} \sim 0.5\ \mu_B$) and AF exchange interactions but the same FCC crystal structure as the HM taenite phase that has $\mu_{Fe} \sim 2.8\ \mu_B$ and predominantly FM interactions, as predicted by several ESCs. This would be the first example where distinct mineral phases can have the same compositions and crystal structures but different electronic structures and associated magnetic, material, and chemical properties.

Rancourt and Scorzelli suggested the mineral name antitaenite for the LM phase and proposed that it may be stabilized by an epitaxial interaction with tetrataenite, since it is always found in microstructural association with the latter phase and with an indistinguishable lattice parameter.

Rancourt et al. (1999b) later provided an experimental proof that antitaenite has an electronic structure that is distinct from that of any known natural or synthetic HM Fe-Ni alloy, in the form of direct local electronic density evaluations from ^{57}Fe Mössbauer spectroscopy. High resolution scanning electron microscopy of an unoxidized piece of the Santa Catharina ataxite showed a nanoscale microstructure consisting of 26-33 nm islands of tetrataenite in a honeycomb matrix phase of antitaenite having wall thicknesses of ~5 nm or less, consistent with the idea of epitaxial stabilization. It was also found that synthetic LM phase material could be produced by mechanical alloying of Fe and Ni, a method known to produce nanophase materials having nanoscale crystallites and nanoscale inter-grain boundaries.

Recently, Lagarec et al. (2001) located the composition-controlled equilibrium LM/HM transition of the synthetic FCC Fe-Ni system for the first time. They also used ESCs to show that the measured changes in local electronic density were precisely of the same magnitudes and signs as those predicted to occur on crossing the LM/HM transition. This work implies that, to the extent that FCC Fe-Ni can be stabilized with respect to the martensitic transition to the BCC structure, the electronic structure that has lowest energy on the bulk FCC structure above ~70 at % Fe is the LM structure. Lagarec et al. also showed that an FCC alloy having a LM ground state (including high temperature, FCC, γ-Fe and possibly high pressure, hexagonal close packed, ϵ-Fe) undergoes an entropic stabilization and gradual transition to a HM state as temperature is increased. Concomitantly, the dominant magnetic exchange interaction becomes less AF, crosses zero, and becomes FM. The latter composition, pressure, and temperature effects on the LM/HM nature of close packed Fe-Ni phases have important repercussions on the geodynamo, since the magnetic nature of Earth's solid core potentially plays an important role (Gilder and Glen 1998, Saxena and Littlewood 2001).

NEW DIRECTIONS: ENVIRONMENTAL MODELLING

What can magnetism do better than other methods? I have stressed that the PM cations (Table 1) are also the ones that can have several different valence states, thereby giving them prominent roles in biogeochemical reactions. Mineral magnetism, therefore, is a mineralogy focussed on the key reactive players in the environmental cycling of nutrients and toxic substances, most of which are nanoparticles or molecular clusters or PM active center metabolites.

Mineral magnetism, the extraction of crystal chemical and nano- and microstructural information from magnetic measurements, is presently underdeveloped. The low temperature magnetic properties of minerals are mostly unexplored yet the potential for widespread applications is high because of the sensitivity of magnetic properties to material properties, including subtle variations that cannot easily be detected by other methods. ESCs and other calculation methods are presently advanced enough for most of the connections between magnetism and underlying structure and chemistry to be made unambiguously. The real challenge is in assembling interdisciplinary teams that combine several measurement methods, appropriate theoretical and calculation methods, laboratory synthesis of realistic natural analogues, and problem-focussed field work.

Ultimately, in the environmental context, all mineral characterizations, including mineral magnetism, must serve to understand environmental systems, on all length scales

from surface reactions, to near cell environments, to weathering depths, to early diagenetic scales, to lake and catchment areas, to continental, ocean, and global scales. Phenomena on all relevant time scales must also be included in realistic models, from local reaction rates, to transport times on all length scales, to reservoir residence times for reservoirs on all length scales, and to paleoclimatic driving times. In constructing environmental models with true predictive and explanatory capabilities, one must strive to work all the way down to the molecular level where nanoparticle properties determine the relevant dissolution and precipitation rates, sorption affinities and capacities, bioavailabilities to different organisms, settling and transport rates, etc. Environmental mineralogists must move from static crystal chemical descriptions to include evaluations of the relevant reactions that geochemists and others attempt to use in their models.

In my own present work, as a member of the Lake Sediment Structure and Evolution (LSSE) group and the Geological Survey of Canada Metals in the Environment (GSC-MITE) Phase-II project, my group provides detailed mineralogical characterizations of selected lacustrine sediment profiles as one input to developing realistic reaction transport models (RTMs) of the evolution of the aquatic sediment profiles. A first step in writing down the relevant reactions is to simply identify and quantify the solid phases, especially the reactive ones. The LSSE/GSC-MITE collaboration also involves a complete suite of biogeochemical characterizations including porewater geochemistry, bacterial enumerations, stable isotope methods, radioactive isotope dating methods, diatom and pollen enumerations, field measurements, etc. We find that one bottleneck in establishing the RTMs is a lack of characterizations of the biogeochemical reactions themselves involving the key solid phases. One problem is that the synthetic model materials used to evaluate reaction parameters in published studies are often not sufficiently characterized and are often not sufficiently realistic.

ACKNOWLEDGMENTS

REFERENCES

Acremann Y, Back CH, Buess M, Portmann O, Vaterlaus A, Pescia D, Melchior H (2000) Imaging precessional motion of the magnetization vector. Science 290:492-495

Aharoni A (1969) Effect of a magnetic field on the superparamagnetic relaxation time. Phys Rev 177:793-796

Aharoni A (1992) Susceptibility resonance and magnetic viscosity. Phys Rev B 46:5434-5441

Allen PD, St-Pierre TG, Street R (1998) Magnetic interactions in native horse spleen ferritin below the superparamagnetic blocking temperature. J Magnet Magnetic Mater 177-181:1459-1460

Altbir D, Vargas P, D'Albuquerque e Castro J, Raff U (1998) Dipolar interaction and magnetic ordering in granular metallic materials. Phys Rev B 57:13604-13609

American Society for Metals (1986) Materials Characterization—ASM Handbook. American Society for Metals International

Amin N, Arajs S (1987) Morin temperature of annealed submicronic α-Fe$_2$O$_3$ particles. Phys Rev B 35:4810-1811

Aragon R, Gehring PM, Shapiro SM (1993) Stoichiometry, percolation, and Verwey ordering in magnetite. Phys Rev Lett 70:1635-1638

Ashcroft NW, Mermin ND (1976) Solid State Physics. Saunders College, Philadelphia, Pennsylvania

Awschalom DD, McCord MA, Grinstein G (1990) Observation of macroscopic spin phenomena in nanometer-scale magnets. Phys Rev Lett 65:783-882

Awschalom DD, Smyth JF, Grinstein G, DiVincenzo DP, Loss D (1992) Macroscopic quantum tunneling in magnetic proteins. Phys Rev Lett 68:3092-3095

Backus G, Parker R, Constable C (1996) Foundations of magnetism. Cambridge University Press, Cambridge, UK

Bacri J-C, Boué F, Cabuil V, Perzynski R (1993) Ionic ferrofluids: Intraparticle and interparticle correlations from small-angle neutron scattering. Colloids Surf A: Physiochem Engin Aspects 80:11-18

Balcells L, Iglesias O, Labarta A (1997) Normalization factors for magnetic relaxation of small-particle systems in a nonzero magnetic field. Phys Rev B 55:8940-8944

Ballet O, Coey JMD (1982) Magnetic properties of sheet silicates; 2:1 layer minerals. Phys Chem Minerals 8:218-229

Banerjee SK (1991) Magnetic properties of Fe-Ti oxides. Rev Mineral 25:107-128

Banfield JF, Nealson KH (eds) (1997) Geomicrobiology: Interactions Between Microbes and Minerals. Rev Mineral 35, 448 p

Barbara B, Chudnovsky EM (1990) Macroscopic quantum tunneling in antiferromagnets. Phys Lett A 145:205-208

Barbara B, Sampaio LC, Marchand A, Kubo O, Takeuchi H (1994) Two-variables scaling of the magnetic viscosity in Ba-ferrite nano-particles. J Magnet Magnetic Mater 136:183-188

Barra A-L, Debrunner P, Gatteschi D, Schulz ChE, Sessoli R (1996) Superparamagnetic-like behavior in an octanuclear iron cluster. EuroPhys Lett 35:133-138

Basso V, Beatrice C, LoBue M, Tiberto P, Bertotti G (2000) Connection between hysteresis and thermal relaxation in magnetic materials. Phys Rev B 61:1278-1285

Bauminger ER, Nowik I (1989) Magnetism in plant and mammalian ferritin. Hyperfine Interactions 50:484-498

Beausoleil N, Lavallée P, Yelon A, Ballet O, Coey JMD (1983) Magnetic properties of biotite. J Appl Phys 54:906-915

Benn K (1999) Applications of magnetic anisotropies to fabric studies of rocks and sediments. Tectonophysics 307:7-10

Berger R, Bissey J-C, Kliava J, Soulard B (1997) Superparamagnetic resonance of ferric ions in devitrified borate glass. J Magnet Magnetic Mater 167:129-135

Berger R, Kliava J, Bissey J-C, Baïetto V (1998) Superparamagnetic resonance of annealed iron-containing borate glass. J Phys: Condensed Matter 10:8559-8572

Berkowitz AE, Kodama RH, Makhlouf SA, Parker FT, Spada FE, McNiff EJ Jr, Foner S (1999) Anomalous properties of magnetic nanoparticles. J Magnet Magnetic Mater 196/197:591-594

Bessais L, Ben Jaffel L, Dormann JL (1992) Relaxation time of fine magnetic particles in uniaxial symmetry. Phys Rev B 45:7805-7815

Binder K, Heermann DW (1992) Monte Carlo Simulation in Statistical Physics. Springer-Verlag, Berlin

Binder K, Young AP (1986) Spin glasses: Experimental facts, theoretical concepts and open questions. Rev Mod Phys 58:801-976

Bitoh T, Ohba K, Takamatsu M, Shirane T, Chikazawa S (1996) Comparative study of linear and nonlinear susceptibilities of fine-particle and spin-glass systems: Quantitative analysis based on the superparamagnetic blocking model. J Magnet Magnetic Mater 154:59-65

Blaes N, Fischer H, Gonser U (1985) Analytical expression for the Mossbauer line shape of ^{57}Fe in the presence of mixed hyperfine interactions. Nuclear Instr Methods Phys Res B9:201-208

Blaes N, Preston RS, Gonser U (1985) Mössbauer spectra for nuclear motion correlated with EFG reorientation. In Applications of the Mössbauer Effect—ICAME-83, Alma-Ata, p 1491-1496

Blaes R, Guillin J, Bominaar EL, Grodzicki M, Marathe VR, Trautwein AX (1987) Spin-polarized SCC-Xα calculations for electronic- and magnetic-structure properties of 2Fe-2s ferrodoxin models. J Phys B 20:5627-5637

Bocquet S (1996) Superparamagnetism and the Mossbauer spectrum of goethite: a comment on a recent proposal by Coey et al. J Phys: Condensed Matter 8:111-113

Bødker F, Hansen MF, Bender Koch C, Lefmann K, Mørup S (2000) Magnetic properties of hematite nanoparticles. Phys Rev B 61:6826-6838

Bodker F, Morup S (2000) Size dependence of the properties of hematite nanoparticles. EuroPhys Lett 52:217-223

Bonet E, Wernsdorfer W, Barbara B, Benoit A, Mailly D, Thiaville A (1999) Three-dimensional magnetization reversal measurements in nanoparticles. Phys Rev Lett 83:4188-4191

Bonnemain B (1998) Superparamagnetic agents in magnetic resonance imaging: Physicochemical characteristics and clinical applications. A review. J Drug Targeting 6:167-174

Bradley JP, McSween Jr HY, Harvey RP (1998) Epitaxial growth of nanophase magnetite in Martian meteorite Allan Hills 84001: Implications for biogenic mineralization. Meteoritics Planet Sci 33:765-773

Braun H-B (1993) Thermally activated magnetization reversal in elongated ferromagnetic particles. Phys Rev Lett 71:3557-3560

Broomberg J, Gélinas S, Finch JA, Xu Z (1999) Review of magnetic carrier technologies for metal ion removal. Magnetic and Electrical Separation 9:169-188

Brown JrWF (1963) Thermal fluctuations of a single-domain particle. Phys Rev 130:1677-1686

Brown JrWF (1979) Thermal fluctuations of fine ferromagnetic particles. I E E E Trans Magnetics 15:1196-1208

Broz JS, Braun HB, Brodbeck O, Baltensperger W, Helman JS (1990) Nucleation of magnetization reversal via creation of pairs of Bloch walls. Phys Rev Lett 65:787-789

Brug JA, Anthony TC, Nickel JH (1996) Magnetic recording head materials. Mater Res Soc Bull, September 1996:23-27

Burton BP (1991) The interplay of chemical and magnetic ordering. Rev Mineral 25:303-321

Cabuil V (2000) Phase behavior of magnetic nanoparticles dispersions in bulk and confined geometries. Current Opinion Colloid Interface Sci 5:44-48

Cahn RW, Lifshin E (1993) Concise Encyclopedia of Materials Characterization. Pergamon Press, Oxford

Campbell WH (2000) Earth Magnetism. Academic Press, New York

Carlin RL (1986) Magnetochemistry. Springer-Verlag, Berlin

Chalupa J (1977) The susceptibilities of spin glasses. Solid State Commun 22:315-317

Chamberlin RV (2000) Mean-field cluster model for the critical behavior of ferromagnets. Nature 408:337-339

Chamberlin RV, Haines DN (1990) Percolation model for relaxation in random systems. Phys Rev Lett 65:2197-2200

Chang C-R, Yang J-S, Klik I (1997) Thermally activated magnetization reversal through multichannels. J Appl Phys 81:5750-5752

Chang S-BR, Kirschvink JL (1985) Possible biogenic magnetite fossils from the late miocene potamida clays of Crete. In Kirschvink JL, Jones DS, MacFadden BJ (eds) Magnetite Miomineralization and Magnetoreception in Organisms—A New Biomagnetism. Plenum Press, New York, p 647-669

Chantrell RW, Walmsley N, Gore J, Maylin M (2000) Calculations of the susceptibility of interacting superparamagnetic particles. Phys Rev B 63:24410-1-24410-14

Chantrell RW, Walmsley NS, Gore J, Maylin M (1999) Theoretical studies of the field-cooled and zero-field cooled magnetization of interacting fine particles. J Appl Phys 85:4340-4342

Chaput F, Boilot J-P, Canva M, Brun A, Perzynski R, Zins D (1993) Permanent birefringence of ferrofluid particles trapped in a silica matrix. J Non-Crystal Solids 160:177-179

Chlachula J, Evans ME, Rutter NW (1998) A magnetic investigation of a late quaternary loess/palaelosol record in Siberia. Geophys J Int'l 132:128-132

Chlachula J, Rutter NW, Evans ME (1997) A late quaternary loess—Paleosol record at Kurtak, southern Siberia. Canadian J Earth Sci 34:679-686

Chowdhury D (1986) Spin Glasses and Other Frustrated Systems. Princeton University Press, Princeton, NJ

Cianchi L, Mancini M, Spina G, Tang H (1992) Mossbauer spectra of ferrihydrite: Superferromagnetic interactions and anisotropy local energy. J Phys—Condensed Matter 4:2073-2077

Clark DA (1983) Comments on magnetic petrophysics. Bull Aust Soc Explor Geophys 14:49-62

Coey JMD (1978) Amorphous magnetic order. J Appl Phys 49:1646-1652

Coey JMD, Ghose S (1988) Magnetic phase transitions in silicate minerals. Adv Phys Geochem 17:162-184

Coey JMD, Readman PW (1973a) New spin structure in an amorphous ferric gel. Nature 246:476-478

Coey JMD, Readman PW (1973b) Characterization and magnetic properties of natural ferric gel. Earth Planet Sci Lett 21:45-51

Coffey WT, Cregg PJ, Crothers DSF, Waldron JT, Wickstead AW (1994a) Simple approximate formulae for the magnetic relaxation time of single domain ferromagnetic particles with unaxial anisotropy. J Magnet Magnetic Mater 131:L301-L303

Coffey WT, Crothers DSF (1996) Comparison of methods for the calculation of superparamagnetic relaxation times. Phys Rev E 54:4768-4774

Coffey WT, Crothers DSF, Dormann JL, Geoghegan LJ, Kalmykov YP, Waldron JT, Wickstead AW (1995a) Effect of an oblique magnetic field on the superparamagnetic relaxation time. Phys Rev B 52:15951-15965

Coffey WT, Crothers DSF, Dormann JL, Geoghegan LJ, Kalmykov YP, Waldron JT, Wickstead AW (1995b) The effect of an oblique magnetic field on the superparamagnetic relaxation time. J Magnet Magnetic Mater 145:L263-L267

Coffey WT, Crothers DSF, Dormann JL, Geoghegan LJ, Kennedy EC, Wernsdorfer W (1998a) Range of validity of Kramers escape rates for non-axially symmetric problems in superparamagnetic relaxation. J Phys: Condensed Matter 10:9093-9109

Coffey WT, Crothers DSF, Dormann JL, Kalmykov YP, Kennedy EC, Wernsdorfer W (1998b) Thermally activated relaxation time of a single domain ferromagnetic particle subjected to a uniform field at an oblique angle to the easy axis: Comparison with experimental observations. Phys Rev Lett 80:5655-5658

Coffey WT, Crothers DSF, Kalmykov YP, Massawe ES, Waldron JT (1993) Exact analytic formulae for the correlation times for single domain ferromagnetic particles. J Magnet Magnetic Mater 127:L254-L260

Coffey WT, Crothers DSF, Kalmykov YP, Massawe ES, Waldron JT (1994b) Exact analytic formula for the correlation time of a single-domain ferromagnetic particle. Phys Rev E 49:1869-1882

Coffey WT, Crothers DSF, Kalmykov YP, Waldron JT (1995c) Constant-magnetic-field effect in Néel relaxation of single-domain ferromagnetic particles. Phys Rev B 51:14947-15956

Coffey WT, Kalmykov YP, Massawe ES (1994c) The effective eigenvalue method and its application to stochastic problems in conjunction with the nonlinear Langevin equation. Adv Chem Phys 85:667-791

Collinson DW (1983) Methods in rock magnetism and paleomagnetism. Chapman & Hall, London

Comello V (1998) Magnetic storage research aiming at high areal densities. R&D Magazine, December 1998, p 14-19

Continentino M, Malozemoff AP (1986) Dynamical susceptibility of spin glasses in the fractal cluster model. Phys Rev B 34:471-474

Cornell RM, Schwertmann U (1996) The Iron Oxides—Structure, properties, reactions, occurrence and uses. VCH, Weinheim

Cowburn RP, Koltsov DK, Adeyeye AO, Welland ME (2000) Sensing magnetic fields using superparamagnetic nanomagnets. J Appl Phys 87:7082-7084

Creer KM, Tucholka P, Barton CE (1983) Geomagnetism of Baked Clays and Recent Sediments. Elsevier Science, Amsterdam

Cregg PJ, Crothers DSF, Wickstead AW (1994) An approximate formula for the relaxation time of a single domain ferromagnetic particle with uniaxial anisotropy and collinear field. J Appl Phys 76:4900-4902

Dang MZ, Rancourt DG (1996) Simultaneous magnetic and chemical order-disorder phenomena in Fe_3Ni, FeNi, and $FeNi_3$. Phys Rev B 53:2291-2301

Dang M-Z, Rancourt DG, Dutrizac JE, Lamarche G, Provencher R (1998) Interplay of surface conditions, particle size, stoichiometry, cell parameters, and magnetism in synthetic hematite-like materials. Hyperfine Interactions 117:271-319

Dang M-Z, Rancourt DG, Lamarche G, Evans ME (1999) Mineralogical analysis of a loess/paleosol couplet from the Chinese loess plateau. In Kodama H, Mermut AR, Torrance JK (eds) Clays for Our Future. Proc 11th Int'l Clay Conf, Ottawa, Canada, p 309-315

de Biasi RS, Devezas TC (1978) Anisotropy field of small magnetic particles as measured by resonance. J Appl Phys 49:2466-2469

de Jongh LJ, Miedema AR (1974) Experiments on simple magnetic model systems. Adv Phys 23:1-260

Deutschlander ME, Borland SC, Phillips JB (1999) Extraocular magnetic compass in newts. Nature 400:324-325

Dickson DPE, Reid NMK, Hunt C, Williams HD, El-Hilo M, O'Grady K (1993) Determination of f_0 for fine magnetic particles. J Magnet Magnetic Mater 125:345-350

Dimitrov DA, Wysin GM (1996) Magnetic properties of superparamagnetic particles by a Monte Carlo method. Phys Rev B 54:9237-9341

Ding ZL, Sun JM, Yang SL, Liu TS (2001) Geochemistry of the Pliocene red clay formation in the Chinese Loess Plateau and implications for its origin, source provenance and paleoclimate change. Geochim Cosmochem Acta 65:901-913

Dixon JB, Weed SB (1989) Minerals in Soil Environments. Soil Science Society of America, Madison, Wisconsin

Djurberg C, Svedlindh P, Nordblad P, Hansen MF, Bodker F, Morup S (1997) Dynamics of an interacting particle system: Evidence of critical slowing down. Phys Rev Lett 79:5154-5157

Domany E (1999) Superparamagnetic clustering of data—The definitive solution of an ill-posed problem. Physica A 263:158-169

Domany E, Blatt M, Gdalyahu Y, Weinshall D (1999) Superparamagnetic clustering of data: Application to computer vision. Computer Phys Commun 121-122:5-12

Dormann JL (1981) La phénomène de superparamagnétisme. Rev Phys Appl 16:275-301

Dormann JL, Bessais L, Fiorani D (1988) A dynamic study of small interacting particles: Super-paramagnetic model and spin-glass laws. J Phys C: Solid State Phys 21:2015-2034

Dormann JL, Cherkaoui R, Spinu L, Noguès M, Lucari F, D'Orazio F, Fiorani D, Garcia A, Tronc E, Jolivet JP (1998) From pure superparamagnetic regime to glass collective state of magnetic moments in γ-Fe₂O₃ nanoparticle assemblies. J Magnet Magnetic Mater 187:L139-L144

Dormann JL, D'Orazio F, Lucari F, Tronc E, Prené P, Jolivet JP, Fiorani D, Cherkaoui R, Noguès M (1996) Thermal variation of the relaxation time of the magnetic moment of γ-Fe₂O₃ nanoparticles with interparticle interactions of various strengths. Phys Rev B 53:14291-14297

Dormann JL, Fiorani D (1995) Nanophase magnetic materials: Size and interaction effects on static and dynamical properties of fine particles (invited paper). J Magnet Magnetic Mater 140-144:415-418

Dormann JL, Fiorani D, El Yamani M (1987) Field dependence of the blocking temperature in the superparamagnetic model: $H^{2/3}$ coincidence. Phys Lett A 120:95-99

Dormann JL, Fiorani D, Tronc E (1997) Magnetic relaxation in fine-particle systems. In Prirogine I, Rice SA (eds) Adv Chem Phys, volume XCVIII. John Wiley & Sons, New York, p 283-494

Dormann JL, Spinu L, Tronc E, Jolivet JP, Lucari F, D'Orazio F, Fiorani D (1998) Effect of interparticle interactions on the dynamical properties of γ-Fe₂O₃ nanoparticles. J Magnet Magnetic Mater 183:L255-L260

Dubowik J, Baszynski J (1968) FMR study of coherent fine magnesioferrite particles in MgO-line shape behavior. J Magnet Magnetic Mater 59:161-168

Dunlop DJ (1990) Developments in rock magnetism. Rep Prog Phys 53:707-792

Dunlop DJ, Özdemir Ö (1997) Rock magnetism. Fundamentals and frontiers. Cambridge University Press, Cambridge, UK

Dzyaloshinsky I (1958) A thermodynamic theory of "weak" ferromagnetism of antiferromagnetics. J Phys Chem Solids 4:241-255

El-Hilo M, O'Grady K, Chantrell RW (1992a) Susceptibility phenomena in a fine particle system. I. Concentration-dependence of the peak. J Magnet Magnetic Mater 114:295-306

El-Hilo M, O'Grady K, Chantrell RW (1992b) The ordering temperature in fine particle systems. J Magnet Magnetic Mater 117:21-28

Essam JW (1980) Percolation theory. Rep Prog Phys 43:833-912

Evans ME, Ding Z, Rutter NW (1996) A high resolution magnetic susceptibility study of a loess/paleosol couplet at Baoji, China. Studia Geophys Geod 40:225-233

Ezzir A, Dormann JL, Hachkachi H, Nogues M, Godinho M, Tronc E, Jolivet JP (1999) Superparamagnetic susceptibility of a nanoparticle assembly: Application of the Onsager model. J Magnet Magnetic Mater 196-197:37-39

Ferchmin AR, Kobe S (1983) Amorphous Magnetism and Metallic Magnetic Materials—Digest. North-Holland Publishing Company, New York

Ferré R, Barbara B, Fruchart D, Wolfers P (1995) Dipolar interacting small particles: Effects of concentration and anisotropy. J Magnet Magnetic Mater 140-144:385-386

Ferris FG (1997) Formation of authigenic minerals by bacteria. In McIntosh JM, Groat LA (eds) Biological-Mineralogical Interactions. Mineral Assoc Canada Short Course Ser 25:187-208

Fiorani D, Dormann JL, Cherkaoui R, Tronc E, Lucari F, D'Orazio F, Spinu L, Nogues M, Garcia A, Testa AM (1999) Collective magnetic state in nanoparticles systems. J Magnet Magnetic Mater 196/197:143-147

Fiorani D, Tholence J, Dormann JL (1986) Magnetic properties of small ferromagnetic particles (Fe-Al₂O₃ granular thin films): Comparison with spin glass properties. J Phys C.: Solid State Phys 19:5495-5507

Fischer KH, Hertz JA (1991) Spin Glasses. Cambridge University Press, Cambridge, UK

Fisher ME, Privman V (1985) First-order transitions breaking O(n) symmetry: Finite-size scaling. Phys Rev B 32:447-464

Fortin D, Ferris FG, Beveridge TJ (1997) Surface-mediated mineral development by bacteria. Rev Mineral 35:161-177

Friedman JR, Sarachik MP, Tejada J, Ziolo R (1996) Macroscopic measurement of resonant magnetization tunneling in high-spin molecules. Phys Rev Lett 76:3830-3833

Friedman JR, Voskoboynik U, Sarachik MP (1997) Anomalous magnetic relaxation in ferritin. Phys Rev B 56:10793-10796

Frost BR (1991) Magnetic petrology: factors that control the occurrence of magnetite in crustal rocks. Rev Mineral 25:489-509

Garanin DA (1996) Integral relaxation time of single-domain ferromagnetic particles. Phys Rev E 54:3250-3256

Garanin DA (1997) Quantum thermoactivation of nanoscale magnets. Phys Rev E 55:2569-2572

Garanin DA (1999) New integral relaxation time for thermal activation of magnetic particles. EuroPhys Lett 48:486-490

Garanin DA, Kladko K, Fulde P (2000) Quasiclassical hamiltonians for large-spin systems. EuroPhys Lett B14:293-300

García-Palacios JL, Lázaro FJ (1997) Anisotropy effects on the nonlinear magnetic susceptibilities of superparamagnetic particles. Phys Rev B 55:1006-1010

García-Palacios JL, Svedlindh P (2000) Large nonlinear dynamical response of superparamagnets: Interplay between precession and thermoactivation in the stochastic Landau-Lifshitz equation. Phys Rev Lett 85:3724-3727

García-Palacios JL, Svedlindh P (2001) Derivation of the basic system equations governing superparamagnetic relaxation by the use of the adjoint Fokker-Planck operator. Phys Rev B 63:172417-1-172417/4

Gatteschi D, Sessoli R (1996) Origin of superparamagnetic-like behavior in large molecular clusters. In Molecule-based Magnetic Materials. American Chemical Society, p 157-169

Gayraud J, Robin E, Rocchia R, Froget L (1996) Formation conditions of oxidized Ni-rich spinel and their relevance to the K/T boundary event. Geol Soc Am 307:425-443

Gazeau F, Bacri JC, Gendron F, Perzynski R, Raikher YuL, Stepanov VI, Dubois E (1998) Magnetic resonance of ferrite nanoparticles: Evidence of surface effects. J Magnet Magnetic Mater 186:175-187

Gazeau F, Dubois E, Hennion M, Perzynski R, Raikher Yu (1997) Quasi-elastic neutron scattering on γ-Fe₂O₃ nanoparticles. EuroPhys Lett 40:575-580

Gee JS, Cande SC, Hildebrand JA, Donnelly K, Parker RL (2000) Geomagnetic intensity variations over the past 780 kyr obtained from near-seafloor magnetic anomalies. Nature 408:827-832

Gider S, Awschalom DD, Douglas T, Mann S, Chaparala M (1995) Classical and quantum magnetic phenomena in natural and artificial ferritin proteins. Science 268:77-80

Gider S, Awschalom DD, Douglas T, Wong K, Mann S, Cain G (1996) Classical and quantum magnetism in synthetic ferritin proteins. J Appl Phys 79:5324-5326

Gilder S, Glen J (1998) Magnetic properties of hexagonal closed-packed iron deduced from direct observations in a diamond anvil cell. Science 279:72-74

Gilles C, Bonville P, Wong KKW, Mann S (2000) Non-Langevin behavior of the uncompensated magnetization in nanoparticles of artificial ferritin. EuroPhys J B17:417-427

Gittleman JI, Abeles B, Bozowski S (1974) Superparamagnetism and relaxation effects in granular Ni-SiO₂ and Ni-Al₂O₃ films. Phys Rev B 9:3891-3897

Golden DC, Ming DW, Schwandt CS, Lauer Jr. HV, Socki RA, Morris RV, Lofgren GE, McKay GA (2001) A simple inorganic process for formation of carbonates, magnetite, and sulfides in Martian meteorite ALH84001. Am Mineral 86:370-375

Goodman AA, Whittet DCB (1955) A point in favor of the superparamagnetic grain hypothesis. Astrophys J 455:L181-L184

Griscom DL, Friebele EJ, Shinn DB (1979) Ferromagnetic resonance of spherical particles of α-iron precipitated in fused silica. J Appl Phys 50:2402-2404

Grodzicki M (1980) A self-consistent charge Xα method I. Theory. J Phys B 13:2683-2690

Grossmann B, Rancourt DG (1996) Simulation of magneto-volume effects in ferromagnets by a combined molecular dynamics and Monte-Carlo approach. Phys Rev B 54:12294-12301

Grun R (2000) Electron spin resonance dating. In Ciliberto E, Spoto G (eds) Modern Analytical Methods in Art and Archaeology. John Wiley & Sons, New York, p 641-679

Grüttner C, Teller J (1999) New types of silica-fortified magnetic nanoparticles as tools for molecular biology applications. J Magnet Magnetic Mater 194:8-15

Gunther L, Mohie-Eldin M-EY (1994) Motional narrowing and magnetostrictive broadening of the Mossbauer spectrum due to superparamagnetism. J Magnet Magnetic Mater 129:334-338

Hansen MF, Bender Koch C, Mørup S (2000) Magnetic dynamics of weakly and strongly interacting hematite nanoparticles. Phys Rev B 62:1124-1135

Hansen MF, Bødker F, Mørup S, Lefmann K, Clausen KN, Lindgård P-A (1997) Dynamics of magnetic nanoparticles studied by neutron scattering. Phys Rev B 79:4910-4913

Hansen MF, Mørup S (1998) Models for the dynamics of interacting magnetic nanoparticles. J Magnet Magnetic Mater 184:262-274

Hanzlik M, Heunemann C, Holtkamp-Rötzler E, Winklhofer M, Petersen N, Fleissner G (2000) Superparamagnetic magnetite in the upper beak tissue of homing pigeons. BioMetals 13:325-331

Hartmann-Boutron F, Politi P, Villain J (1996) Tunneling and magnetic relaxation in mesoscopic molecules. Int'l J Modern Phys B 10:2577-2639

Hawkins C, Williams JM, Hudson AJ, Andrews SC, Treffry A (1994) Mossbauer studies of the ultrafine antiferromagnetic cores of ferritin. Hyperfine Interactions 91:827-833

Hawthorne FC (ed) (1988) Spectroscopic Methods in Mineralogy and Geology. Rev Mineral 18, 698 p

Hayashi M, Susa M, Nagata K (1997) Magnetic interaction between magnetite particles dispersed in calciumsilicate glasses. J Magnet Magnetic Mater 171:170-178

Heller F, Evans ME (1995) Loess magnetism. Rev Geophys 33:211-240

Himpsel FJ, Ortega JE, Mankey GJ, Willis RF (1998) Magnetic nanostructures. Adv Phys 47:511-597

Hohenberg PC (1967) Existence of long-range order in one and two dimensions. Phys Rev 158:383-386
Honda H, Kawabe A, Shinkai M, Kobayashi T (1998) Development of Chitosan-conjugated magnetite for magnetic cell separation. J Fermentation Bioengin 86:191-196
Hopkins PF, Moreland J, Malhotra SS, Liou SH (1996) Superparamagnetic magnetic force microscopy tips. J Appl Phys 79:6448-6450
Ibrahim MM, Darwish S, Seehra MS (1995) Nonlinear temperature variation of magnetic viscosity in nanoscale FeOOH particles. Phys Rev B 51:2955-2959
Ibrahim MM, Edwards G, Seehra MS, Ganguly B, Huffman GP (1994) Magnetism and spin dynamics of nanoscale FeOOH particles. J Appl Phys 75:5873-5875
Ibrahim MM, Zhao J, Seehra MS (1992) Determination of particle size distribution in an Fe_2O_3-based catalyst using magnetometry and X-ray diffraction. J Mater Res 7:1856-1860
Ignatchenko VA, Mironov YE (1991) Magnetic structures with a finite number of domain walls. J Magnet Magnetic Mater 94:170-178
Jacobs JA (1991) Geomagnetism. Academic Press, London
Jambor JL, Dutrizac JE (1998) Occurrence and constitution of natural and synthetic ferrihydrite, a widespread iron oxyhydroxide. Chem Rev 98:2549-2585
Jiles DC, Atherton DL (1984) Theory of ferromagnetic hysteresis (invited). J Appl Phys 55:2115-2120
Jones DH, Srivastava KKP (1989) A re-examination of models of superparamagnetic relaxation. J Magnet Magnetic Mater 78:320-328
Jönsson P, Jonsson T, García-Palacios JL, Svedlindh P (2000) Nonlinear dynamic susceptibilities of interacting and noninteracting magnetic nanoparticles. J Magnet Magnetic Mater 222:219-226
Jonsson T, Mattsson J, Djurberg C, Khan FA, Nordblad P, Svedlindh P (1995b) Aging in a magnetic particle system. Phys Rev Lett 75:4138-4141
Jonsson T, Mattsson J, Nordblad P, Svedlindh P (1997) Energy barrier distribution of a noninteracting nano-sized magnetic particle system. J Magnet Magnetic Mater 168:269-277
Jonsson T, Nordblad P, Svedlindh P (1998) Dynamic study of dipole-dipole interaction effects in a magnetic nanoparticle system. Phys Rev B 57:497-504
Jonsson T, Svedlindh P, Hansen MF (1998) Static scaling on an interacting magnetic nanoparticle system. Phys Rev Lett 81:3976-3979
Jonsson T, Svedlindh P, Nordblad P (1995a) AC susceptibility and magnetic relaxation studies on frozen ferrofluids. Evidence for magnetic dipole-dipole interactions. J Magnet Magnetic Mater 140-144:401-402
Jung CW, Rogers JM, Groman EV (1999) Lymphatic mapping and sentinel node location with magnetite nanoparticles. J Magnet Magnetic Mater 194:210-216
Kahn O (1999) The magnetic turnabout. Nature 399:21-23
Kalmykov YP (2000) Longitudinal dynamic susceptibility and relaxation time of superparamagnetic particles with cubic anisotropy: Effect of a biasing magnetic field. Phys Rev B 61:6205-6212
Kalmykov YP, Titov SV (1999) Calculating coefficients for a system of moment equations used to describe the magnetization kinetics of a superparamagnetic particle in a fluctuating field. Phys Solid State 41:1854-1861
Kalmykov YP, Titov SV (2000) Derivation of matrix elements for the system of moment equations governing the kinetics of superparamagnetic particles. J Magnet Magnetic Mater 210:233-243
Kechrakos D, Trohidou KN (1998a) Effects of dipolar interactions on the magnetic properties of granular solids. J Magnet Magnetic Mater 177-181:943-944
Kechrakos D, Trohidou KN (1998b) Magnetic properties of dipolar interacting single-domain particles. Phys Rev B 58:12169-12177
Kirschvink JL (1989) Magnetite biomineralization and geomagnetic sensitivity in higher animals: An update and recommendations for future study. Bioelectromagnetics 10:239-259
Kirschvink JL, Jones DS, MacFadden BJ (1985) Magnetite Biomineralization and Magnetoreception in Organisms—A New Biomagnetism. Plenum Press, New York
Kirschvink JL, Kirschvink-Kobayashi A, Woodford BJ (1992) Magnetite biomineralization in the human brain. Proc Natl Acad Sci 89:7683-7687
Kleemann W, Petracic O, Binek Ch, Nakazei GN, Pogorelov YuG, Sousa JB, Cardoso S, Freitas PP (2001) Interacting ferromagnetic nanoparticles in discontinuous $Co_{80}Fe_{20}/Al_2O_3$ multilayers: From superspin glass to reentrant superferromagnetism. Phys Rev B 63:134423-1-134423/5
Klein C, Hurlbut CS Jr (1999) Manual of Mineralogy. John Wiley & Sons, New York
Kliava J, Berger R (1999) Size and shape distribution of magnetic nanoparticles in disordered systems: Computer simulations of superparamagnetic resonance spectra. J Magnet Magnetic Mater 205:328-342
Kneller E (1968) Magnetic-interaction effects in fine-particle assemblies and in thin films. J Appl Phys 39:945-955

Kneller E, Puschert W (1966) Pair interaction models for fine particle assemblies. IEEE Trans Magnetics MAG-2:250
Kodama RH (1999) Magnetic nanoparticles. J Magnet Magnetic Mater 200:359-372
Kodama RH, Berkowitz AE (1999) Atomic-scale magnetic modeling of oxide nanoparticles. Phys Rev B 59:6321-6336
Kröckel M, Grodzicki M, Papaefthymiou V, Trautwein AX, Kostikas A (1996) Tuning of electron delocalization in polynuclear mixed-valence clusters by super-exchange and double exchange. J Biol Inorg Chem 1:173-176
Krupicka S, Novak P (1982) Oxide Spinels. *In* Wohlfarth EP (ed) Ferromagnetic Materials. North-Holland, Amsterdam, p 189-304
Kryder MH (1996) Ultrahigh-density recording technologies. Mater Res Bull, September 1996, 17-22
Kukla G (1987) Loess stratigraphy in Central China. Quaternary Sci Rev 6:191-219
Kukla G, An Z (1989) Loess stratigraphy in Central China. Palaeogeogr Palaeoclimatol Palaeoecol 72:203-225
Kundig W, Bommel H, Constabaris G, Lindquist RH (1966) Some properties of supported small α-Fe_2O_3 particles determined with the Mossbauer effect. Phys Rev 142:327-333
Kyte FT (1998) A meteorite from the Cretaceous/Tertiary boundary. Nature 396:237-239
Kyte FT, Bohor BF (1995) Nickel-rich magnesiowüstite in Cretaceous/Tertiary boundary spherules crystallized from ultramafic, refractory silicate liquids. Geochim Cosmochem Acta 59:4967-4974
Kyte FT, Bostwick JA (1995) Magnesioferrite spinel in Cretaceous/Tertiary boundary sediments of the Pacific basin: Remnants of hot, early ejecta from the Chicxulub impact? Earth Planet Sci Lett 132:113-127
Lagarec K, Rancourt DG (2000) Fe_3Ni-type chemical order in $Fe_{65}Ni_{35}$ films grown by evaporation: Implications regarding the Invar problem. Phys Rev B 62:978-985
Lagarec K, Rancourt DG, Bose SK, Sanyal B, Dunlap RA (2001) Observation of a composition-controlled high-moment/low-moment transition in the face centered cubic Fe-Ni system: Invar effect is an expansion, not a contraction. J Magnet Magnetic Mater (in press)
Lalonde AE, Rancourt DG, Ping JY (1998) Accuracy of ferric/ferrous determinations in micas: A comparison of Mössbauer spectroscopy and the Pratt and Wilson wet-chemical methods. Hyperfine Interactions 117:175-204
Lear PR (1987) The role of iron in nontronite and ferrihydrite. PhD Dissertation. University of Illinois, Champagne-Urbana
Lifshin E (1992) Characterization of Materials, Part I. VCH, Weinheim
Lifshin E (1994) Characterization of Materials, Part II. VCH, Weinheim
Ligenza S, Dokukin EB, Nikitenko YuV (1995) Neutron depolarization studies of magnetization process in superparamagnetic cluster structures. J Magnet Magnetic Mater 147:37-44
Lin D, Nunes AC, Majkrzak CF, Berkowitz AE (1995) Polarized neutron study of the magnetization density distribution within a $CoFe_2O_4$ colloidal particle II. J Magnet Magnetic Mater 145:343-348
Liou SH, Malhotra SS, Moreland J, Hopkins PF (1997) High resolution imaging of thin-film recording heads by superparamagnetic magnetic force microscopy tips. Appl Phys Lett 70:135-137
Liu C, Zou B, Rondinone AJ, Zhang ZJ (2000) Reverse micelle synthesis and characterization of superparamagnetic $MnFe_2O_4$ spinel ferrite nanocrystallites. J Phys Chem B 104:1141-1145
Liu T (1988) Loess in China. Springer-Verlag, Berlin
Liu T, Liu T (1991) Loess, Environment and Global Change. Science Press Beijing, China
Lodder JC (1995) Magnetic microstructures of perpendicular magnetic-recording media. Mater Res Soc Bull, October 1995:59-63
López A, Lázaro FJ, García-Palacios JL, Larrea A, Pankhurst QA, Martínez C, Corma A (1997) Superparamagnetic particles in ZSM-5-type ferrisilicates. J Mater Chem 12:1519-1529
Lowes FJ (1989) Geomagnetism and Paleomagnetism. Kluwer Academic Publishers, Boston
Lucinski T, Elefant D, Reiss G, Verges P (1966) The concept of the existence of interfacial superparamagnetic entities in Fe/Cr multilayers. J Magnet Magnetic Mater 162:29-37
Luo W, Nagel SR, Rosenbaum TF, Rosensweig RE (1991) Dipole interactions with random anisotropy in a frozen ferrofluid. Phys Rev Lett 67:2721-2724
Madsen MB, Morup S, Koch CJW (1986) Magnetic properties of ferrihydrite. Hyperfine Interactions 27:329-332
Maher BA, Thompson R (1999) Quaternary climates, environments and magnetism. Cambridge University Press, Cambridge, UK
Makhlouf SA, Parker FT, Berkowitz AE (1997b) Magnetic hysteresis anomalies in ferritin. Phys Rev B 55:R14717-R14720
Makhlouf SA, Parker FT, Spada FE, Berkowitz AE (1997a) Magnetic anomalies in NiO nanoparticles. J Appl Phys 81:5561-5563

Malaescu I, Marin CN (2000) Deviation from the superparamagnetic behavior of fine-particle systems. J Magnet Magnetic Mater 218:91-96

Mamiya H, Nakatani I, Furubayashi T (1998) Blocking and freezing of magnetic moments for iron nitride fine particle systems. Phys Rev Lett 80:177-180

Marin ML, Ortuno M, Hernandez A, Abellan J (1990) Percolative treatment of the Verwey transition in cobalt-iron and nickel-iron ferrites. Physica Status Solidi (B) 157:275-280

McElhinny MW, McFadden PL (1999) Paleomagnetism. Academic Press, New York

McVitie S, Chapman JN (1995) Coherent Lorentz imaging of soft thin-film magnetic materials. Mater Res Soc Bull, October 1995:55-58

Menear S, Bradbury A, Chantrell RW (1984) A model of the properties of colloidal dispersions of weakly interacting fine ferromagnetic particles. J Magnet Magnetic Mater 43:166-176

Mermin ND, Wagner H (1966) Absence of ferromagnetism or antiferromagnetism in one-or-two-dimensional isotropic Heisenberg models. Phys Rev Lett 17:1133-1136

Merrill RT, McElhinny MW, McFadden PL (1998) The Magnetic Field of the Earth. Academic Press, London

Miltat J, Thiaville A (2000) Magnets fast and small. Science 290:466-467

Mira J, López-Pérez JA, López-Quintela MA, Rivas J (1997) Magnetic iron oxide nanoparticles synthesized via microemulsions. Mater Sci Forum 235-238:297-302

Moriya T (1960) Anisotropic superexchange interaction and weak ferromagnetism. Phys Rev 120:91-98

Morris RV, Golden DC, Ming DW, Shelfer TD, Jorgensen LC, Bell III JF, Graff TG, Mertzman SA (2001) Phyllosilicate-poor palagonitic dust from Mauna Kea Volcano (Hawaii): A mineralogical analogue for magnetic Martian dust? J Geophys Res 106:5057-5083

Morris RV, Golden DG, Shelfer TD, Lauer Jr. HV (1998) Lepidocrocite to maghemite to hematite: A pathway to magnetic and hematitic martian soil. Meteoritics Planet Sci 33:743-751

Morup S (1994a) Superparamagnetism and spin glass ordering in magnetic nanocomposites. EuroPhys Lett 28:671-676

Morup S (1994b) Superferromagnetic nanostructures. Hyperfine Interactions 90:171-185

Morup S, Bodker F, Hendriksen PV, Linderoth S (1995) Spin-glass-like ordering of the magnetic moments of interacting nanosized maghemite particles. Phys Rev B 52:287-294

Morup S, Madsen MB, Franck J, Villadsen J, Koch CJW (1983) A new interpretation of Mossbauer spectra of microcrystalline goethite: "super-ferromagnetism" or "super-spin-glass" behavior? J Magnet Magnetic Mater 40:163-174

Morup S, Topsoe H, Lipka J (1976) Modified theory for Mossbauer spectra of superparamagnetic particles: Application to Fe₃O₄. J Physique, Colloque C6, Suppl n° 12:C6-287–C6-291

Morup S, Tronc E (1994) Superparamagnetic relaxation of weakly interacting particles. Phys Rev Lett 72:3278-3281

Moskowitz BM, Frankel RB, Walton SA, Dickson DPE, Wong KKW, Douglas T, Mann S (1997) Determination of the preexponential frequency factor for superparamagnetic maghemite particles in magneto-ferritin. J Geophys Res 102:22671-22680

Mullins CE, Tite MS (1973) Magnetic viscosity, quadrature susceptibility, and frequency dependence of susceptibility in single-domain assemblies of magnetite and maghemite. J Geophys Res 78:804-809

Murad E, Bowen LH, Long GL, Quin TG (1988) The influence of crystallinity on magnetic ordering in natural ferrihydrites. Clay Minerals 23:161-173

Nagata T (1961) Rock Magnetism. Maruzen, Tokyo

Néel L (1949a) Théorie du trainage magnétique des ferromagnétiques en grains fins avec applications aux terres cuites. Annal Géophys 5:99-136

Néel L (1949b) Influence des fluctuations thermiques sur l'aimantation de grains ferromagnétiques très fins. Comptes-rendus des séances de l'Académie des sciences 228:664-666

Néel L (1953) L'anisotropie superficielle des substances ferromagnétiques. Comptes-rendus des séances de l'Académie des sciences 237:1468-1470

Néel L (1954) Anisotropie magnétique superficielle et surstructures d'orientation. Journal de physique et le radium 15:225-239

Néel L (1955) Some theoretical aspects of rock magnetism. Adv Phys 4:191-243

Néel L (1961a) Superparamagnétisme des grains très fins antiferromagnétiques. Comptes-rendus des séances de l'Académie des sciences 252:4075-4080

Néel L (1961b) Superantiferromagnétisme dans les grains fins. Comptes-rendus des séances de l'Académie des sciences 253:203-208

Néel L (1961c) Superposition de l'antiferromagnétisme et du superparamagnétisme dans un grain très fin. Comptes-rendus des séances de l'Académie des sciences 253:9-12

Néel L (1961d) Sur le calcul de la susceptibilité additionnelle superantiferromagnétique des grains fins et sa variation thermique. Comptes-rendus des séances de l'Académie des sciences 253:1286-1291

Nordström L, Singh DJ (1996) Noncollinear intra-atomic magnetism. Phys Rev Lett 76:4420-4423

Nowak U, Chantrell RW, Kennedy EC (2000) Monte Carlo simulation with time step quantification in terms of Langevin dynamics. Phys Rev Lett 84:163-166

Nowak U, Hinzke D (1999) Magnetization switching in small ferromagnetic particles: Nucleation and coherent rotation. J Appl Phys 85:4337-4339

Nuth III JA, Wilkinson GM (1995) Magnetically enhanced coagulation of very small iron grains: A correction of the enhancement factor due to dipole-dipole interactions. Icarus 117:431-434

O'Reilly W (1984) Rock and Mineral Magnetism. Blackie, Glasgow and London

Oka T, Grun R, Tani A, Yamanaka C, Ikeya M, Huang HP (1997) ESR microscopy of fossil teeth. Radiation Measurements 27:331-337

Omari R, Prejean JJ, Souletie J (1983) Critical measurements in the spin glass CuMn. J Physique 44:1069-1083

Onodera S, Kondo H, Kawana T (1996) Materials for magnetic-tape media. Mater Res Soc Bull, September 1996:35-41

Opdyke ND, Channell JET (1996) Magnetic Stratigraphy. Academic Press, New York

Pankhurst QA, Pollard RJ (1992) Structural and magnetic properties of ferrihydrite. Clays Clay Minerals 40:268-272

Pankhurst QA, Pollard RJ (1993) Fine-particle magnetic oxides. J Phys: Condensed Matter 5:8487-8508

Parker FT, Foster MW, Margulies DT, Berkowitz AE (1993) Spin canting, surface magnetization, and finite-size effects in γ-Fe₂O₃ particles. Phys Rev B 47:7885-7891

Parkinson WD (1983) Introduction to geomagnetism. Scottish Academic Press, Edinburgh

Pastor GM, Dorantes-Davila J, Pick S, Dreyssé H (1995) Magnetic anisotropy of 3d transition-metal clusters. Phys Rev Lett 75:326-329

Pathria RK (1988) Statistical Mechanics. Pergamon Press, Exeter, UK

Petersen N, von Dobeneck T, Vali H (1986) Fossil bacterial magnetite in deep-sea sediments form the South Atlantic Ocean. Nature 320:611-615

Pfannes H-D (1997) Simple theory of superparamagnetism and spin-tunneling in Mossbauer spectroscopy. Hyperfine Interactions 110:127-134

Pfannes H-D, Mijovilovich A, Magalhães-Paniago R, Paniago R (2000) Spin-lattice-relaxation-like model for superparamagnetic particles under an external magnetic field. Phys Rev B 62:3372-3380

Pieters CM, Taylor LA, Noble SK, Keller LP, Hapke B, Morris RV, Allen CC, McKay DS, Wentworth S (2000) Space weathering on airless bodies: Resolving a mystery with lunar samples. Meteoritics Planet Sci 35:1101-1107

Pietzsch O, Kubetzka A, Bode M, Wiesendanger R (2001) Observation of magnetic hysteresis at the nanometer scale by spin-polarized scanning tunneling spectroscopy. Science 292:2053-2056

Pindor AJ, Staunton J, Stocks GM, Winter H (1983) Disordered local moment state of magnetic transition metals: A self-consistent KKR CPA calculation. J Phys F: Metal Phys 13:979-989

Politi P, Rettori A, Hartmann-Boutron F, Villain J (1995) Tunneling in mesoscopic magnetic molecules. Phys Rev Lett 75:537-540

Pollard RJ, Cardile CM, Lewis DG, Brown LG (1992) Characterization of FeOOH polymorphs and ferrihydrite using low-temperature, applied-field, Mössbauer spectroscopy. Clay Minerals 27:57-71

Popkov AF, Savchenko LL, Vorotnikova NV (1999) Thermally activated transformation of magnetization-reversal modes in ultrathin nanoparticles. JETP Lett 69:596-602

Popplewell J, Sakhnini L (1995) The dependence of the physical and magnetic properties of magnetic fluids on particle size. J Magnet Magnetic Mater 149:72-78

Preisach F (1935) Über die magnetische Nachwirkung. Z Physik 94:277-302

Prozorov R, Yeshurun Y, Prozorov T, Gedanken A (1999) Magnetic irreversibility and relaxation in assembly of ferromagnetic nanoparticles. Phys Rev B 59:6956-6965

Pshenichnikov AF, Mekhonoshin VV (2000) Equilibrium magnetization and microstructure of the system of superparamagnetic interacting particles: Numerical simulation. J Magnet Magnetic Mater 213:357-369

Qiu ZQ, Bader SD (1995) Surface magnetism and Kerr spectroscopy. Mater Res Soc Bull, October 1995:34-37

Quin TG, Long GL, Benson CG, Mann S, Williams RJP (1988) Influence of silicon and phosphorus on structural and magnetic properties of synthetic goethite and related oxides. Clays Clay Minerals 36:165-175

Raikher YL, Shliomis MI (1975) Theory of dispersion of the magnetic susceptibility of fine ferromagnetic particles. Soviet Physics JETP 40:526-532

Raikher YL, Shliomis MI (1994) The effective field method in the orientational kinetics of magnetic fluids and liquid crystals. Adv Chem Phys 87:595-751

Raikher YL, Stepanov VI (1995) Intrisic magnetic resonance in superparamagnetic systems. Phys Rev B 51:16428-16431

Raikher YL, Stepanov VI (1995a) Stochastic resonance and phase shifts in superparamagnetic particles. Phys Rev B 52:3493-3498

Raikher YL, Stepanov VI (1995b) Magnetic resonances in ferrofluids: temperature effects. J Magnet Magnetic Mater 149:34-37

Raikher YL, Stepanov VI (1997) Linear and cubic dynamic susceptibilities of superparamagnetic fine particles. Phys Rev B 55:15005-15017

Rancourt DG (1985) New theory for magnetic GICs: Superferromagnetism in two dimensions. J Magnet Magnetic Mater 51:133-140

Rancourt DG (1986) Low temperature behavior of Ising magnetic chains; decorated solitons, locally enhanced exchange and diffusive propagation. Solid State Commun 58:433-440

Rancourt DG (1987) Magnetic phenomena in layered and intercalated compounds. In Legrand AP, Flandrois S (eds) Chemical Physics of Intercalation. Plenum, New York, p 79-103

Rancourt DG (1988) Pervasiveness of cluster excitations as seen in the Mossbauer spectra of magnetic materials. Hyperfine Interactions 40:183-194

Rancourt DG (1994a) Mossbauer spectroscopy of minerals. I. Inadequacy of lorentzian-line doublets in fitting spectra arising from quadrupole splitting distributions. Phys Chem Minerals 21:244-249

Rancourt DG (1994b) Mossbauer spectroscopy of minerals. II. Problem of resolving cis and trans octahedral Fe^{2+} sites. Phys Chem Minerals 21:250-257

Rancourt DG (1998) Mossbauer spectroscopy in clay science. Hyperfine Interactions 117:3-38

Rancourt DG, Dang MZ (1996) Relation between anomalous magneto-volume behavior and magnetic frustration in Invar alloys. Phys Rev B 54:12225-12231

Rancourt DG, Dang M-Z, Lalonde AE (1992) Mossbauer spectroscopy of tetrahedral Fe^{3+} in trioctahedral micas. Am Mineral 77:34-43

Rancourt DG, Daniels JM (1984) Influence of unequal magnetization direction probabilities on the Mossbauer spectra of superparamagnetic particles. Phys Rev B 29:2410-2414

Rancourt DG, Daniels JM, Nazar LF, Ozin GA (1983) The superparamagnetism of very small particles supported by zeolite-Y. Hyperfine Interactions 15/16:653-656

Rancourt DG, Dube M, Heron PRL (1993) General method for applying mean field theory to disordered magnetic alloys. J Magnet Magnetic Mater 125:39-48

Rancourt DG, Ferris FG, Fortin D (1999a) Sorbed iron on the cell wall of Bacillus subtilis characterized by Mössbauer spectroscopy: In Evidence for Bioreduction. Ferris FG (ed) Abstracts: Int'l Symp Environ Biogeochem, Hunstville, Canada. XIV:27

Rancourt DG, Flandrois S, Biensan P, Lamarche G (1990a) Magnetism of a graphite bi-intercalation compound with two types of ferromagnetic layers: Double hysteretic transition in $CrCl_3-NiCl_2-C$. Canadian J Phys 68:1435-1439

Rancourt DG, Fortin D, Pichler T, Thibault P-J, Lamarche G, Morris RV, Mercier PHJ (2001b) Mineralogy of a natural As-rich hydrous ferric oxide coprecipitate formed by mixing of hydrothermal fluid and seawater: Implications regarding surface complexation and color banding in ferrihydrite deposits. Am Mineral 86:1-18 (in press)

Rancourt DG, Julian SR, Daniels JM (1985) Mossbauer characterization of very small superparamagnetic particles: Application to intra-zeolitic α-Fe_2O_3 particles. J Magnet Magnetic Mater 49:305-316

Rancourt DG, Lagarec K, Densmore A, Dunlap RA, Goldstein JI, Reisner RJ, Scorzelli RB (1999b) Experimental proof of the distinct electronic structure of a new meteoritic Fe-Ni alloy phase. J Magnet Magnetic Mater 191:L255-L260

Rancourt DG, Lamarche G, Tume P, Lalonde AE, Biensan P, Flandrois S (1990b) Dipole-dipole interactions as the source of spin-glass behavior in exchangewise two-dimensional ferromagnetic layer compounds. Canadian J Phys 68:1134-1137

Rancourt DG, Meschi C, Flandrois S (1986) S = 1/2 antiferromagnetic finite chains effectively isolated by frustration: $CuCl_2$ graphite intercalation compounds. Phys Rev B 33:347-255

Rancourt DG, Ping JY (1991) Voigt-based methods for arbitrary-shape static hyperfine parameter distributions in Mössbauer spectroscopy. Nuclear Instruments and Methods in Physics Research B (NIMB) 58:85-97

Rancourt DG, Ping JY, Berman RG (1994) Mossbauer spectroscopy of minerals. III. Octahedral-site Fe^{2+} quadrupole splitting distributions in the phlogopite-annite series. Phys Chem Minerals 21:258-267

Rancourt DG, Scorzelli RB (1995) Low-spin γ-Fe-Ni(γ_{LS}) proposed as a new mineral in Fe-Ni-bearing meteorites: Epitaxial intergrowth of γ_{LS} and tetrataenite as a possible equilibrium state at ~20-40 at % Ni. J Magnet Magnetic Mater 150:30-36

Rancourt DG, Thibault P-J, Ferris FG (2001a) Resolution and quantification of Fe sorbed to bacterial cell walls, biogenic ferrihydrite, and abiotic ferrihydrite by cryogenic ^{57}Fe Mössbauer spectroscopy. Proc of ICOBTE-2001, 6th Int'l Conf Biogeochemistry of Trace Elements. Extended abstr GO448, p 360

Ribas R, Labarta A (1996a) Magnetic relaxation of a one-dimensional model for small particle systems with dipolar interaction: Monte Carlo simulation. J Appl Phys 80:5192-5199

Ribas R, Labarta A (1996b) Monte Carlo simulation of magnetic relaxation in small-particle systems with dipolar interactions. J Magnet Magnetic Mater 157-158:351-352

Ricci TF, Scherer C (1997) Linear response and stochastic resonance of superparamagnets. J Statist Phys 86:803-819

Richter C, van der Pluijm BA (1994) Separation of paramagnetic and ferrimagnetic susceptibilities using low temperature magnetic susceptibilities and comparison with high field methods. Phys Earth Planet Inter 82:113-123

Rikitake T, Honkura Y (1986) Solid earth geomagnetism. D Reidel Pub Co, Dordrecht, The Netherlands

Roberts AP, Cui Y, Verosub KL (1995) Wasp-waisted hysteresis loops: Mineral magnetic characteristics and discrimination of components in mixed magnetic systems. J Geophys Res 100:17909-17924

Robin E (1996) Le verdict du spinelle: les derniers vestiges de la météorite elle-même ont été retrouvés. La Recherche 293:58-60

Roch A, Muller RN (1999) Theory of proton relaxation induced by superparamagnetic particles. J Chem Phys 110:5403-5411

Rochette P, Fillion G (1988) Identification of multicomponent anisotropies in rocks using various field and temperature values in a cryogenic magnetometer. Phys Earth Planet Interiors 51:379-386

Ronov AB, Yaroshevsky AA (1969) The Earth's Crust and Upper Mantle. American Geophysical Union, Washington, DC

Rose K, Gurewitz E, Fox GC (1990) Statistical mechanics and phase transitions in clustering. Phys Rev Lett 65:945-948

Rosensweig RE (1985) Ferrohydrodynamics. Cambridge University Press, Cambridge, UK

Rubens SM (1979) William Fuller Brown, Jr. I E E E Trans Magnetics 15:1192-1195

Sabourin N, Rancourt DG, Dang M-Z, Evans ME (2001) Mineral magnetic, and mineralogical, and geochemical study of a Siberian loess/paleosol sequence. (manuscript in preparation)

Sadykov EK, Isavnin AG (1996) Theory of dynamic magnetic susceptibility in uniaxial superparamagnetic particles. Phys Solid State 38:1160-1164

Safarik I, Safarikova M (1997) Copper phthalocyanine dye immobilized on magnetite particles: An efficient adsorbent for rapid removal of polycyclic aromatic compounds from water solutions and suspensions. Separation Sci Technol 32:2385-2392

Sappey R, Vincent E, Hadacek N, Chaput F, Boilot JP, Zins D (1997a) Nonmonotonic field dependence of the zero-field cooled magnetization peak in some systems of magnetic nanoparticles. Phys Rev B 56:14551-14559

Sappey R, Vincent E, Ocio M, Hammann J, Chaput F, Boilot JP, Zins D (1997b) A new experimental procedure for characterizing quantum effects in small magnetic particle systems. EuroPhys Lett 37:639-644

Saxena SS, Littlewood PB (2001) Iron cast in exotic role. Nature 412:290-291

Scheinfein MR, Schmidt KE, Heim KR, Hembree GG (1996) Magnetic order in two-dimensional arrays of nanometer-sized superparamagnets. Phys Rev Lett 76:1541-1544

Schmidt H, Ram RJ (2001) Coherent magnetization reversal of nanoparticles with crystal and shape anisotropy. J Appl Phys 89:507-513

Seehra MS, Babu VS, Manivannan A (2000) Neutron scattering and magnetic studies of ferrihydrite nanoparticles. Phys Rev B 61:3513-3518

Sestier C, Da-Silva MF, Sabolovic D, Roger J, Pons JN (1998) Surface modification of superparamagnetic nanoparticles (ferrofluid) studied with particle electrophoresis: Application to the specific targeting of cells. Europhoresis 19:1220-1226

Sestier C, Sabolovic D (1998) Particle electrophoresis of micrometic-sized superparamagnetic particles designed for magnetic purification of cells. Europhoresis 19:2485-2490

Sharma R, Saini S, Ros PR, Hahn PF, Small WC, de Lange EE, Stillman AE, Edelman RR, Runge VM, Outwater EK, Morris M, Lucas M (1999) Safety profile of ultrasmall superparamagnetic iron oxide ferumoxtran-10: Phase II clinical trial data. J Magnet Reson Imaging 9:291-294

Sharma VK, Baiker A (1981) Superparamagnetic effects in the ferromagnetic resonance of silica supported nickel particles. J Chem Phys 75:5596-5601

Sharma VK, Waldner F (1977) Superparamagnetic and ferrimagnetic resonance of ultrafine Fe_3O_4 particles in ferrofluids. J Appl Phys 48:4298-4302

Sibilia JP (1996) A Guide to Materials Characterization and Chemical Analysis. VCH Publishers, Weinheim, FRG

Simkiss K, Taylor MG (2001) Trace element speciation at cell membanes: aqueous, solid and lipid phase effects. J Environ Monitoring 3:15-21

Smith NV, Padmore HA (1995) X-ray magnetic circular dichroism spectroscopy and microscopy. Mater Res Soc Bull October:41-44

Soltis FG (2001) Magnetic storage: How much longer can it keep going? News/400, February 2001:25-29

Song T, Roshko RM (2000) Preisach model for systems of interacting superparamagnetic particles. IEEE Trans Magnetics 36:223-230

Spinu L, Stancu A (1998) Modelling magnetic relaxation phenomena in fine particles systems with a Preisach-Néel model. J Magnet Magnetic Mater 189:106-114

Srivastava KKP, Jones DH (1988) Toward a microscope description of superparamagnetism. Hyperfine Interactions 42:1047-1050

St-Pierre TG, Chan P, Bauchspiess KR, Webb J, Betteridge S, Walton S, Dickson DPE (1996) Synthesis, structure and magnetic properties of ferritin cores with varying composition and degrees of structural order: Models of iron oxide deposits in iron-overload diseases. Coordination Chem Rev 151:125-143

St-Pierre TG, Jones DH, Dickson DPE (1987) The behavior of superparamagnetic small particles in applied magnetic fields: A Mossbauer spectroscopy study of ferritin and haemosiderin. J Magnet Magnetic Mater 69:276-284

St-Pierre TG, Webb J, Mann S (1989) Ferritin and hemosiderin: Structural and magnetic studies of the iron core. In Mann S, Webb J, Williams RJP (eds) Biomineralization—Chemical and Biochemical Perspectives. VCH Publishers, Weinheim, p 295-344

Stacey FD, Banerjee SK (1974) Physical principles of rock magnetism. In Developments in Solid Earth Geophysics. Elsevier, Amsterdam

Stacey GD (1963) The physical theory of rock magnetism. Adv Phys 12:45-133

Stamp PCE (1991) Quantum dynamics and tunneling of domain walls in ferromagnetic insulators. Phys Rev Lett 66:2802-2805

Stancu A, Spinu L (1998) Temperature- and time-dependent Preisach model for a Stoner-Wohlfarth particle system. IEEE Trans Magnetics 34:3867-3875

Stein DL (1992) Spin glasses and biology. World Scientific, Singapore

Steiner M, Villain J, Windsor G (1976) Theoretical and experimental studies on one-dimensional magnetic systems. Adv Phys 25:87-209

Stokroos I, Litinetsky L, van der Want JJL, Ishay JS (2001) Keystone-like crystals in cells of hornet combs. Nature 411:654

Stoner EC, Wohlfarth EP (1948) A mechanism of magnetic hysteresis in heterogeneous alloys. Philos Trans Royal Soc London 240:599-644

Street R, Woolley JC (1949) A study of magnetic viscosity. Proc Phys Soc A 62:562-572

Suber L, Fiorani D, Imperatori P, Foglia S, Montone A, Zysler R (1999) Effects of thermal treatments on structural and magnetic properties of acicular α-Fe$_2$O$_3$ nanoparticles. NanoStructured Mater 11:797-803

Suber L, Santiago AG, Fiorani D, Imperatori P, Testa AM, Angiolini M, Montone A, Dormann JL (1998) Structural and magnetic properties of α-Fe$_2$O$_3$ nanoparticles. Appl Organometal Chem 12:347-351

Sutton AP (1993) Electronic Structure of Materials. Clarendon Press, Oxford, UK

Suzuki T (1996) Magneto-optic recording materials. Mater Res Soc Bull, September 1996:42-47

Svedlindh P, Jonsson T, García-Palacios JL (1997) Intra-potential-well contribution to the AC susceptibility of a noninteracting nano-sized magnetic particle system. J Magnet Magnetic Mater 169:323-334

Szabo A, Ostlund NS (1996) Modern quantum chemistry. Introduction to advanced electronic structure theory. Dover, New York

Tarduno JA (1995) Superparamagnetism and reduction diagenesis in pelagic sediments: Enhancement or depletion? Geophys Res Lett 22:1337-1340

Tarling DH, Hrouda P (1993) The Magnetic Anisotropy of Rocks. Chapman and Hall, New York

Tauxe L, Mullender TAT, Pick T (1996) Potbellies, wasp-waists, and superparamagnetism in magnetic hysteresis. J Geophys Res 101:571-583

Tejada J, Zhang XX (1994) On magnetic relaxation in antiferromagnetic horse-spleen ferritin proteins. J Phys: Condensed Matter 6:263-266

Tejada J, Zhang XX, del Barco E, Hernández JM, Chudnovsky EM (1997) Macroscopic resonant tunneling of magnetization in ferritin. Phys Rev Lett 79:1754-1757

Tejada J, Ziolo RF, Zhang XX (1996) Quantum tunneling of magnetization in nanostructured materials. Chem Mater 8:1784-1792

Thibault P-J (2001) Charactérization de la ferrihydrite authigénique synthétisée sous différentes conditions. MsC Thesis, Department of Earth Sciences, University of Ottawa (submitted)

Thomas L, Lionti F, Ballou R, Gatteschi D, Sessoli R, Barbara B (1996) Macroscopic quantum tunnelling of magnetization in a single crystal of nanomagnets. Nature 383:145-147

Thompson R, Oldfield F (1986) Environmental Magnetism. Allen & Unwin, St. Leonards, UK

Tiefenauer LX, Kühne G, Andres RY (1993) Antibody-magnetite nanoparticles: In vitro characterization of a potential tumor-specific contrast agent for magnetic resonance imaging. Bioconjugate Chem 4:347-352

Upadhyay RV, Sutariya GM, Mehta RV (1993) Particle size distribution of a laboratory-synthesized magnetic fluid. J Magnet Magnetic Mater 123:262-266

Uyeda C (1993) Diamagnetic anisotropies of oxide minerals. Phys Chem Minerals 20:77-81

Vacquier V (1972) Geomagnetism in Marine Geology. Elsevier Science, Amsterdam

Van Der Giessen AA (1967) Magnetic properties of ultra-fine iron (3) oxide-hydrate particles prepared from iron (3) oxide-hydrate gels. J Phys Chem Solids 28:343-346

van der Kraan AM (1971) Superparamagnetism of small alpha-Fe$_2$O$_3$ crystallites studied by means of the Mossbauer effect. J Physique 32:C1-1034-C1-1036

Van der Woude F, Dekker AJ (1965a) Interpretation of Mössbauer spectra of paramagnetic materials in a magnetic field. Solid State Commun 3:319-321

Van der Woude F, Dekker AJ (1965b) The relation between magnetic properties and the shape of Mossbauer spectra. Physica Status Solidi 9:775-786

van Lierop J, Ryan DH (2001) Mossbauer spectra of single-domain fine particle systems described using a multiple-level relaxation model for superparamagnets. Phys Rev B 63:64406-1-64406-8

Van Ruitenbeek JM, Van Leeuwen DA, De Jongh LJ (1994) Magnetic properties of metal cluster compounds. In De Jongh LJ (ed) Physics and Chemistry of Metal Cluster Compounds. Kluwer Academic Publishers, Dordrecht, The Netherlands, p 277-306

Van Vleck JH (1959) The Theory of Electric and Magnetic Susceptibilities. Oxford University Press, London

Vandenberghe RE, Barrero CA, da Costa GM, Van San E, De Grave E (2000) Mossbauer characterization of iron oxides and (oxy)hydroxides: The present state of the art. Hyperfine Interactions 126:247-259

Vasçuez-Mansilla M, Zysler RD, Arciprete C, Dimitrijewits MI, Saragovi C, Greneche JM (1999) Magnetic interaction evidence in α-Fe$_2$O$_3$ nanoparticles by magnetization and Mössbauer measurements. J Magnet Magnetic Mater 204:29-35

Vaz C, Godinho M, Dormann JL, Nogués M, Ezzir A, Tronc E, Jolivet JP (1997) Superparamagnetic regime in γ-Fe$_2$O$_3$ nanoparticle systems; effect of the applied magnetic field. Mater Sci Forum 325-238:813-817

Victora RH (1989) Predicted time dependence of the switching field for magnetic materials. Phys Rev Lett 63:457-460

Vincent E, Yuan Y, Hammann J, Hurdequint H, Guevara F (1996) Glassy dynamics of nanometric magnetic particles. J Magnet Magnetic Mater 161:209-219

Wang J-S, Swendsen RH (1990) Cluster Monte Carlo algorithms. Physica A 167:565-579

Warren LA, Ferris FG (1998) Continuum between sorption and precipitation of Fe(3) on microbial surfaces. Environ Sci Technol 32:2331-2337

Watson JHP, Cressey BA, Roberts AP, Ellwood DC, Charnock JM, Soper AK (2000) Structural and magnetic studies on heavy-metal-adsorbing iron sulphide nanoparticles produced by sulphate-reducing bacteria. J Magnet Magnetic Mater 214:13-30

Weaver JC, Vaughan TE, Astumian RD (2000) Biological sensing of small field differences by magnetically sensitive chemical reactions. Nature 405:707-709

Weiss PR (1948) The application of the Bethe-Peierls method to ferromagnetism. Phys Rev 74:1493-1504

Wernsdorfer W, Orozco EB, Hasselbach K, Benoit A, Barbara B, Demoncy N, Loiseau A, Pascard H, Mailly D (1997a) Experimental evidence of the Néel-Brown model of magnetization reversal. Phys Rev Lett 78:1791-1794

Wernsdorfer W, Orozco EB, Hasselbach K, Benoit A, Mailly D, Kubo O, Nakano H, Barbara B (1997b) Macroscopic quantum tunneling of magnetization of single ferrimagnetic nanoparticles of barium ferrite. Phys Rev Lett 79:4014-4017

Wickman HH, Klein MP, Shirley DA (1966) Paramagnetic hyperfine structure and relaxation effects in Mossbauer spectra: Fe^{57} in ferrichrome. Phys Rev 152:345-357

Wiltschko R, Wiltschko W (1995) Magnetic Orientation in Animals. Springer-Verlag, Berlin

Wiser N (1996) Phenomenological theory of the giant magnetoresistance of superparamagnetic particles. J Magnet Magnetic Mater 159:119-124

Wohlfarth EP (1964) A review of the problem of fine-particle interactions with special reference to magnetic recording. J Appl Phys 35:783-790

Worm H-U (1998) On the superparamagnetic-stable single domain transition for magnetite, and frequency dependence of susceptibility. Geophys J Int'l 133:201-206

Xu J, Hickey BJ, Howson MA, Greig D, Cochrane R, Mahon S, Achilleos C, Wiser N (1997) Giant magnetoresistance in AuFe alloys: Evidence for the progressive unblocking of superparamagnetic particles. Phys Rev B 56:14602-14606

Yeh T-C, Zhang W, Ildstad ST, Ho C (1993) Intracellular labeling of T-cells with superparamagnetic contrast agents. MRM (Magnetic Resonance in Medicine) 30:617-625

Yelon A, Movaghar B (1990) Microscopic explanation of the compensation (Meyer-Neldel) rule. Phys Rev Lett 65:618-620

Zarutskaya T, Shapiro M (2000) Capture of nanoparticles by magnetic filters. J Aerosol Sci. 31:907-921

Zhang P, Molnar P, Downs WR (2001) Increased sedimentation rates and grain sizes 2-4 Myr ago due to the influence of climate change on erosion rates. Nature 410:891-897

Zhao J, Huggins FE, Feng Z, Huffman GP (1996) Surface-induced superparamagnetic relaxation in nanoscale ferrihydrite particles. Phys Rev B 54:3403-3407

Zhu J-G (1995) Micromagnetic modeling: Theory and applications in magnetic thin films. Mater Res Soc Bull, October 1995:49-54

Zysler RD, Fiorani D, Testa AM (2001) Investigation of magnetic properties of interacting Fe_2O_3 nanoparticles. J Magnet Magnetic Mater 224:5-11

7 Magnetism of Earth, Planetary, and Environmental Nanomaterials

Denis G. Rancourt

NANOPARTICLES AND THE ENVIRONMENT

CONTENTS

REVIEWS in MINERALOGY and GEOCHEMISTRY

Volume 44   2001

NANOPARTICLES AND THE ENVIRONMENT

Editors:

JILLIAN F. BANFIELD   *Department of Geology & Geophysics*
University of Wisconsin
Madison, Wisconsin

ALEXANDRA NAVROTSKY   *Department of Chemical*
Engineering & Materials Science
University of California-Davis
Davis, California

COVER: Colorized, high-resolution transmission electron microscope lattice-fringe image of seven nanoparticles of UO_2 produced by the activity of sulfate-reducing bacteria. Note that the largest uraninite particle is <3 nm in diameter (Suzuki and Banfield, in preparation).

Graphic provided by Jill Banfield, Yohey Suzuki, and Mary Diman.

*Series Editor for MSA: **Paul H. Ribbe***

Virginia Polytechnic Institute and State University
Blacksburg, Virginia

MINERALOGICAL SOCIETY of AMERICA